2005

POWER SPECTRAL DENSITY ANALYSIS OF PRINTER DEFECT

Il-Won Shin
University of Kentucky, ishin0@engr.uky.edu

ABSTRACT OF THESIS

POWER SPECTRAL DENSITY ANALYSIS OF PRINTER DEFECT

A potential characterization tool for printer quality is the power spectral density (PSD) analysis of flat-field printer outputs. This thesis explains the relationship between the PSD and characteristics of printer defects using examples of scanned printer outputs. In addition, a protocol is also presented for scanning flat fields and performing a PSD analysis. The protocol considers sampling and windowing issues to best focus on defects or quality issues of interest. The main objective of this work is to determine the interactive relationships of print defect patterns such as graininess, streaking, and banding under flat-field hardcopy outputs. The additive and multiplicative models are considered for describing the interaction between printer defects. Simulated print defect patterns and metrics base on the PSD are used to demonstrate the patterns generated by multiplicative and additive processes. These results are compared the PSD of actual flat-field prints from digital printers to draw conclusion concerning actual artifact interaction. For all defects examined the additive model is shown to be a good model of the interactions between printer defects.

KEYWORDS: Printer Defect, Additive and Multiplicative Models, Power Spectral Density, Graininess, Streaking, Banding

Il-Won Shin

December 12, 2005

POWER SPECTRAL DENSITY ANALYSIS OF PRINTER DEFECT

By

Il-Won Shin

Dr. Kevin D. Donohue
Director of Thesis

Dr. YuMing Zhang
Director of Graduate Studies

December 12, 2005

RULES FOR THE USE OF THESES

Unpublished theses submitted for the Master's degree and deposited in the University of Kentucky Library are as a rule open for inspection, but are to be used only with due regard to the rights of the authors. Bibliographical references may be noted, but quotations or summaries of parts may be published only with the permission of the author, and with the usual scholarly acknowledgments.

Extensive copping or publication of the thesis in whole or in part also requires the consent of the Dean of the Graduate school of the University of Kentucky.

A library that borrows this thesis for use by its patrons is expected to secure the signature of each user.

Name	Date

THESIS

Il-Won Shin

The Graduate School

University of Kentucky

2005

POWER SPECTRAL DENSITY ANALYSIS OF PRINTER DEFECT

THESIS

A thesis submitted in partial fulfillment of the
requirements for the degree of Master of Science in the
College of Engineering
at the University of Kentucky

By

Il-Won Shin

Lexington, Kentucky

Director: Dr. Kevin D. Donohue, Associate Professor of

Electrical Engineering, Lexington, Kentucky

2005

DEDICATION

To my family, friends and teachers

ACKNOWLEDGEMENTS

There are lots of people I would like to thank for a huge variety of reasons.

Firstly, I would like to thank my Advisor, Dr. Kevin D. Donohue. I could not have imagined having a better advisor and mentor for my Master, and without his common-sense, knowledge, perceptiveness and cracking-of-the-whip I would never have finished. His capacity to combine critique with an immediate empathy and commitment towards workers and others engaged in struggle will always inspire me.

I would also like to thank Dr. Laurence G. Hassebrook and Dr. Daniel D. Lau for agreeing to take part in my committee and for letting me proceed my own way until I needed some mid-course guidance, and for being right there with the thrusters when asked.

I would also like to thank my lab mates Vijay, Nathir, Elios, and Wei and the respondents of my study for their help and their patience in enduring me through these days.

Finally, I am forever indebted to my parents and Gil Kim for their understanding and support, endless patience and encouragement when it was most required.

TABLE OF CONTENTS

LIST OF TABLES

LIST OF FIGURES

LIST OF FILES

IWThesis.pdf……...7870 KB

CHAPTER 1

Introduction and Literature Review

Recent advances in digital imaging technology and multimedia applications have renewed research interests in image quality. Image Quality (IQ) has conventionally been evaluated in two different methods. One approach to the image quality evaluation is image quality metrics, which are objective measurements of an image based on mathematical calculations [5, 11-15]. The other approach is an image preference, which is a subjective measurement of overall image based on many observers [6-10, 11, 15]. A central issue in the analysis of image quality is the understanding of the Human Visual System (HVS), which is critical in the development of image quality metrics.

Section 1.1 of this chapter discusses the image quality description. Section 1.2 details features of the Human Visual System (HVS). Section 1.3 introduces the approaches of the InterNational Committee on Information Technology (INCITS) W1.1, which is the U.S. representative of ISO/IEC JTC1/SC28 and the standardization committee on image quality for printer system. This chapter concludes with a hypothesis statement and overall organization of the thesis in Section 1.4 and 1.5, respectively.

1.1 Image Quality Description

Keelan [1] defines image quality as follows:

"*The quality of an image is defined to be an impression of its merit or excellence, as perceived by an observer neither associated with the act of photography, nor closely involved with the subject matter depicted.*"

As mention before, image quality is usually separated into two classes [11,15]

1. Objective image quality is evaluated through physical measurements of image properties. In the case of digital imaging this is achieved with special software evaluating the digital file.
2. Subjective image quality is evaluated through judgment by human observers. The final goal of image quality assessment research is to find objective image quality metrics that automatically respond to the subjective values from the human observers.

The common objective metrics in image quality analysis are Mean Square Error (MSE) [5], Peak Signal to Noise Ration (PSNR), Modulation Transfer Function (MTF) of the imaging system [1], and the Noise Power Spectra (NPS) [21]. In this thesis, the two-dimensional NPS is the characterization tool, the details of which are described in Chapter 2. These metrics are easy computed, but the values do not correlate well with subjective quality measures by human observers. Therefore, it is not possible to develop objective image quality metrics without understanding the Human Visual System (HVS). In the last two decades, the analysis of the HVS features has been emphasized to develop objective metrics and the following section details features of the HVS.

1.2 HVS Features

Perceptual image quality is correlated with various HVS features [6, 7, 8, 9, 10]. The most commonly used features are luminance contrast sensitivity, frequency contrast sensitivity, and masking effects.

Luminance contrast sensitivity is referred to as the amplitude nonlinearity of the visual system. Ernst Weber, a 19^{th} century experimental psychologist, observed the following relationship, known since as Weber's Law [16]

$$\frac{\Delta I}{I} = K, \tag{1-1}$$

where I is the initial stimulus magnitude, ΔI is the difference threshold and K is a constant. More simply stated, the size of the just noticeable difference (ΔI) is proportional to original stimulus value (I).

Many researchers have performed experiments to measure the contrast sensitivity function (CSF) of the human vision system over a variety of frequencies. Mannos and Sakrison defined a general form for the CSF [17]:

$$CSF\ (f) = a(b + cf)e^{(-df)^g}, \tag{1-2}$$

where parameters a=2.6, b=0.0192, c=0.114, d=0.114, and g=1.1. The CSF describes the variations in visual sensitivity as a function of spatial frequency and viewing distance. In addition, the CSF can be thought of as a band-pass characteristic, much more sensitive to middle spatial frequency range. An example of the CSF is shown in Figure 1.1 along a single orientation. A 2-D NPS for obtaining a perceptually weighted metric for the printer defects such as graininess, streaking, and banding can weight the 2-D CSF.

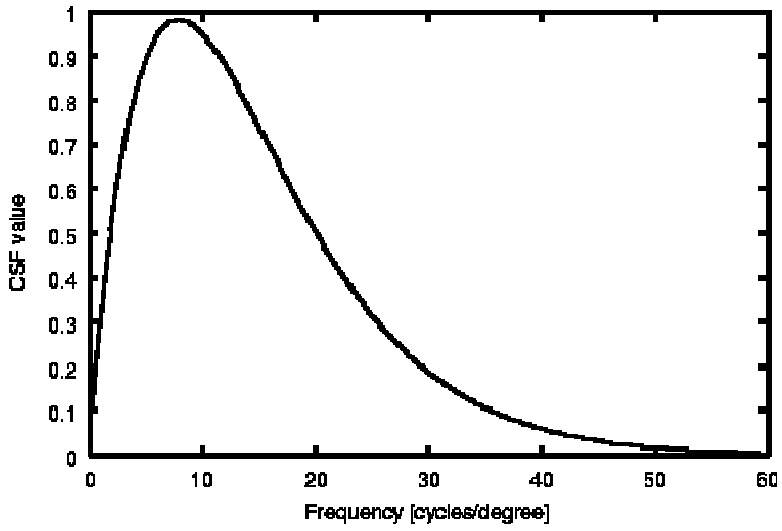

Figure 1.1 Contrast Sensitivity Function adapted from [17]

The masking effect is dynamic HVS feature where the presence of a signal component influences the way the other signal components are perceived. In other words, the stimulus in one sub-band will raise the detection threshold other stimulus in the same sub-band [17]. This feature is useful for the improvement of image coding efficiency and the design of image quality metrics, even though the theoretical formulation has not been able to prove various forms of masking [18].

1.3 The Approach of the INCITS W1.1 Process

The InterNational Committee on Information Technology (INCITS) W1.1 is the U.S. representative of ISO/IEC JTC1/SC28 and the standardization committee on image quality for printer system. The paper [11] proposes the perceived image quality could be described by a small set of broad-based attributes. In addition, it focuses on evaluating the overall image quality of hardcopy output from printer systems so that the systems can be compared in a meaningful way. The idea of this thesis is strongly influenced by the methodology laid out in [11], where the main objective of this thesis is to analyze the interaction of the printer defects on the flat-field hardcopy output from any printer systems. The process for developing the Image Quality of Printer Standards is described in [4]. There are currently six ad hoc W1.1 teams, each team working on one or more of these image quality attributes, which enable evaluation of overall image quality.

Image quality of printer systems can categorize three different domains as objective image quality metrics, image preference, and image quality attributes. The disadvantage of objective metrics is that they do not directly model high-level image quality descriptors and not enough is know about the higher-level cognitive processes to combine the large number of various metrics in a meaningful way. For examples, if someone

wants to compare the overall image quality using image quality metrics, he or she would need to compare thousands of numerical values. This is difficult to do in a meaningful manner that models the human quality judgment process. The disadvantage of image preference is that it is difficult to quantify and is strongly dependent on image content. Moreover, even though color rendering is one of the weaker links in the overall image quality, the influence of color rendering on preference is a major concern. Because of these inherent drawbacks associated with image quality metrics and image preference, image quality attributes have been introduced for the overall image quality of a printer system from W1.1 Process.

1.3.1 Image Quality Attributes

Image quality attributes used at Xerox are those specified by the DAC (Document Appearance Characterization) system [11] and a high-level image quality descriptor. As mention in Section 1.1, a long-term goal is to be able to predict image quality from measurements on analytical images using statistical correlations. Image quality attributes combine some of the best features of both image quality metrics and image preference because they can correlate with image quality attributes. Figure 1.2 shows the current DAC attributes that are rated on an absolute scale of 0 to 100, with 100 indicating the best quality.

This thesis focuses on the uniformity such as Macro-uniformity and Micro- uniformity. The contributors of Macro-uniformity are streaks, bands, mottle, gradients, moiré, etc and the contributors of Micro-uniformity are streaks, bands, voids, mottle, granularity, textures, noise, etc. While both attributes are similar because they focus on uniformity, the scale of analysis is the key different.

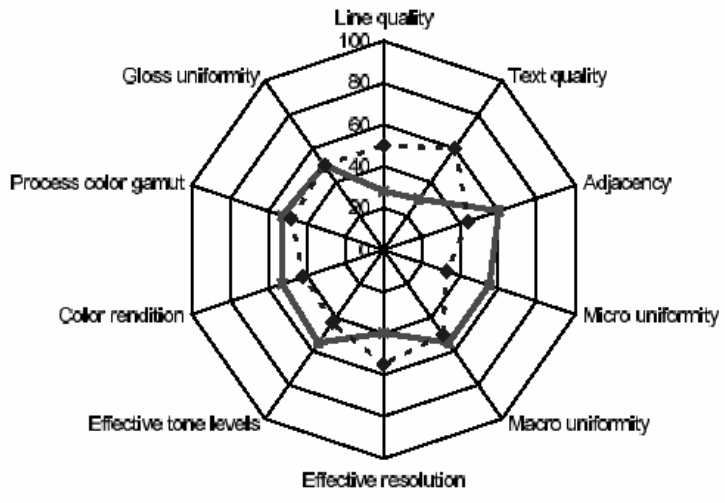

Figure 1.2 The DAC image quality attributes adapted from [11]. The solid and dotted lines illustrate the image quality of two hypothetical printers.

Defect that are noticeable over 2 cm patches or less are considered micro-uniformity defects and this over large areas up to the whole page are Macro-uniformity attributes. While the DAC system defines major categories of image attributes it does not specify how to quantify the defects or printer artifacts that directly affect each attribute. The contribution of this thesis focuses on finding the interaction between printer defects that affect uniformity such as graininess, streaking, and banding, and being able to model these interactions in the NPS. An understanding of this interaction could lead to better models for combining metrics for perceptual scoring of image quality.

1.4 Motivation and Hypothesis

Paul J. Kane [21] suggested the additive interactions of graininess, streaking, and banding artifacts. The printer gear created banding noise in the images, which are also created by the halftoning. The location of halftoning depends on the density of banding artifact, and it seems to be the multiplicative interaction between two components. Therefore, our

motivation of this thesis is to find the multiplicative interaction of suggested three printer artifacts.

The hypothesis of this thesis is that multiplicative models better describe the interaction between printer artifacts. If this hypothesis is rejected, we assume additive model is more realistic model than multiplicative models.

1.5 Approach

The goal of this thesis is to determine the interactive relationships of print defect patterns such as graininess, streaking, and banding under flat-field hardcopy outputs. The characterization tool used in this work is the power spectral density (PSD) of flat-field printer outputs. Two types of models were considered for describing the interaction between printer defects, which are the additive model and the multiplicative model. In other words when two or more defects are present, do their variations add or multiply to results in the final observed non-uniformity. Simulated print defect patterns and metrics based on the NPS are used to demonstrate the patterns generated by multiplicative and additive processes. These results are compared the noise power spectrum of actual flat-field prints from digital printers to draw conclusion concerning actual artifact interaction.

1.6 Organization of the Thesis

Chapter 2 discusses the experimental setup and modeling of printer artifacts such as graininess, streaking, and banding. Chapter 3 presents the discussion of two types of interaction models (additive and multiplicative) and analysis for digital printers. Chapter 4 presents the results and discussions followed by Chapter 5 that presents conclusions and directions for future research.

CHAPTER 2

Experiment Setup and Modeling of Printer Artifacts

ISO (the International Organization for Standardization) and IEC (the International Electrical Commission) document 13660 specifies guidelines of image quality on hardcopy print quality assessment [2]. These guidelines contain the schema of image quality and attributes for two categories of printed areas: Large area density attributes, and character and line attributes. This thesis only focuses on the large area density, i.e., flat field images which have three dominant printer defects such as graininess, streaking, and banding. This chapter introduces the experiment setup for measuring common printer defects. The discussion on the overview of data collection is presented in Section 2.1. Section 2.2 discusses characterizing defect patterns with parameters estimated from the 2-D NPS. Finally, Section 2.3 describes the modeling of three printer artifacts with the power spectrum density.

2.1 Data Collections

The data collection for the printer quality analysis can be explained with the help of a flow chart shown in Figure 2.2.

The general procedure of analysis of printer quality is explained below [3]:

1. Test patterns are stored in compressed PDF file format download from [4]. Figure 2.1 shows the one of the test patterns (reduced from actual size). The primary content is a 178mm by 211mm flat field region at a specific gray level between 0 (white) and 100% (black). The purpose of the smaller intensity fields is for calibration over the range of luminance values. From a single print the small area

can be used to find the test pattern densities that are closest to CIE L* levels of 40, 60, and 80. These test patterns are printed along with the 100%K pattern on the printer system to be assessed. In the experiments described in this work, Figure 2.1 was printed with two inkjet printers and two laser printers.

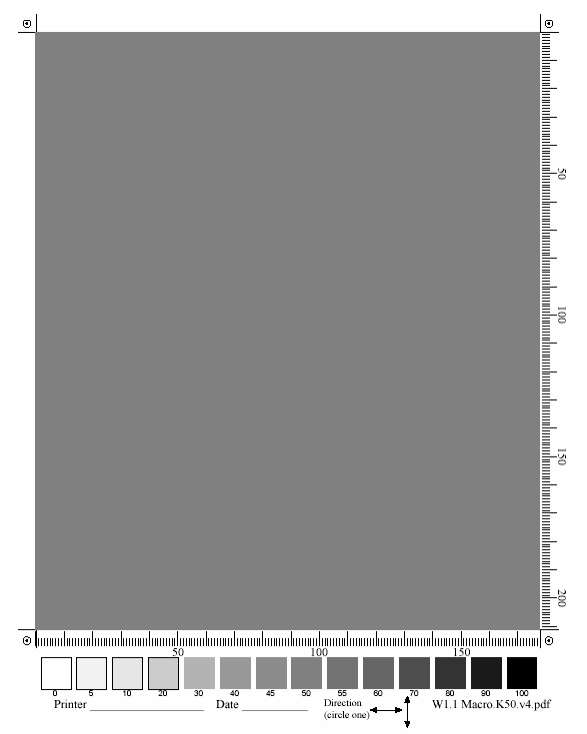

Figure 2.1 The "W1.1.Macro.K50" (version 4) test pattern, reduced to approximately 50% size.

2. With 4 printers and 4 prints, a total of 16 hardcopy patterns will be analyzed. The properties of specific printers are shown below in Appendix A.

3. The target hardcopy images are then mounted on a scanning device, and scanned at the multiple resolutions such as 300, 600, 1200, and 1600dpi to find most effective resolution for printer defects. Appendix B shows the setup properties of the flatbed scanner (Epson 1650). The scanned images are then saved to disk in

uncompressed TIFF format. The region of interest (ROI) for analyzing the artifacts and the Block Averaging Method (BAM) are presented in Figure 2.3.

4. Once scanned and saved to disk, the reproduced test targets are read and analyzed by 2-D NPS estimates.

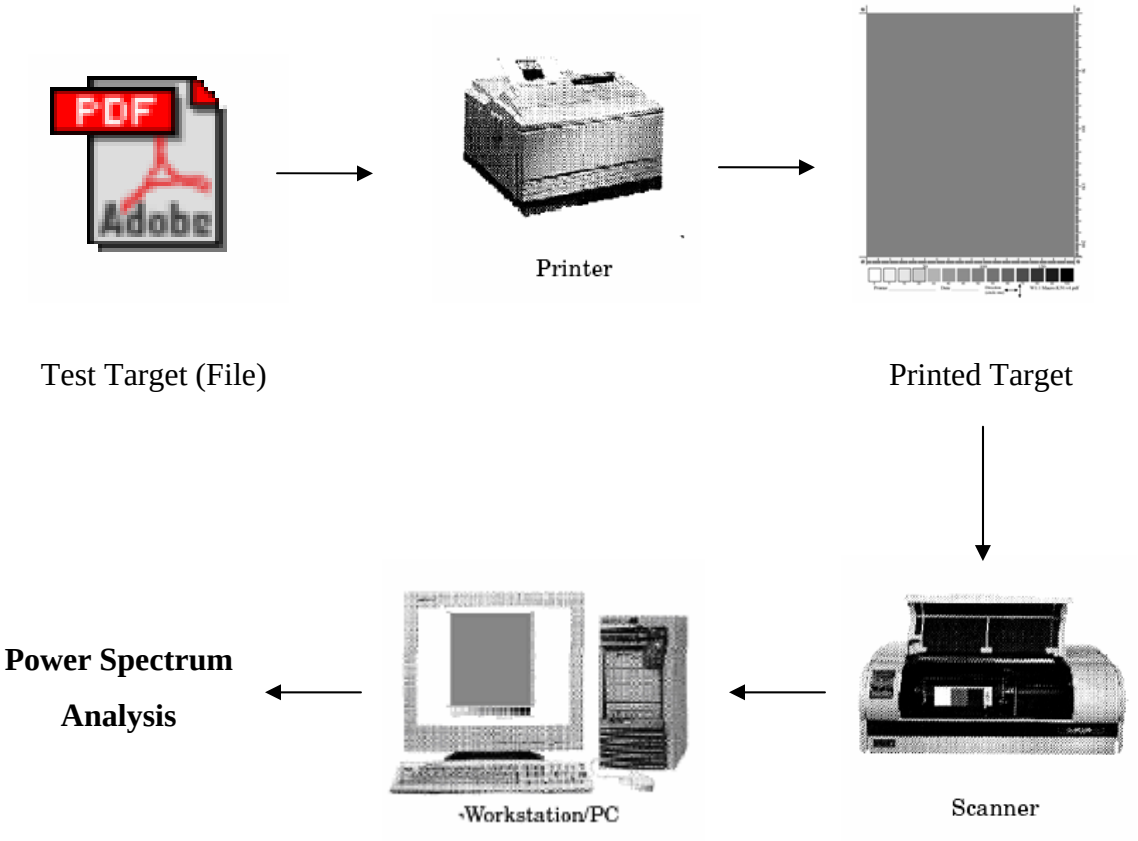

Figure 2.2 Overview of print quality analysis with the Matlab software adapted from [3]

In addition, the drivers, the modes, the substrates and so forth, are kept fixed throughout the procedure. It is very important that all test patterns be printed with the exact same printer setup, and with the same set of materials (inks, toners, substrates). 2-D NPS shows noise spectrum synthesis in frequency domain and its theoretical representation and estimation parameters will be introduced in the next Section.

2.2 Two-Dimensional Noise Power Spectrum

The 2-D NPS or the Wiener spectrum [19-29], which is a function that indicates the power distribution of random signal as a function of spatial frequency, is introduced for analyzing scanned images described in Section 2.1. The noise power spectrum of a stationary signal of the artifact pattern statistics has been applied to the analysis of many imaging systems. The NPS plays a central role in the measure of image quality and provides the means of characterizing image noise.

2.2.1 Theoretical Representation

For two-dimensional isotropic random noise, the NPS of imaging processes is defined for stationary processes in terms of the expected value of the squared magnitude of the Fourier transform of the random signal. Equation (2-1) is the 2-D Discrete Fourier Transform of an analysis window within the ROI of the original image $d(x, y)$. This is denoted by:

$$\hat{D}(u, v) = \sum_{x=1}^{N_x} \sum_{y=1}^{N_y} \Delta d(x, y) e^{-j2\pi(ux\Delta x + vy\Delta y)}, \qquad (2\text{-}1)$$

where $\Delta d(x, y)$ represents the density deviation from the mean of image at position x and y as measured in two dimension with block length N_x and N_y which are the number of data points in x direction per block and y direction per block. Equation (2-2) is the 2-D NPS estimator [21, 25], given by:

$$W(u,v) = \frac{1}{K}\frac{\Delta x \Delta y}{N_x N_y}\sum_{k=1}^{K}\left|\hat{D}(u,v)\right|^2 , \qquad (2\text{-}2)$$

The mean of the image is subtracted out and the remaining variation is assumed to be a wide sense stationary process. K is the number of blocks, and δx and δy are the sampling increments in the x and y directions, respectively. The algorithm of 2-D NPS in this paper used the Block Averaging Method (BAM) for Wiener spectrum estimation as shown in Figure 2.3(b) [27]. The BAM partitions the density data (i.e. scanned flat field images) into analysis window blocks with 50 % overlapping, and the Discrete Fourier Transom of each block is computed by a Matlab program. In addition, all divided blocks were tapered with a hanning window for reduce sidelobes [24, 30]. The expectation of squared-magnitude Discrete Fourier Transforms (DFTs) of the signal blocks was calculated at each frequency to reduce the variance of the estimate.

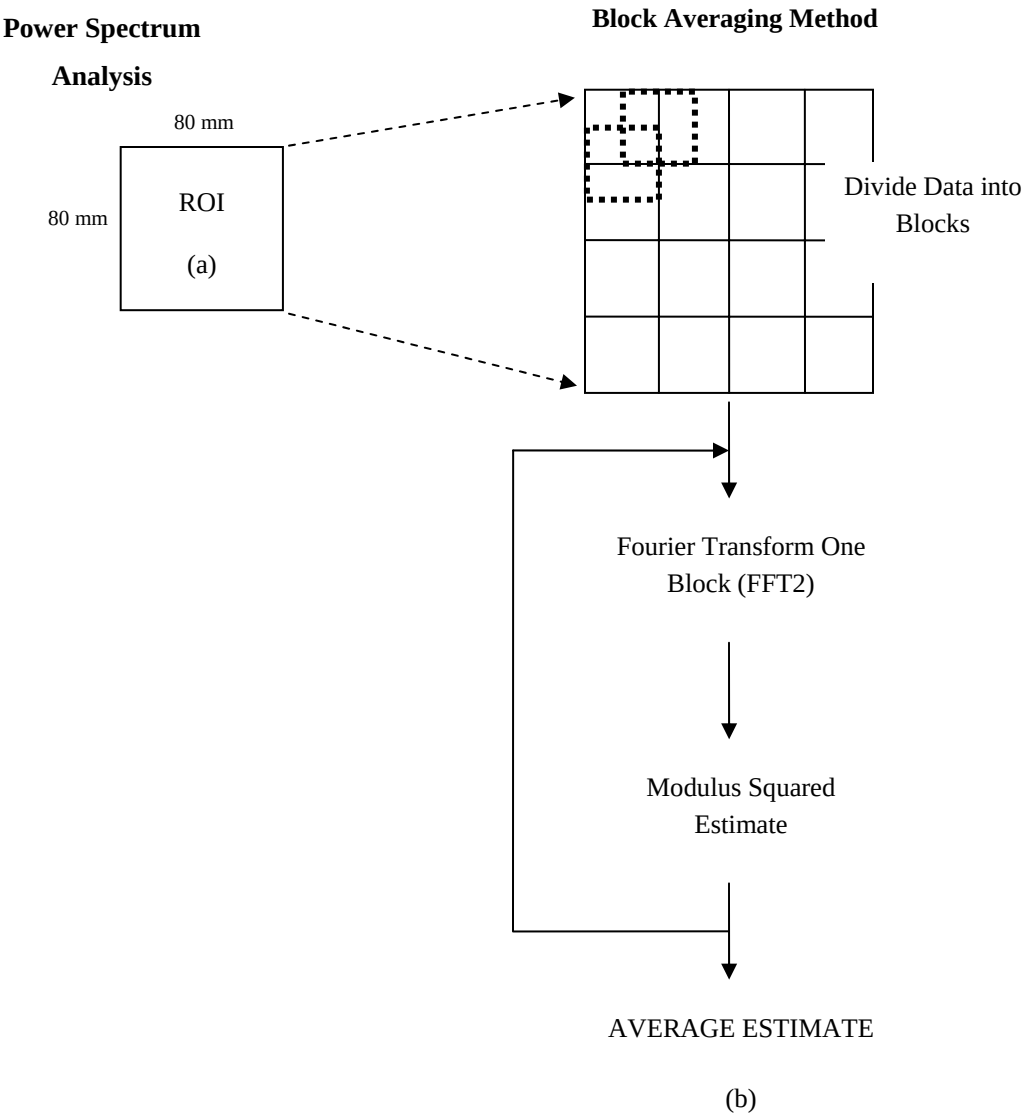

Figure 2.3 (a) Region of Interest (ROI) for analyzing three artifacts is the square area and physical size of the ROI is around 80 * 80 mm (b) The Block Averaging Method (BAM) for Wiener Spectrum Estimation [27] of scanned images and dotted squares show the 50% overlapping.

2.2.2 NPS Estimation Parameters

Sampling Frequency of the scanned images and Block Size of the NPS estimation are critical parameters for proper analysis of the particular printer defect. The effect of the sampling frequency on the NPS will be demonstrated with test pattern of L* levels of 60 by first laser printer. The most effective sampling frequency will be the lowest rate that does not exhibit effects of aliasing. The sampling frequency governs the frequency range of the NPS estimation. For example, if the patterns is scanned at 300dpi, the highest frequency that will not be aliased is the Nyquist frequency and corresponds to 6 cycles/mm. Nyqusit frequencies at 6, 12, 24, and 32 cycles/mm correspond to the sampling frequencies at 300, 600, 1200, and 1600dpi, respectively. Therefore defect patterns with frequency content above these frequencies will be distorted by aliasing.

The method of finding the most effective sampling frequency for analyzing printer defects is determined by comparing the different NPS results. Figure 2.4 presents 2-D NPS of the L* 60 sample from "W1.1.Macro.K50" (version 4) test pattern shown in Figure 2.1. Distinct feature of the NPS in Figure 2.4 is changed by the sampling frequencies. For example, we can see peaks inside ellipses of Figure 2.4(a)-(c) but we cannot see their peaks in Figure 2.4(d) (same corresponding frequency region). For simplicity and easier observation, the horizontal and vertical profiles of 2-D NPS will also be plotted and compared to find aliasing components.

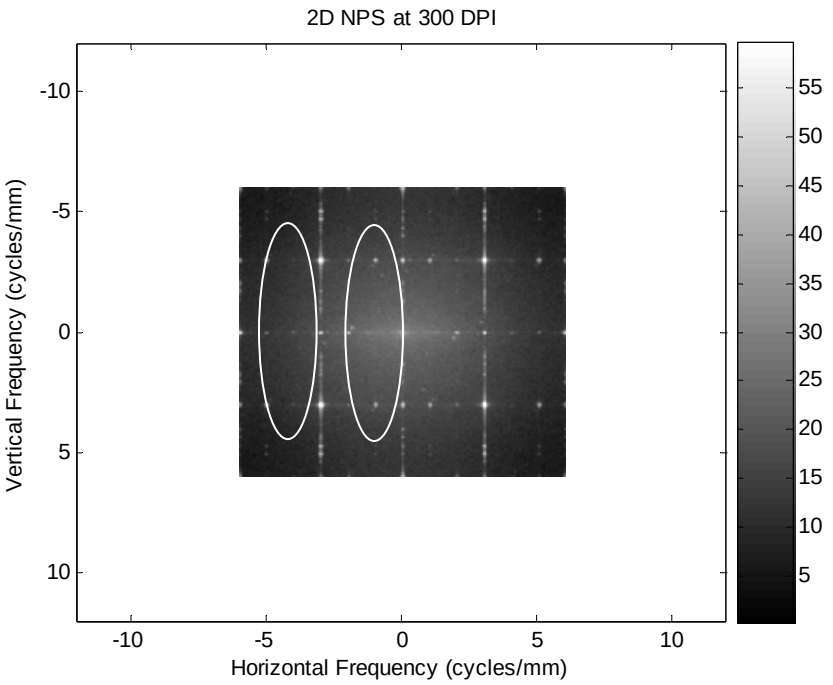
2D NPS at 300 DPI
Vertical Frequency (cycles/mm)
Horizontal Frequency (cycles/mm)
-10
-5
0
5
10
55
50
45
40
35
30
25
20
15
10
5

(a)

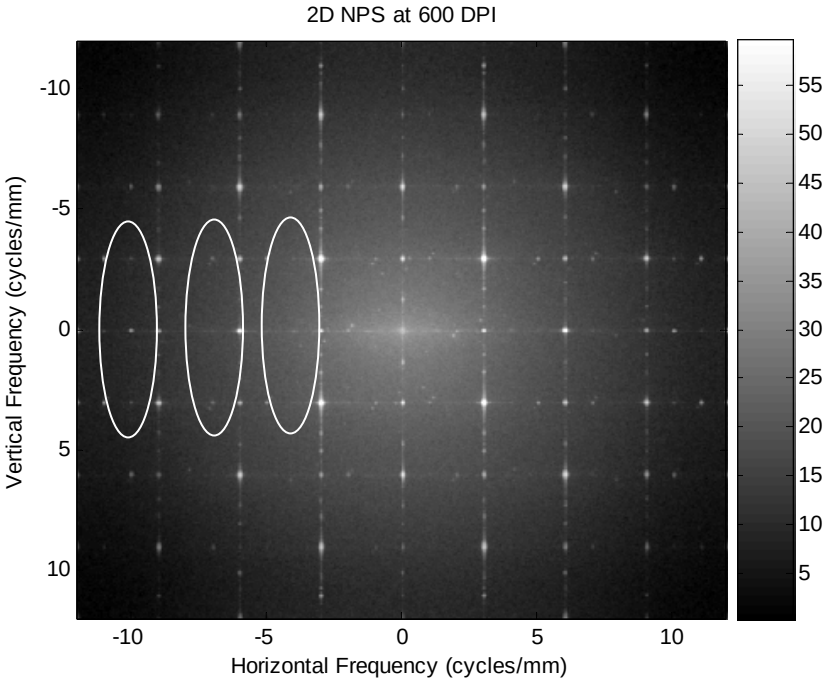
2D NPS at 600 DPI
Vertical Frequency (cycles/mm)
Horizontal Frequency (cycles/mm)
-10
-5
0
5
10
55
50
45
40
35
30
25
20
15
10
5

(b)

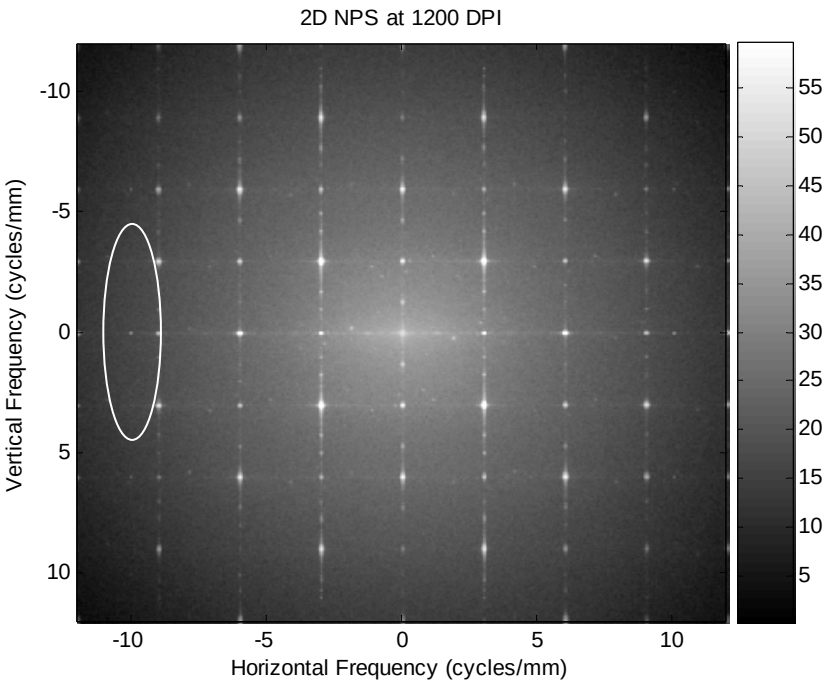

(c)

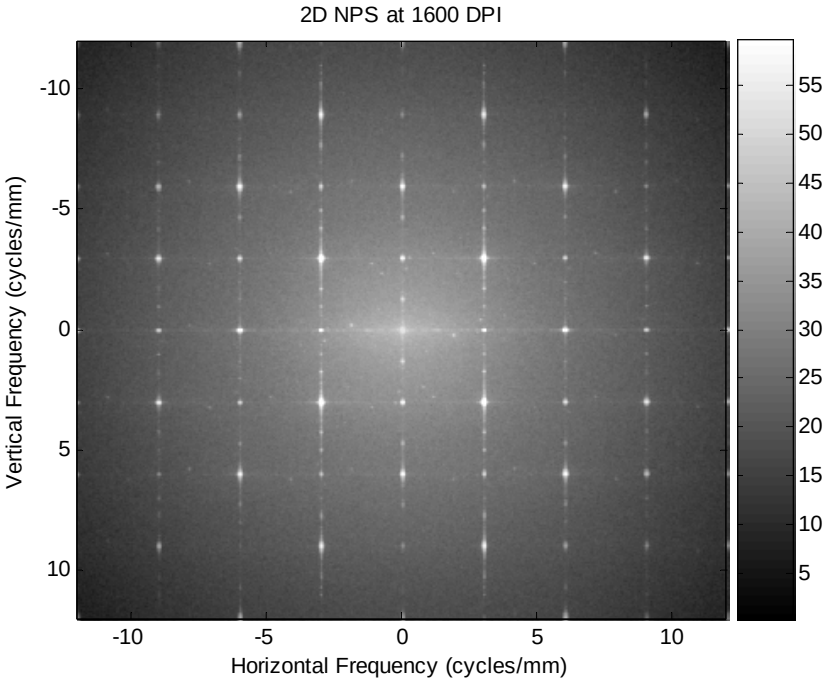

(d)

Figure 2.4 The NPS on -12 to 12 cycles/mm range of Scanned images (ROI) of the test pattern from first laser printer using four sampling frequencies of (a) 300dpi, (b) 600dpi, (c) 1200dpi, and (d) 1600dpi. The physical size of the ROI is around 80 * 80 mm as mentioned in Figure 2.3(a).

The non-aliased features due to the actual printer artifacts are independent of the sampling frequencies using 300, 600, 1200, and 1600dpi. For example, in the horizontal (fast-scan) direction as shown in Figure 2.5 the line components near 3, 6, 9, 12, 15, and 18 cycles/mm are independent of the sampling frequencies. However, the line components of 2, 4, 5, 10, 11 cycles/mm in the horizontal profile, and 2, 4, 5, 8, 10, 11, 16, 19 cycles/mm in the vertical profile change with the sampling frequencies and are therefore assumed to be due to aliasing. So sampling frequencies of 300dpi, 600dpi, and 1200dpi result in the aliasing components in both of horizontal and vertical direction, and the sampling frequency of 1600dpi is most effective for the frequency range of interest. It is reasonable to choose sampling frequency of 1600dpi not only without aliasing but also efficient number of data points for analyzing the artifacts.

Humans cannot perceive frequencies above 10 cycles/mm at a 35 cm viewing distance [17, 46]. Even though a sampling frequency of 1600dpi far exceed that, i.e., Nyquist frequency is a 32 cycles/mm, the higher rate will ensure that higher frequency components of the artifact do not alias back in to the visible range. In addition, the analyzed range will depend on the modulate transfer function (MTF) of considered scanner.

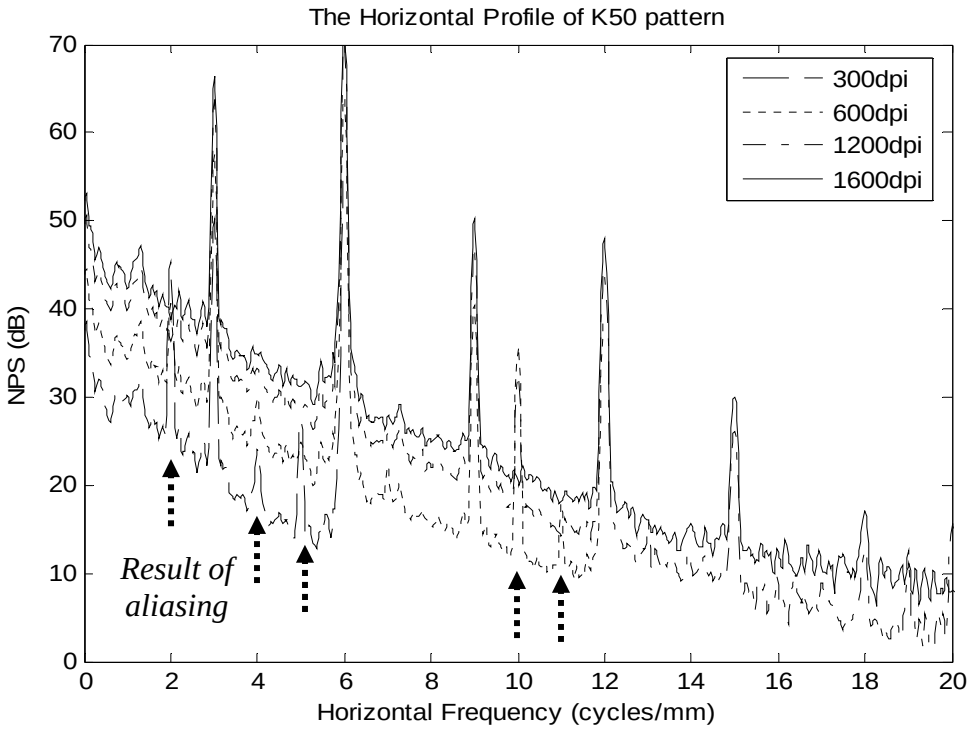

(a)

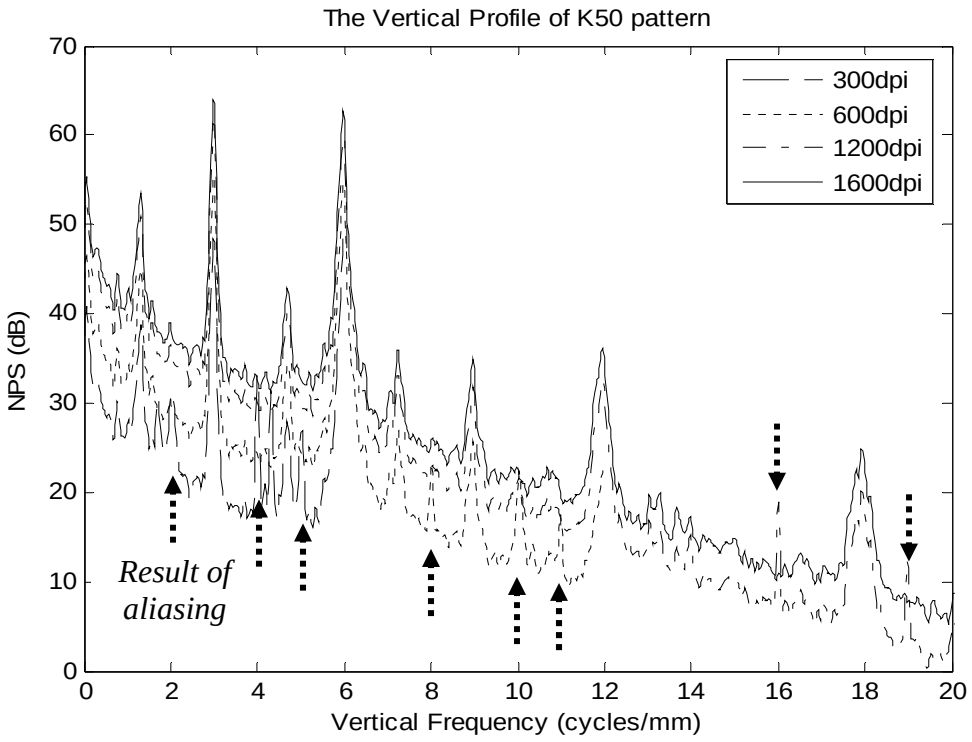

(b)

Figure 2.5 (a) The horizontal (fast-scan) direction and (b) the vertical (slow-scan) direction of 2D NPS in Figure 2.4.

The other estimation parameter of the NPS is the block size. The NPS shown in Figure 2.4 used a 20mm block size, which is one fourth of ROI. The appropriate block size is critical for obtaining the best power spectrum resolution particularly at lower frequencies with sufficient averaging (i.e. smaller block sizes allow for more averages but less frequency resolution). The ROI size is 80mm, and the four different block sizes were chosen, these are 80/2 (40mm), 80/4 (20mm), 80/8 (10mm), and 80/16 (5mm). Defect patterns must be consistently present in the ROI (if it is periodic or quasi-periodic). The block must be large enough to contain full periods of the defect oscillations, while small enough to result in enough averages to reduce noise fluctuation. Therefore, if we choose the large block size, the power spectrum has high resolution and more detail results, at the expense of more noise in the power spectrum estimation.

The selection of optical block size depends on the particular printer defects of interest. The most hard copy images scanned for this experiment had artifacts exhibiting full dynamics within a 20mm window. In addition, the resolution from 5 to 20 improves while the noise power content does not increase significantly. In particular in going from 20 to 40 the resolution does not improves significantly while the noise power content increases significantly. Therefore, the analysis block size of one-fourth the ROI (20mm) was chosen with a 50 % overlapping to reduce noise fluctuation. The noise power spectra for various block sizes are shown in Figure 2.6.

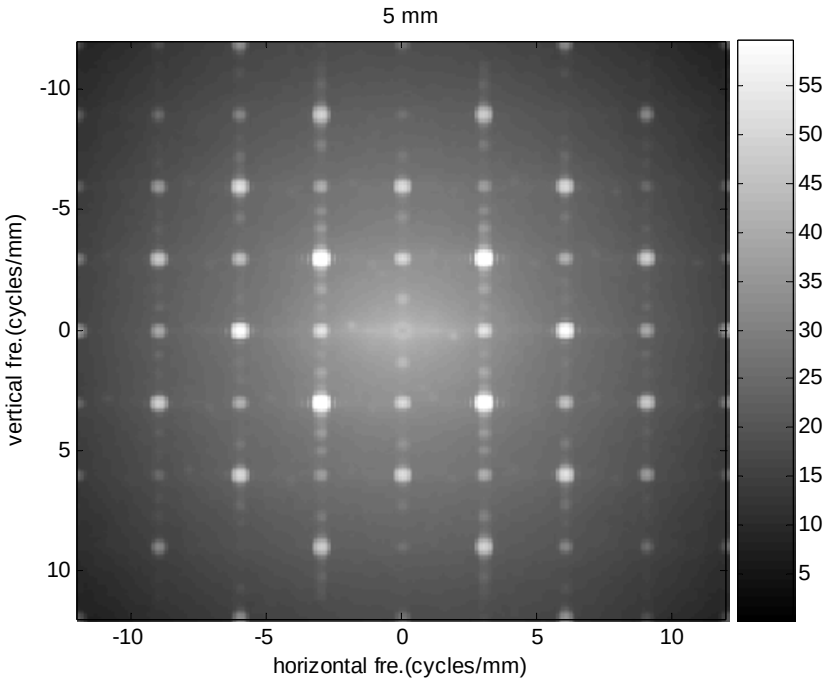
5 mm
vertical fre.(cycles/mm)
horizontal fre.(cycles/mm)
-10
-5
0
5
10
55
50
45
40
35
30
25
20
15
10
5

(a)

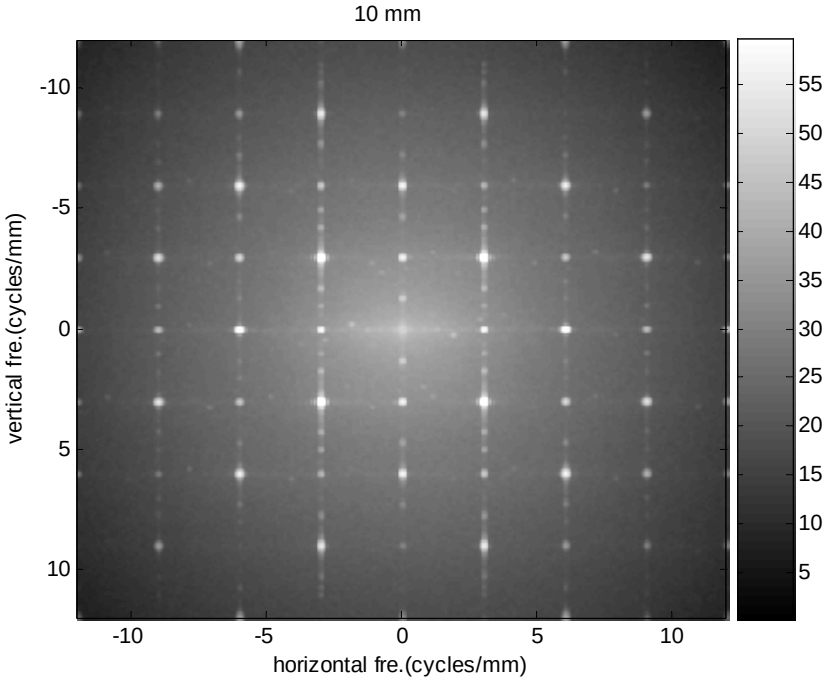
10 mm
vertical fre.(cycles/mm)
horizontal fre.(cycles/mm)
-10
-5
0
5
10
55
50
45
40
35
30
25
20
15
10
5

(b)

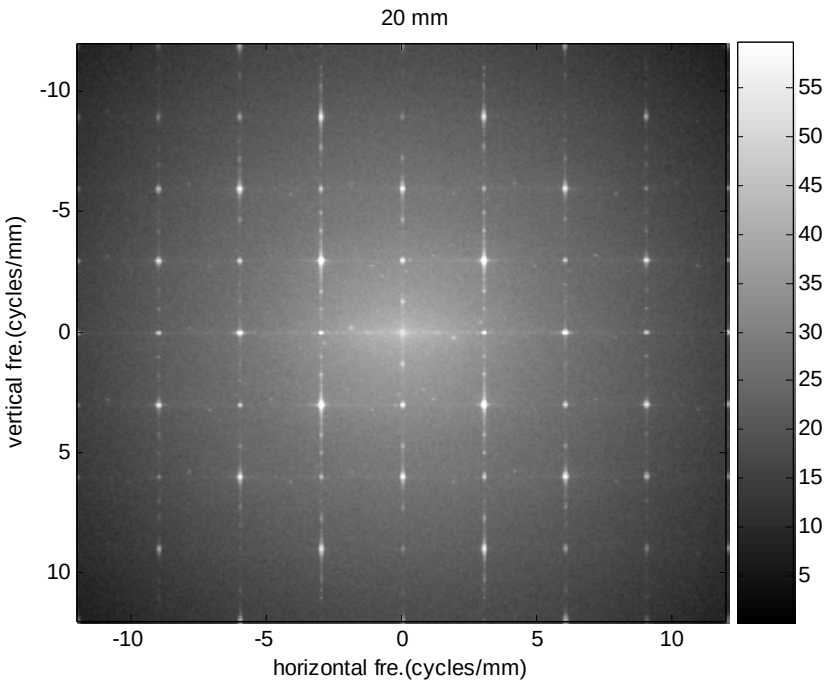

(c)

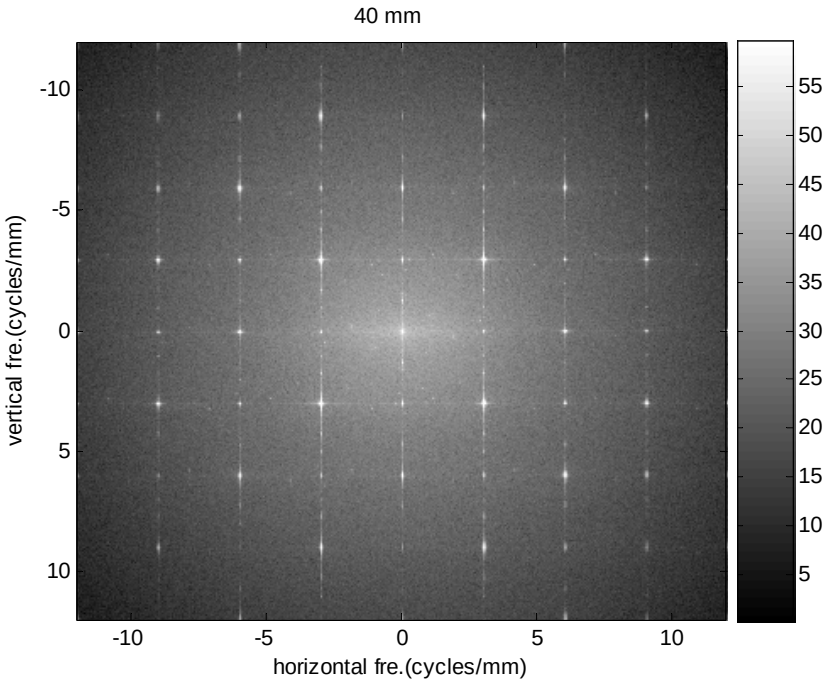

(d)

Figure 2.6 The 2-D NPS of four different analysis block sizes such as (a) 5mm (b) 10mm (c) 20mm (d) 40mm

2.2.3 Modulate Transfer Function (MTF) of the Scanner

Our goal is to get a MTF; however getting a true impulse signal is difficult since we have to crate a dot smaller than the system resolution and strong enough that it exceeds the sensitivity of the system. If we don't know a lot about the system beforehand, this cannot be done practically. So we will obtain a step response and take the derivative of that to get an impulse response. We use a circle because we can effectively get a step signal with any orientation.

For example, we create the small dot on the white paper of 1-inch size and the dot was scanned with 1600dpi resolution using a flatbed scanner. Figure 2.7 shows the steps of getting MTF of the scanner. With a horizontal profile firstly, the profile was differentiated by given in Equation (2-3), and convolved with same profile in shown as Figure 2.7 (c)-(d) because we want to compare MTF with power spectrum.

$$\frac{dU(t)}{dt} = \delta(t) \tag{2-3}$$

The ellipse of Figure 2.7 (d) is the point spread function (PSF) of the horizontal profile as same as Figure 2.7 (e). In addition, the PSF is the output of the image system for an input point source. Finally, we can find the MTF of the scanner by the Fourier transform of the PSF. Furthermore; we did same steps for getting the vertical and diagonal MTF of scanner. The horizontal MTF and all different MTF of scanner are shown in Figure 2.7 (f) and (g), respectively. We can use this to also discuss the spectral shape due to the MTF of the scanner.

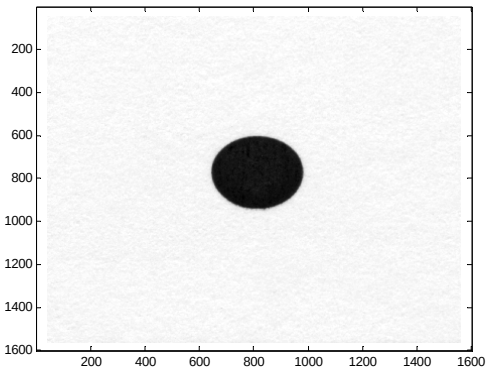
200
400
600
800
1000
1200
1400
1600

(a)

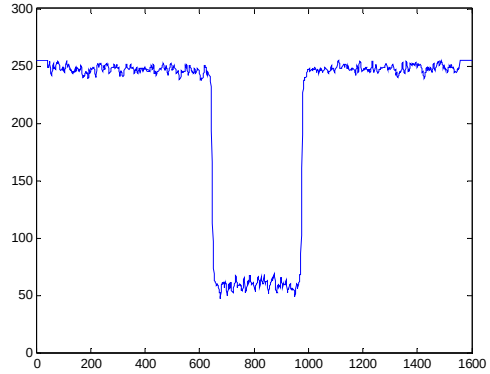
300
250
200
150
100
50
0
0
200
400
600
800
1000
1200
1400
1600

(b)

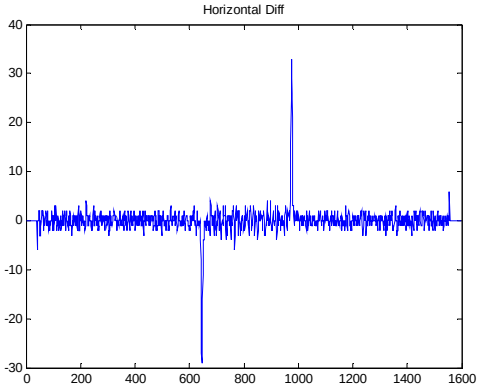
Horizontal Diff
40
30
20
10
0
-10
-20
-30
0
200
400
600
800
1000
1200
1400
1600

(c)

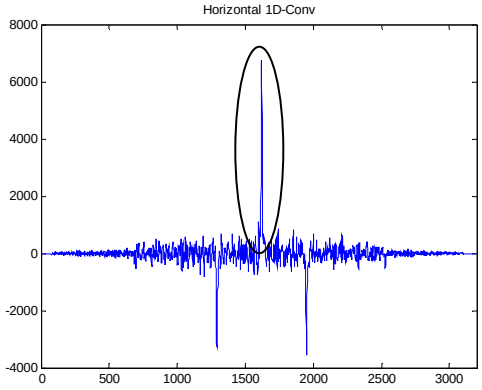
Horizontal 1D-Conv
8000
6000
4000
2000
0
-2000
-4000
0
500
1000
1500
2000
2500
3000

(d)

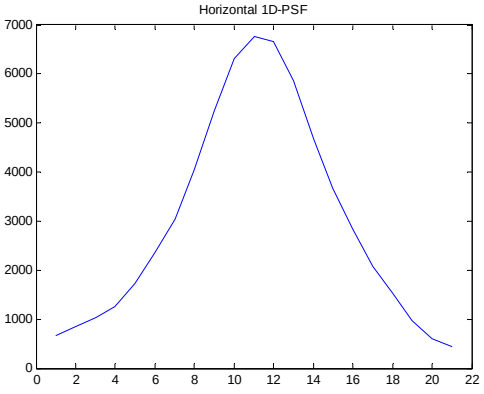
Horizontal 1D-PSF
7000
6000
5000
4000
3000
2000
1000
0
0
2
4
6
8
10
12
14
16
18
20
22

(e)

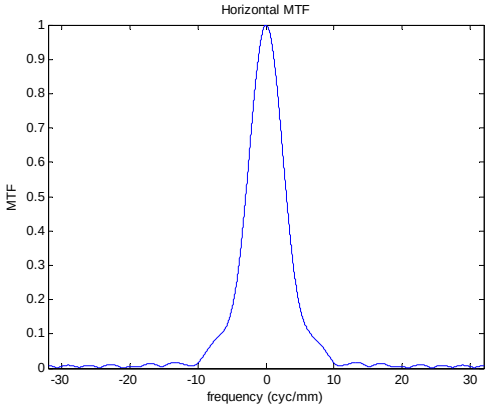
Horizontal MTF
MTF
1
0.9
0.8
0.7
0.6
0.5
0.4
0.3
0.2
0.1
0
-30
-20
-10
0
10
20
30
frequency (cyc/mm)

(f)

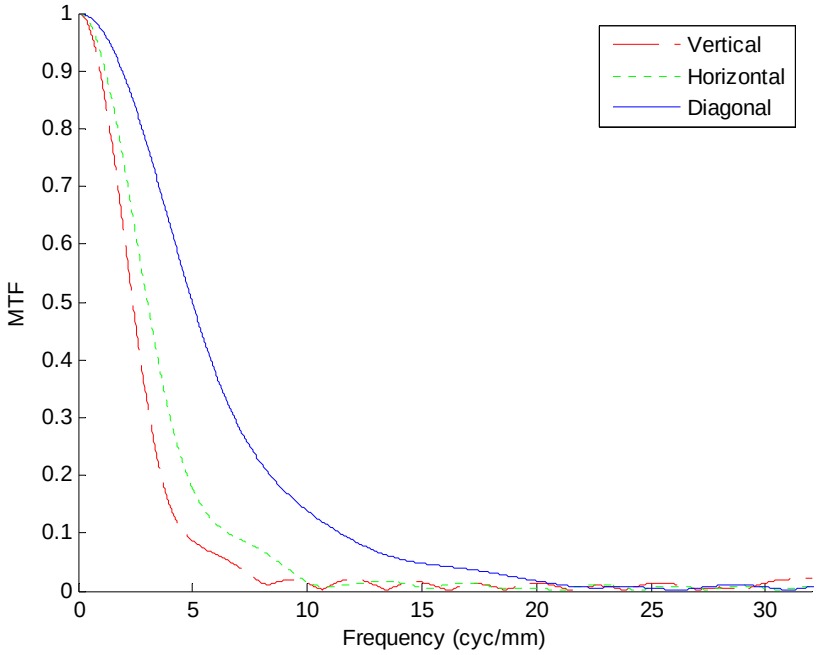

(g)

Figure 2.7 (a) scanned dot of 1 inch size (b) the horizontal profile of the scanned dot at the vertical center point (c) differentiated horizontal profile (d) convolved horizontal profile by the same profile (e) the PSD of the horizontal profile (f) the MTF of the horizontal profile (g) three profile MTF of the scanner

2.3 Modeling of Printer Artifacts

The NPS is an analysis tool for the printer artifacts on the spectral domain. All three types of isotropic noise (graininess), streaking, and banding noise are most obvious in slowly varying areas of an image, especially flat-field image. Each of these types of artifact will be described and generated based on their description in several references [1, 2, 21, 31, 36, 41].

2.3.1 Grain defect Description and Generation

Grain defect or graininess defined at International Standard ISO/IEC document 13660 is perceived two-dimensional, generally random, and aperiodic fluctuations of density at a spatial frequency greater than 0.4 cycles per millimeter in all directions [2]. In addition, graininess artifact, such as that caused by film grain, produces a speckled appearance because the density fluctuations are random in both spatial dimensions [1]. Figure 2.8, adapted from [1, 2] is shown the example of general graininess in space and spectral domain. The origin of Figure 2.8(b) located in the center of the area shown, and this noise is broadband in nature and rotationally symmetric.

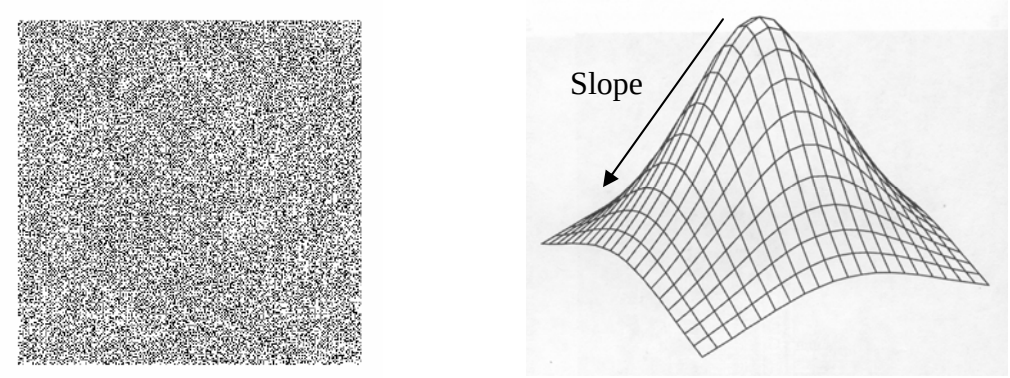

(a) (b)

Figure 2.8 (a) Graininess adapted from [2] in space domain (b) 2-D NPS for graininess noise adapted from [1] in spectral domain

The graininess of a spatial frequency was assumed from 0.4 to a 10 cycles/mm, which is known human visual spectral limit at a 35 cm viewing distance [17, 46]. With a specific spatial frequency from 0.4 to 10 cycles/mm, the graininess will be simulated from its natural characteristic.

Many phenomena can be classified as scale-invariant noise having the general spectral form defined by Equation (2-4) [31-35]. The noise power spectrum *N*, of spatial frequency *f* in cycles per mm will be:

$$N(f) = \frac{1}{f^{\alpha}} \tag{2-4}$$

The value of α is the parameter of grain defect for simulating the defect generated by printer systems and the other words; it is the spectral slope on a log-log scale of graininess. If the slope is steep (large negative α), the variation of graininess in space domain changes slowly, i.e., the grain defect has most low frequency defects. Otherwise, the grain defect has high frequency components. The graininess pattern was simulated by passing white Gaussian noise through a filter with a spectrum, which is given by Equation (2-4). Simulated spectrum with a log-log scale in all directions was used negative slope values, which obtained from the real profiles of 2D NPS.

The same pattern, which is the "W1.1.Macro.K50" (version 4) test pattern as shown in Figure 2.1 used to simulate the graininess, and other test patterns also follow this steps in the next chapter. The pattern was printed by the first laser printer, and scanned by suggested sampling resolution such as 1600dpi. Figure 2.9(a) shows the scanned test pattern of one block size. Furthermore, the 2D NPS of the test pattern produced by the suggested block size in the previous section as shown in Figure 2.9(b). The 2D NPS of the Figure 2.9(b) is same as the Figure 2.6(c). The x- and y-axes of 2-D NPS are spatial frequency in cycles per mm and z-axis is NPS density in dB.

The diagonal profile used to get the slope of graininess because streaking and banding artifacts typically exist only on the horizontal or vertical spectral axes. In this section, we only focus on the diagonal profile. In addition, streaking and banding artifacts are 1D random and periodic noise, respectively, and their description and generation follow in the next sections.

Figure 2.9(c) shows the diagonal deconvolved NPS obtained by dividing of the diagonal MTF and the NPS is a function of frequency on a log-log scale. The fitted line generated between 0.4 and 10 cyc/mm. Furthermore, the general frequency pattern in this plot is a line with a negative slope, implying that the NPS is inversely proportional to the frequency.

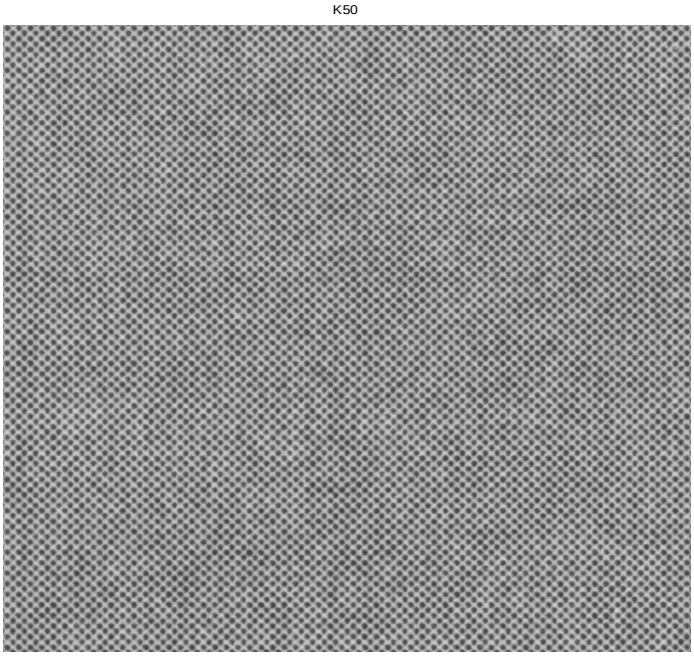

(a)

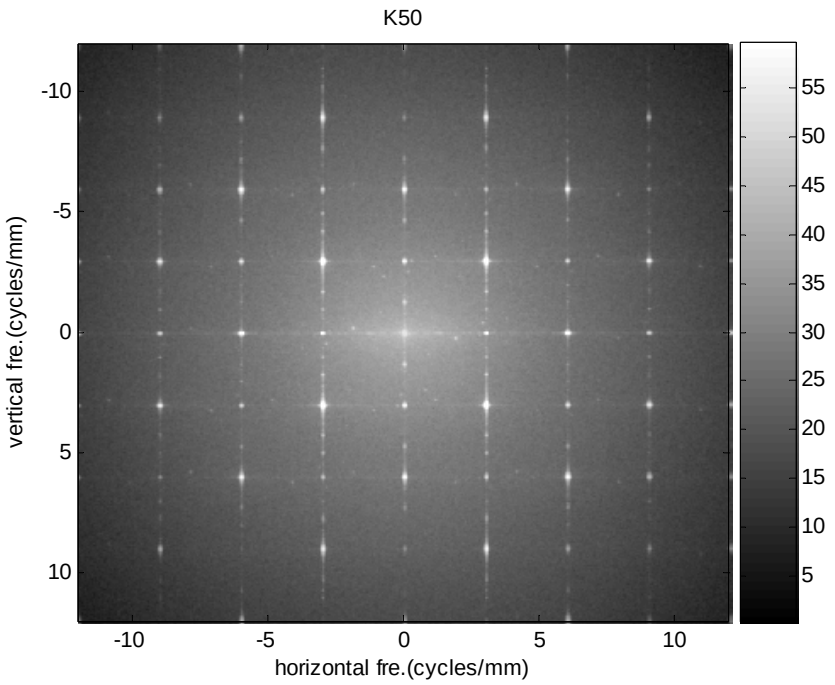

(b)

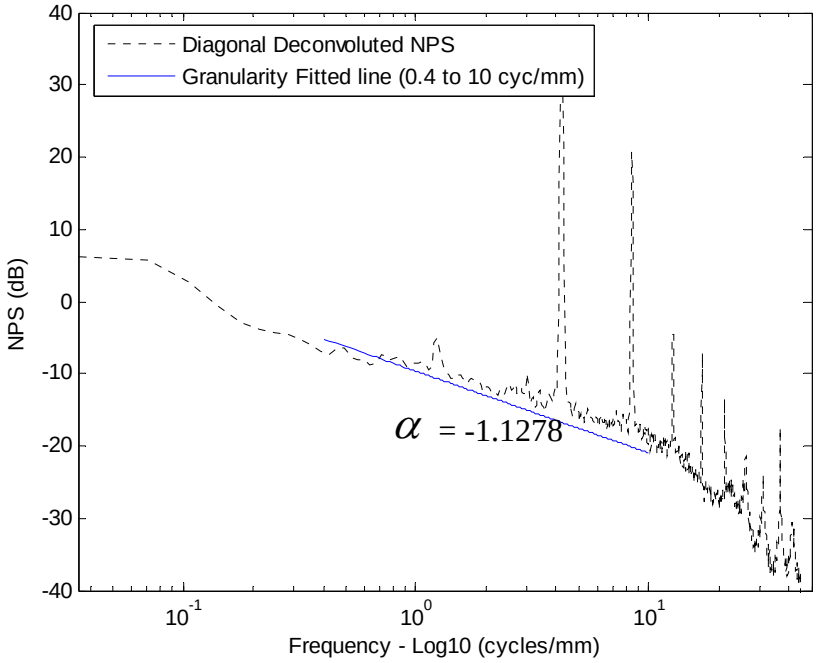

(c)

Figure 2.9 (a) Scanned K50 test pattern (b) 2-D NPS of the "W1.1.Macro.K50" by first laser printer using suggested NPS estimation parameters (c) the fitted line between 0.4 and 10 cyc/mm.

We found the slope of graininess (α), and the value will be the parameter of simulated graininess. As we mentioned before, the graininess pattern was simulated by passing white Gaussian noise through a filter with slope parameter of -1.1278 (circularly symmetric over all orientations). The graininess was simulated with same analysis block size because we can only analyze the defects in the analysis block size, and four different amplitudes as shown in Figure 2.10(a). 2D NPS of simulated graininess and the diagonal profile represent in the Figure 2.10(b) and (c). In addition, we can check the slope of graininess in the diagonal profile. It will be identified to simulate graininess artifact of other test patterns in the next chapters. Appropriate amplitude will also be adopted to find the better model.

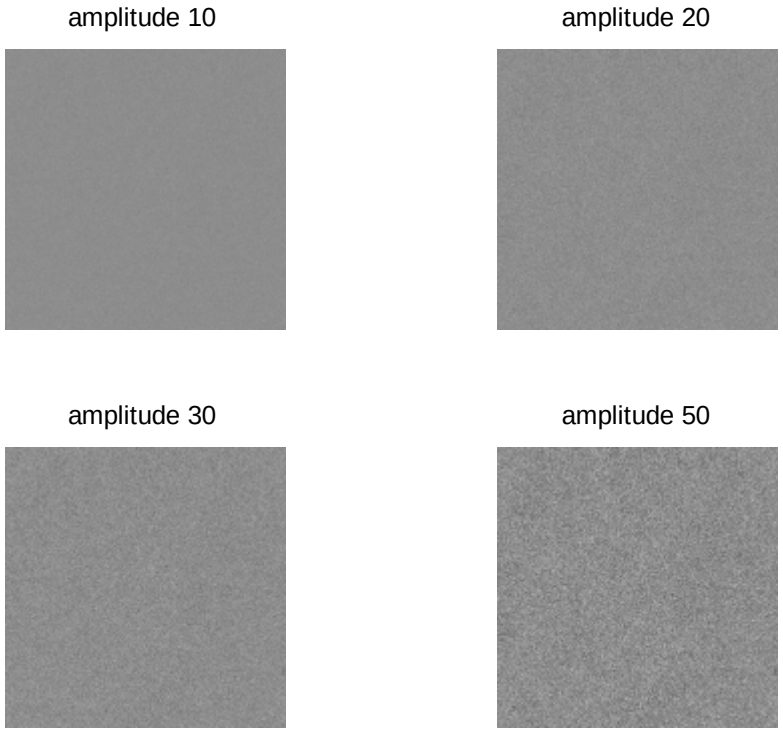

(a)

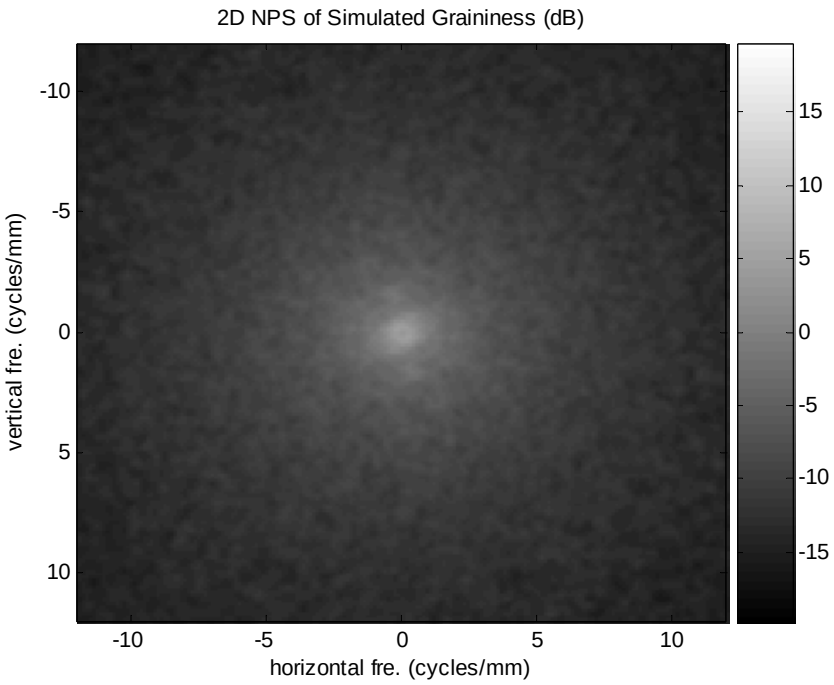

(b)

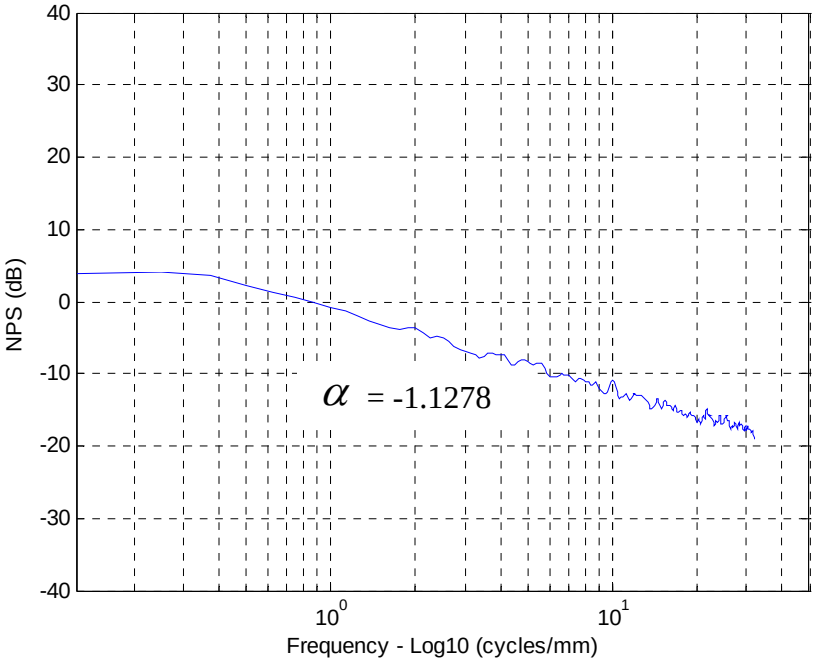

(c)

Figure 2.10 (a) Simulated graininess with four different amplitudes (b) 2D NPS of simulated graininess (c) the diagonal profile of simulated graininess

2.3.2 Streaking defect Description and Generation

Streaking defect can be characterized by a 1/f noise frequency spectrum similar to grain defect, except without circular symmetry. The isotropic noise (graininess) is random with equal variance in both spatial frequency directions as shown in Figure 2.8(b), but streaking is a random noise in one direction but deterministic (or less random, tighter variance) in the other. It is illustrated in Figure 2.11 [1, 36].

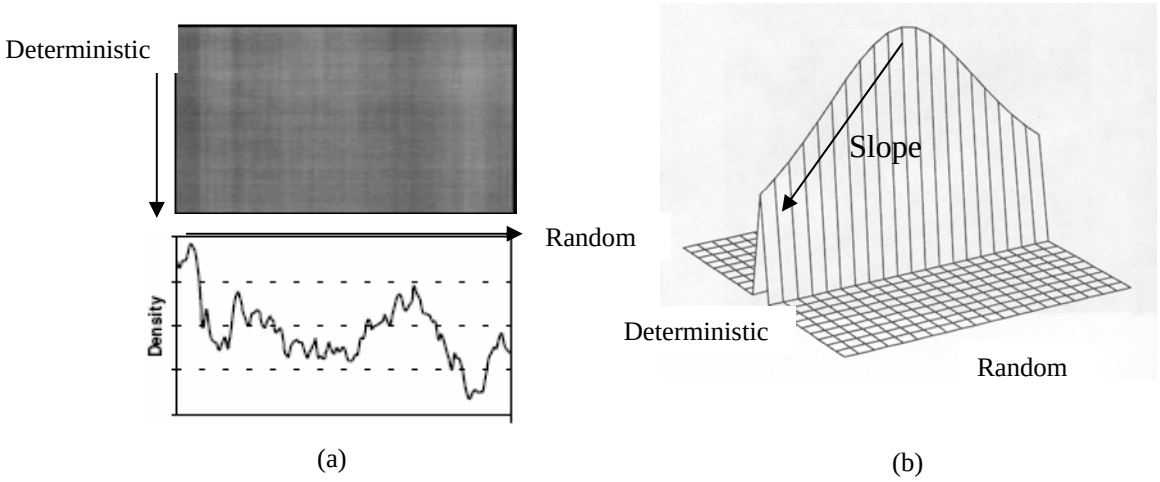

Figure 2.11 Streaking defect a) adapted from [36] in space domain (top) and horizontal profile (bottom) (b) 2-D NPS for streaking noise adapted from [1] in spectral domain.

The streaking defect is anisotropic and primarily exists only on the horizontal and/or vertical axis, for example, Figure 2.11(a) shows that the density varies in the horizontal direction randomly and in the vertical direction constantly. This is called vertical streaking. In addition, the trend of the spectrum for random streaking is roughly linear only on the horizontal and/or vertical axis [37]. Though the spectral range of the linear pattern is not known, we assume the range of linear trend at the horizontal and vertical profiles. In this specific example, we chose the range of streaking between 0.4 and 2 cycles/mm as shown in Figure 2.12. The comparison of the horizontal or vertical profile with the diagonal profile indicates how much streaking exists. Figure 2.12 shows

horizontal and vertical profile with streaking fitted line and granularity fitted line. The granularity fitted line is same as the Figure 2.9(c). Each horizontal and vertical profile has more energy than diagonal profile, indicating the presence of a streaking component in the artifacts. With the values of α_{HS} and α_{VS}, random streaking was simulated with four different amplitudes and presented in the Figure 2.13. In addition, the slope of vertical profile (α_{VS} = -0.9771) is steeper than the slope of horizontal profile (α_{HS} = -0.5173). Therefore, vertical streaking changes more slowly (thicker streaks) along the horizontal direction as shown in Figure 2.13(b). In next chapter, other random streaking from different densities and different printer technologies will be simulated with their own trend.

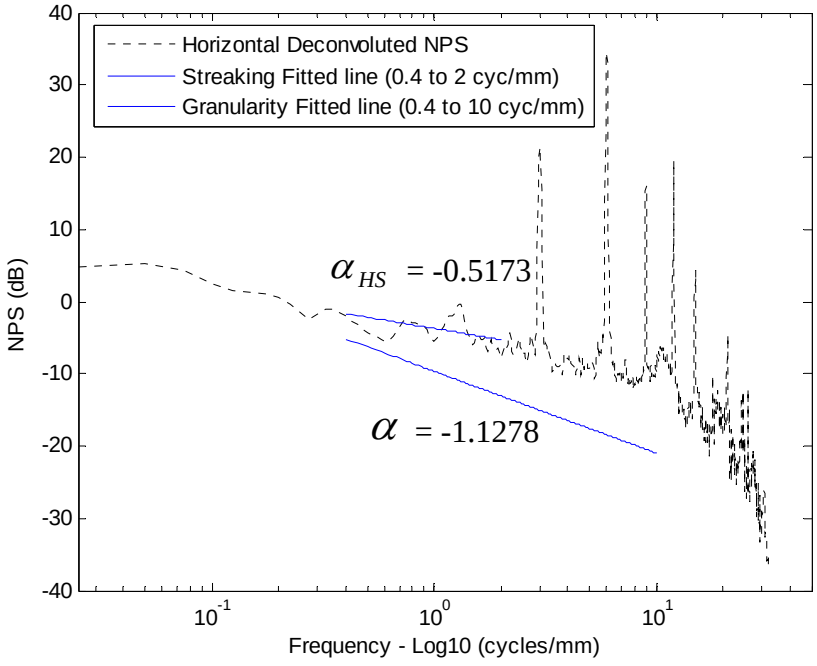

(a)

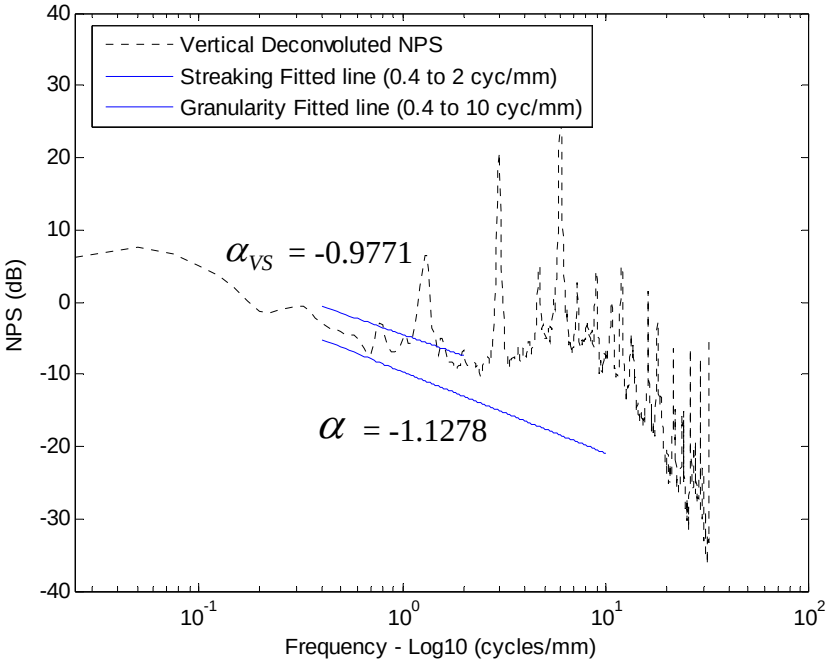

(b)

Figure 2.12 (a) Horizontal deconvolved NPS, horizontal fitted line, and granularity fitted line (b) Vertical deconvolved NPS, vertical fitted line, and granularity fitted line

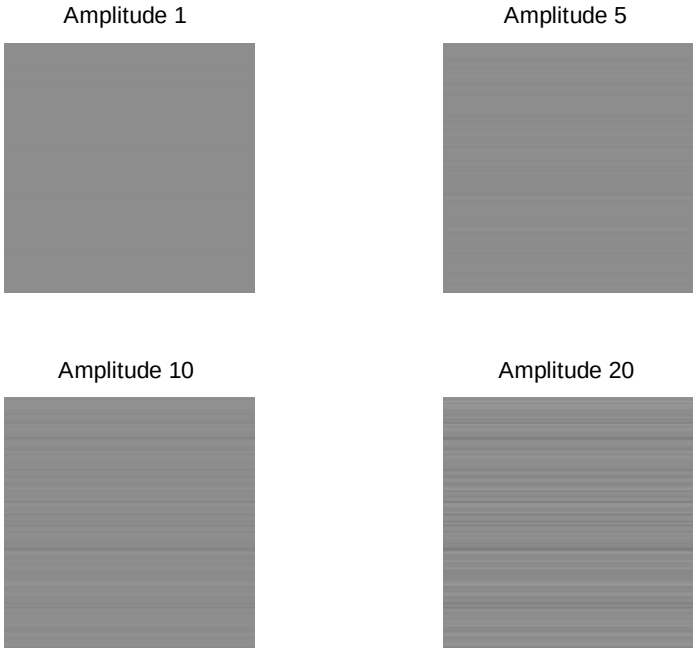

(a)

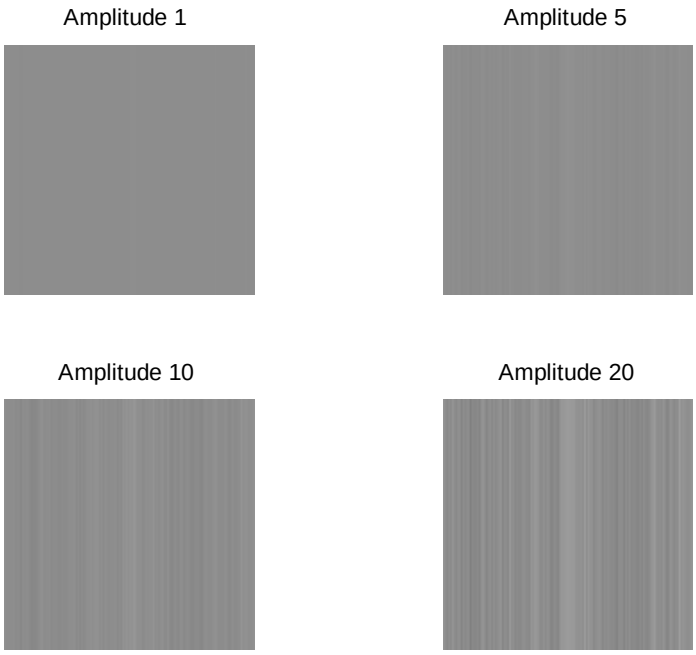

(b)

Figure 2.13 (a) Simulated horizontal streaking using α_{HS} = -0.5173 with four different amplitudes (b) Simulated vertical streaking using α_{VS} = -0.9771 with four different amplitudes

2.3.3 Banding defect Description and Generation

Banding is often the most objectionable type of noise. It is characterized by periodicity in one direction and constant in the other direction. Its NPS exists only at the frequency of the periodic variation, and Figure 2.14 shows the only one type of banding in the x direction in assumed as $b_x(x)$ [1, 21, 36, 41-45].

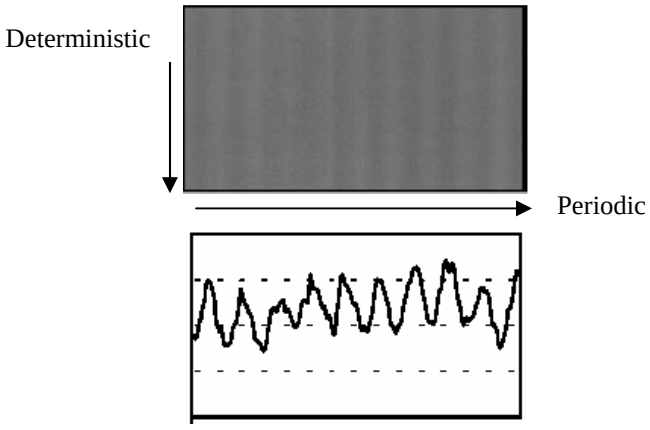

Fig. 2.14: a) Banding adapted from [36] in space domain (top) and horizontal profile (bottom)

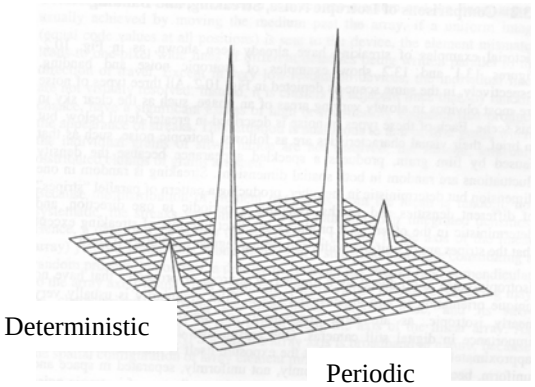

Fig. 2.14: b) Two-dimensional NPS for isotropic noise adapted from [1] in spectral domain

Figure 2.14 Banding defect adapted from [1, 36]

Similarly, $b_y(y)$ is a one-dimensional zero mean periodic function representing the banding in the y direction. The following model assumed to be characterized as the banding [21]:

$$b_x(x) = \sum_i a_i \cos(2\pi v_i x + \phi_i)$$
$$b_y(y) = \sum_j a_j \cos(2\pi v_j y + \phi_j) \qquad (2\text{-}5)$$

where a_i, v_i, and ϕ_i are the amplitude, spatial frequency and phase of the i^{th} component in the x direction, and a_j, v_j, and ϕ_j are the amplitude, spatial frequency and phase of

the j^{th} component in the y direction, respectively. In addition, considering the Fourier transform of Equation (2-5) with ignoring the phase angles ϕ_i and ϕ_j:

$$B_x(v_x) = \left(\frac{1}{2}\right)\sum_i a_i\left[\delta(v_x + v_i)\delta(v_y) + \delta(v_x - v_i)\delta(v_y)\right]$$
$$B_y(v_y) = \left(\frac{1}{2}\right)\sum_j a_j\left[\delta(v_y + v_j)\delta(v_x) + \delta(v_y - v_j)\delta(v_x)\right] \quad (2\text{-}6)$$

The one-dimensional periodic components such as horizontal banding, $b_y(y)$ and vertical banding, $b_x(x)$ generate a series of delta function along the x and y direction as shown in the Equation (2-6). Therefore, the banding is observed along these axes and the two-dimensional NPS of a banding defect has power along the axis of periodic variation at a fundamental frequency and its harmonics (2x the fundamental frequency, 3x the fundamental frequency, etc), as shown in Figure 2.14(b). In Figure 2.15, we can find the fundamental frequency of real noise spectrum in the x and y direction, that is around 1.3 cycles/mm. In addition, the periodic peaks such as 3, 6, 9, 12, 15, and 18 cycles/mm is not the banding defect but halftone screen frequencies as mention in previous section. Figure 2.15(a) represents horizontal and vertical deconvolved NPS using the NPS and frequency of log – log scale and Figure 2.15(b) is the same profile except log – linear scale and the range of frequency. Vertical banding has more energy than horizontal banding, and the vertical banding is clearly visible on the hardcopy image. Halftone frequencies have a lot of energy and especially horizontal halftone frequencies have more energy than vertical halftone because horizontal halftoning is not relative to the banding defect and vertical halftoning does. In other word, we can see the multiplicative components between the banding defect at 1.3 cycles/mm and halftoning at 6 and 12

cycles/mm along with vertical profile. Though a halftoning is beyond concept of this paper, but we can consider with banding defects. Simply, this specific laser printer have multiplicative component between halftoning and banding defects. We can also simulate any banding defect if we find the fundamental frequencies from NPS and their harmonic energy distribution.

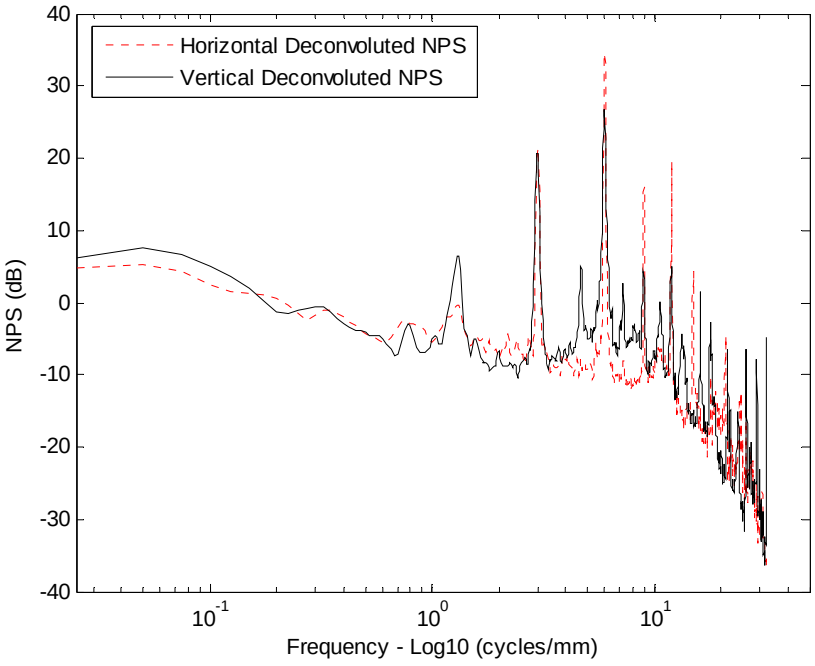

(a)

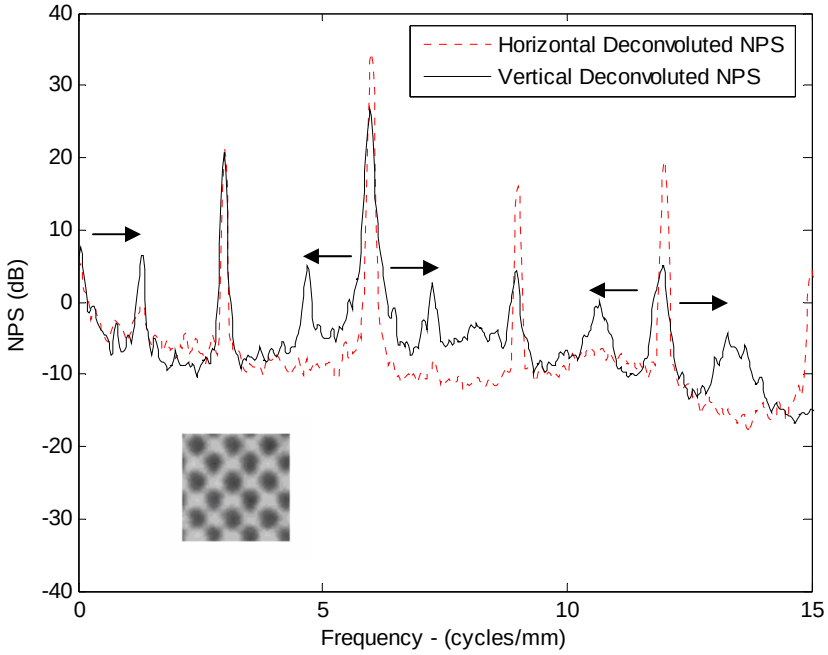

(b)

Figure 2.15 (a) Horizontal and vertical deconvolved NPS using the NPS and frequency of log – log scale (b) Same profile as (a) using log – Linear scale. The image at left-bottom corner is real scanned image with 1mm*1mm block size.

However, NPS only analyze the analysis block that is smaller than our ROI. For simulating banding defect, we better choose the Spectral Autocorrelation Function (SAF) than NPS. Figure 2.16 shows the procedures for simulating the banding artifact by SAF. First, the 1D profile is made from 2D scanned image by average. We can average horizontal or vertical direction for horizontal banding or vertical banding, respectively. Second, 1D vertical profile, i.e. $\tilde{I}_m(y)$, taken the discrete Fourier transform (DFT) such as $\hat{IM}(f)$ and we take just the positive half of $\hat{IM}(f)$ for $f > 0$ and $f < \frac{f_s}{2}$. The Equation (2-7) shows the SAF.

$$\hat{H}(f) = \hat{IM}(f), \qquad 0 < f < \frac{f_s}{2}$$

$$SAF(\Delta) = \sum_f \hat{H}(f)\hat{H}(f-\Delta)^*, \qquad 0 < \Delta < L \tag{2-7}$$

Note for a stationary random process $SAF(0)$ is equivalent to the Power Spectral Density (PSD), which is the average power of the stationary random process, expressed as a function of frequency. In addition, we can find the fundamental frequency and its harmonics until fourth harmonics along to the SAF profile as shown in Figure 2.16(f). The filtered profile was taken Inverse Fourier transform to get 1D banding profile. Finally, Figure 2.16(i) shows the 2D simulated banding artifacts with four different amplitudes and adds to mean value of real scanned image. The simulated image size is the same as the analysis block size, which is one of fourth of ROI.

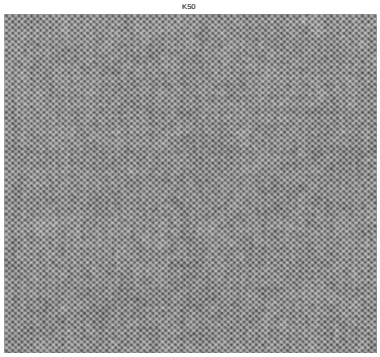

(a)

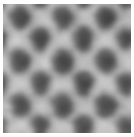

(b)

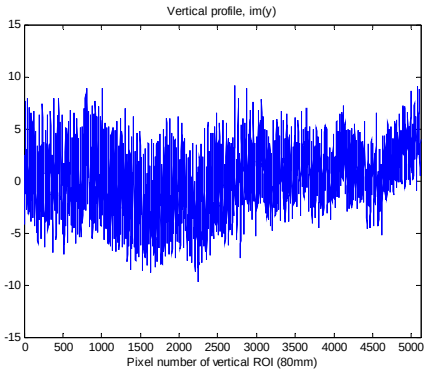
Vertical profile, im(y)
Pixel number of vertical ROI (80mm)

(c)

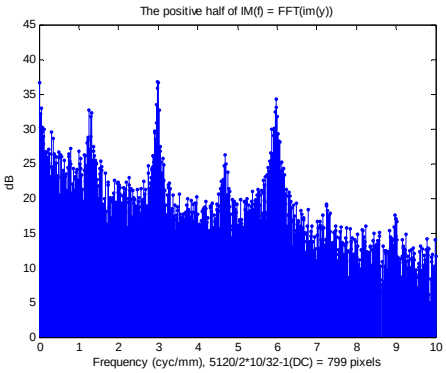
The positive half of IM(f) = FFT(im(y))
dB
Frequency (cyc/mm), 5120/2*10/32-1(DC) = 799 pixels

(d)

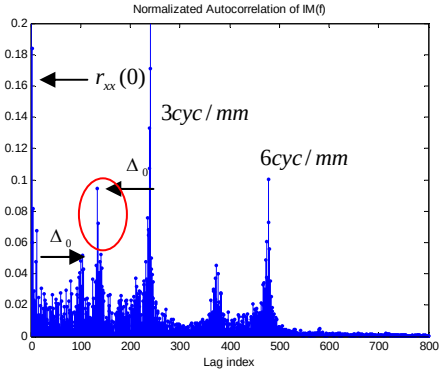
Normalizated Autocorrelation of IM(f)
$r_{xx}(0)$
3cyc / mm
6cyc / mm
Δ_0
Δ_0
Lag index

(e)

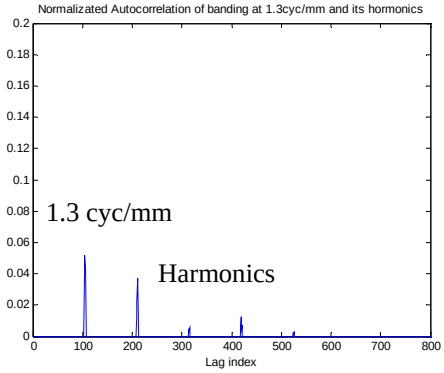
Normalizated Autocorrelation of banding at 1.3cyc/mm and its hormonics
1.3 cyc/mm
Harmonics
Lag index

(f)

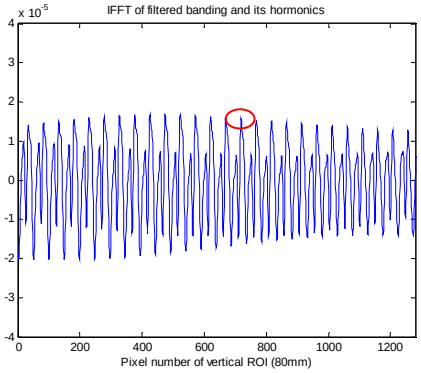
IFFT of filtered banding and its hormonics
x 10^-5
Pixel number of vertical ROI (80mm)

(g)

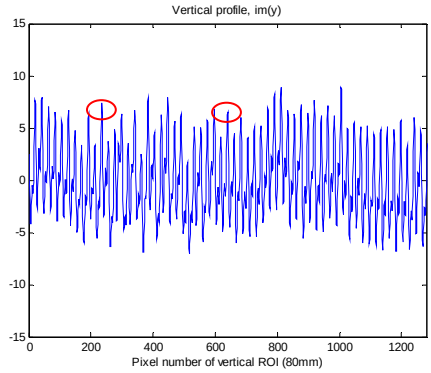
Vertical profile, im(y)
Pixel number of vertical ROI (80mm)

(h)

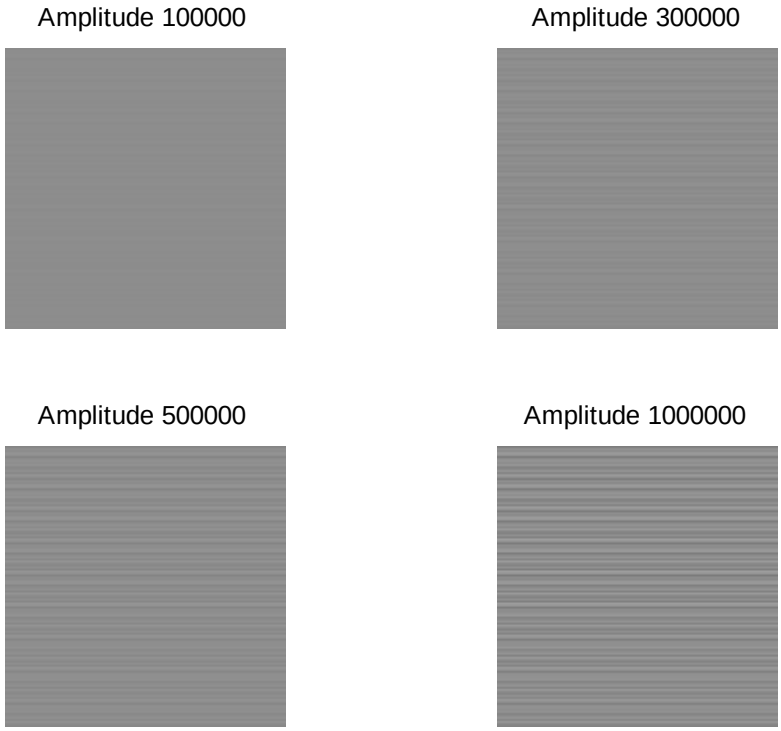

(i)

Figure 2.16 The procedures for simulating the banding artifacts

(a) Scanned K50 pattern (b) 1mm size of scanned K50 pattern (c) Averaged vertical profile (d) 1D discrete Fourier transform (DFT) of averaged vertical profile (e) Normalized Autocorrelation of 1D DFT (f) Filtered Autocorrelation at 1.3 cyc/mm and harmonics (g) IFFT of banding at 1.3 cyc/mm and harmonics (h) Same profiles as (c) except the range to compare with (g); (i) Simulated vertical banding with four different amplitudes

CHAPTER 3

Comparison of Additive Model and Multiplicative Model

The primary goal of this thesis is to find the relationship of the interactions between real printer defects such as graininess, streaking, and banding. The suggested models are the additive and multiplicative interaction. The NPS of real printer flat field output will be the potential characterization tool of our analysis and ultimately compared to interaction of the simulated printer defects, where the model for the interaction is known. In other words, the interaction of each defect will be compared with real NPS for reference to find which model is more appropriate than the other. The measurement technique and the quantities involved in the measurement formulas will be explained in depth in the Chapter 3. Section 3.1 discusses the additive model and multiplicative model of printer defects. Section 3.2 indicates the parameter values of graininess and streaking for simulating these defects as well as the real NPS of four different density patterns from four different printers.

3.1 Additive Model and Multiplicative Model

The simplest assumption is that two-dimensional random noise (graininess), streaking, and banding components are additively superimposed [21]. Equation (3-1) is the simplest assumption of additive model, given by:

$$d(x,y) = \overline{d} + g_{2D}(x,y) + s_x(x) + s_y(y) + b_x(x) + b_y(y), \qquad (3\text{-}1)$$

where $d(x,y)$ represents a two-dimensional data trace across a flat field, $g_{2D}(x,y)$ is a two-dimensional zero mean stationary random process representing the image

granularity, $s_x(x)$ and $s_y(y)$ are one-dimensional zero mean stationary random processes representing the streaking in the x and y direction, respectively, and $b_x(x)$ and $b_y(y)$ are one-dimensional zero mean periodic functions representing the banding in the x and y directions, respectively.

Second assumption is whether the multiplicative component of each printer defect exists on the real NPS. Equation (3-2) is the simplest assumption of multiplicative model of graininess, streaking, and banding given by:

$$\begin{aligned} d(x,y) &= (\overline{d_1} + G_{2D}) * (\overline{d_2} + S) * (\overline{d_3} + B) \\ &= \overline{d_1}\overline{d_2}\overline{d_3} + \overline{d_2}\overline{d_3}G_{2D} + \overline{d_1}\overline{d_3}S + \overline{d_1}\overline{d_2}B \\ &+ \overline{d_3}G_{2D} * S + \overline{d_2}G_{2D} * B + \overline{d_1}S * B + G_{2D} * S * B \end{aligned} \tag{3-2}$$

This multiplicative equation also has an additive equation and the multiplicative values of three artifacts. Therefore, if we find the multiplicative values in the real PSD, we can conclude the multiplicative model is more realistic to the real data. Otherwise, an additive model is more realistic to the real data. For simplicity, we analyzed two defects of graininess, streaking, and banding to find their interaction. For examples, we analyzed the graininess and streaking, graininess and banding, and banding and streaking.

Before we apply for the additive model and multiplicative model by given in Equations, following section discusses the parameter values of graininess and streaking and the real NPS of four different printers. In addition, with 4 printers (2 Laser printers and 2 Inkjet printers) and 4 prints (K20, K50, K80, and K100), a total of 16 hardcopy patterns will be analyzed as mention in Chapter 2.

3.2 Analysis for Digital Printers

This section focuses on the NPS of actual flat-field prints from digital printers that are two laser printers and two inkjet printers. Like the same method to simulate three printer defects in section 2.3, we will find the parameter values of grain defects from diagonal spectral axis of all real noise power spectra. All streaking defects will be simulated by the parameters from the horizontal and/or vertical axis. In addition, banding defects can be simulated by the fundamental frequencies and their harmonic distribution though we did not mention in this section.

3.2.1 Analysis for First Laser Printer

Three printer defects in four different density patterns, i.e., K20, K50, K80, and K100, from first laser printer can be simulated if we find their parameter values that are mentioned in the modeling of printer artifacts. Figure 3.1 shows the 2D NPS of four patterns from first laser printer and each NPS will be compared to simulated NPS by additive and multiplicative interaction in next chapter. Intuitively, the NPS of these actual flat-field prints have graininess, a little vertical streaking, one horizontal banding at 1.3 cycles/mm, and dominant halftone components. The energy of horizontal or vertical streaking on the NPS of K20 test pattern is almost zero. In other words, there does not exist streaking defect on this test pattern. Therefore, we do not need to analyze the relationship between streaking and graininess or between streaking and banding with K20 test pattern.

We can see the graininess, vertical streaking, and horizontal banding defect on the K50, K80, and K100 flat-field prints. Figure 3.2, 3.3, 3.4, and 3.5 represent three profiles of K20, K50, K80, and K100, respectively. The difference of left and right in Figure 3.2,

3.3, 3.4, and 3.5 is the range of the graininess and streaking fitted lines, which are the spectral slope on a log-log scale of graininess and streaking defects. Grain defect or graininess defined at International Standard ISO/IEC document 13660 is perceived two-dimensional, generally random, and aperiodic fluctuations of density at a spatial frequency greater than 0.4 cycles per millimeter in all directions [2]. However, the graininess of K100 flat-field print in Figure 3.5(a) does not follow this definition. Therefore, the frequency greater than 1.3 cycs/mm used for the graininess in the first laser printer. The spectral slopes on log-log scale of graininess and streaking defects are presented in Table 3.1, and the spectral ranges of graininess and streaking are from 1.3 to 10 cyc/mm.

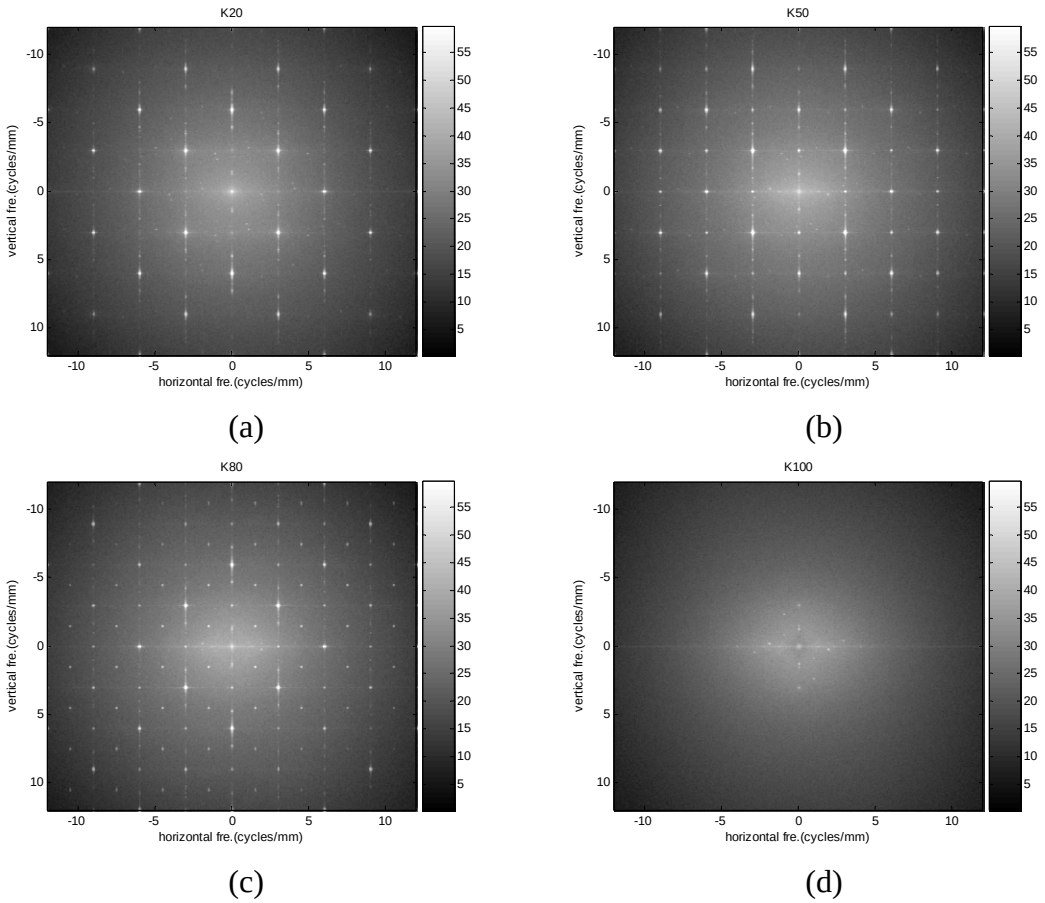

Figure 3.1 (a) 2D NPS of K20 test pattern (b) 2D NPS of K50 test pattern (c) 2D NPS of K80 test pattern (d) 2D NPS of K100 test pattern from first laser printer

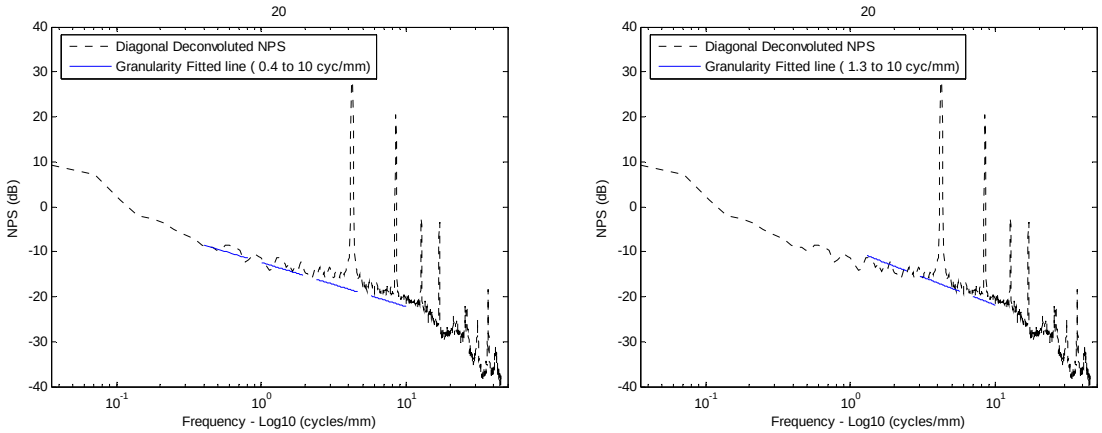

(a)

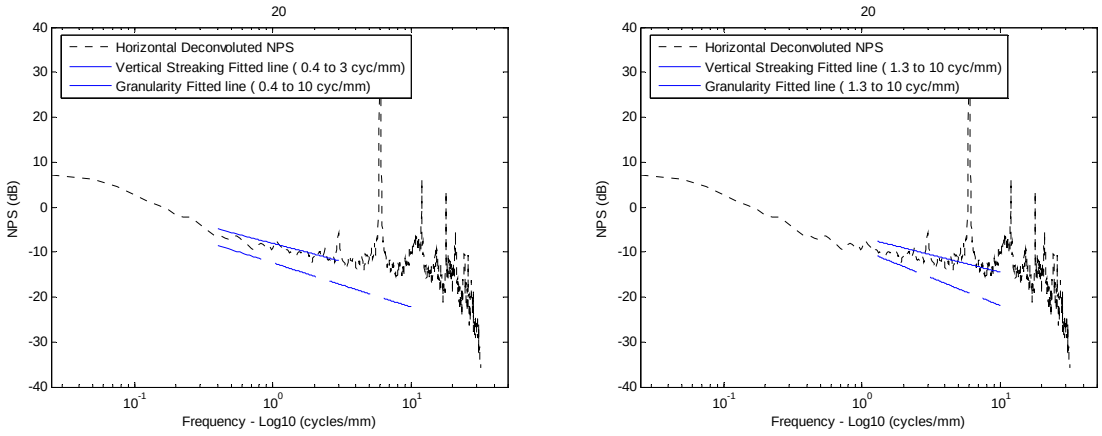

(b)

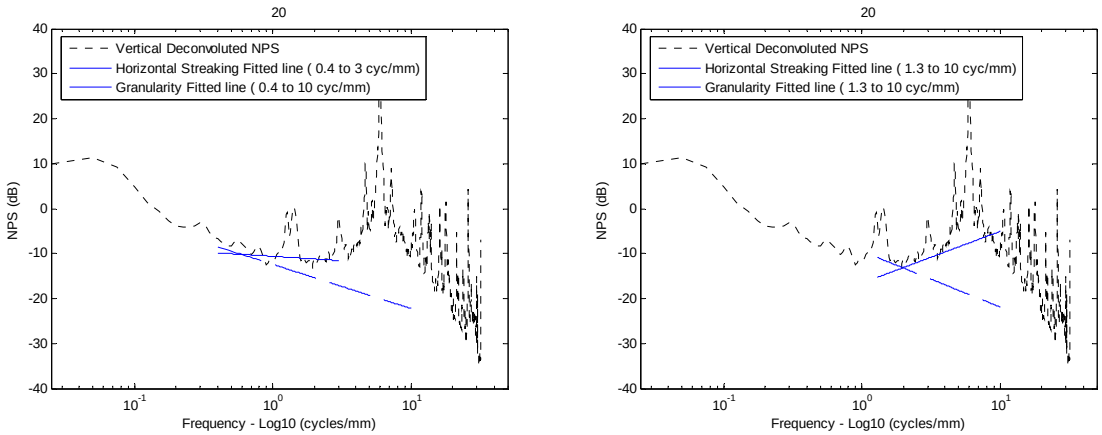

(c)

Figure 3.2 (a) The granularity fitted line on the Diagonal profile (b) Comparison of vertical streaking and granularity fitted lines on the Horizontal profile (c) Comparison of horizontal streaking and granularity fitted lines on the Vertical profile of K20 test pattern

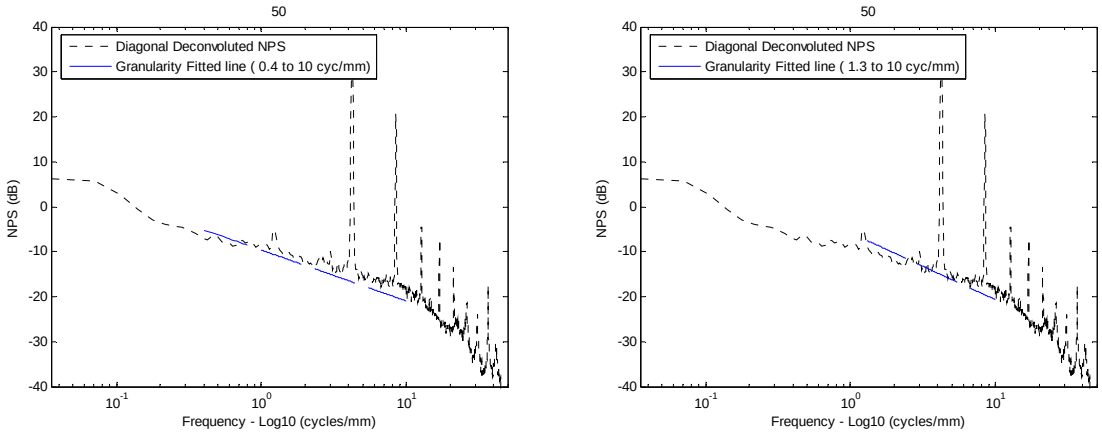

(a)

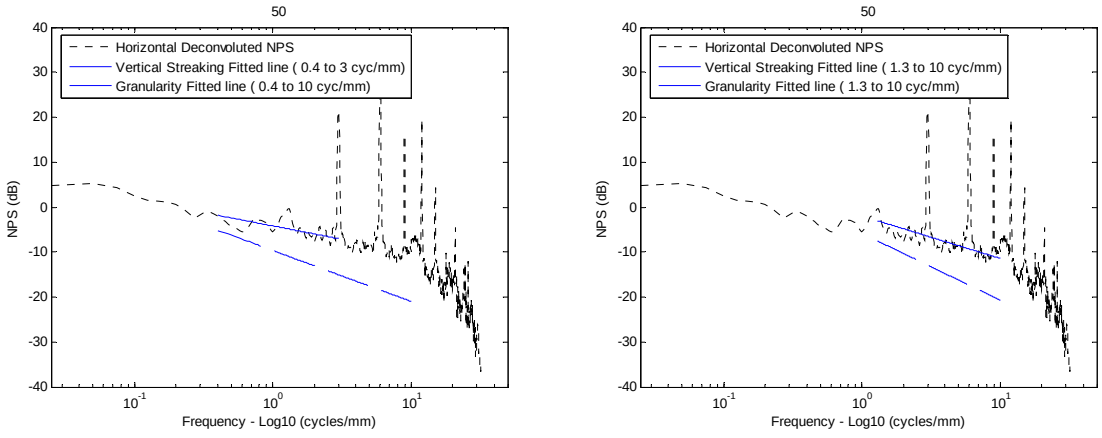

(b)

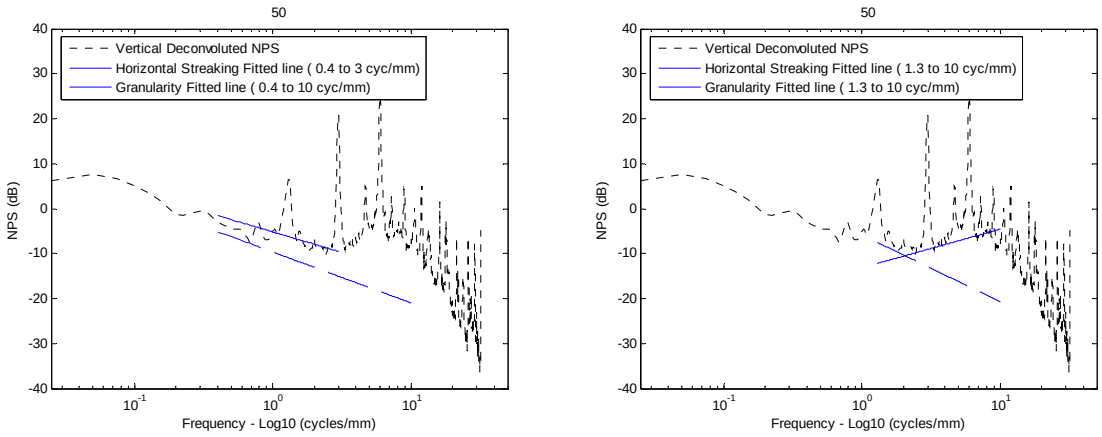

(c)

Figure 3.3 (a) The granularity fitted line on the Diagonal profile (b) Comparison of vertical streaking and granularity fitted lines on the Horizontal profile (c) Comparison of horizontal streaking and granularity fitted lines on the Vertical profile of K50 test pattern

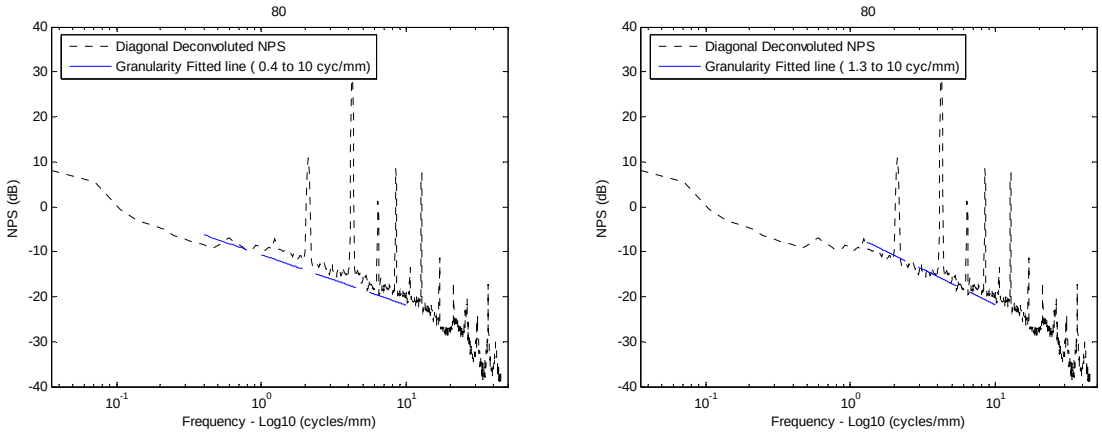

(a)

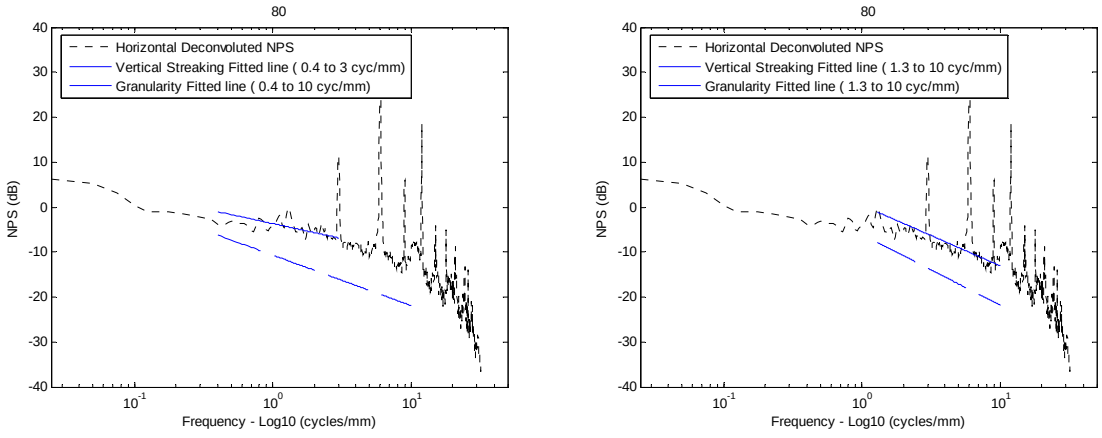

(b)

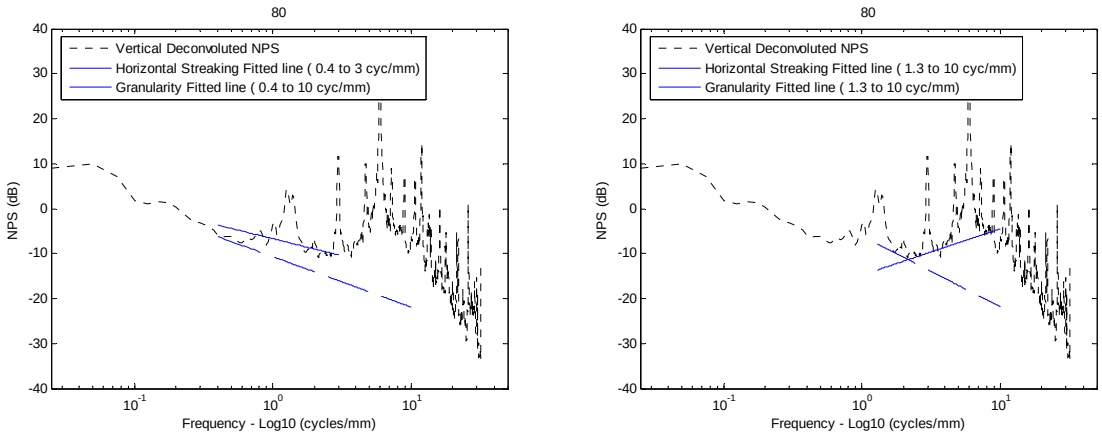

(c)

Figure 3.4 (a) The granularity fitted line on the Diagonal profile (b) Comparison of vertical streaking and granularity fitted lines on the Horizontal profile (c) Comparison of horizontal streaking and granularity fitted lines on the Vertical profile of K80 test pattern

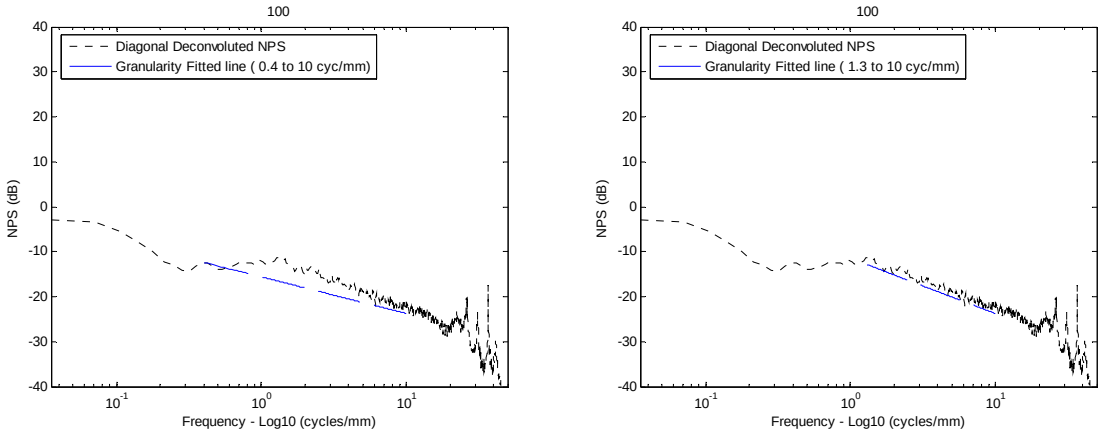

(a)

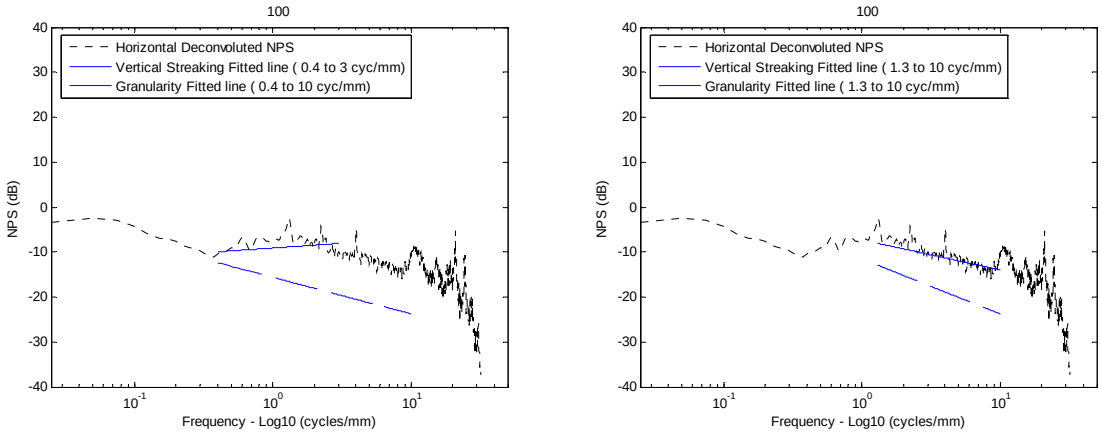

(b)

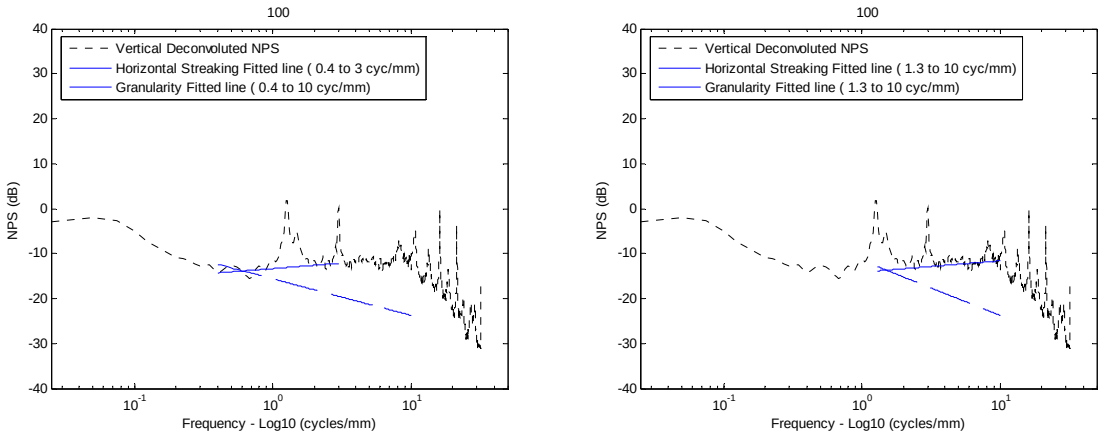

(c)

Figure 3.5 (a) The granularity fitted line on the Diagonal profile (b) Comparison of vertical streaking and granularity fitted lines on the Horizontal profile (c) Comparison of horizontal streaking and granularity fitted lines on the Vertical profile of K100 test pattern

3.2.2 Analysis for Second Laser Printer

Three printer defects will be simulated as same methods that we explained in previous section. The 2D NPS of four patterns from second laser printer is shown as in Figure 3.6, and each NPS will be compared to simulated NPS by additive and multiplicative interaction in next chapter. Though halftone components exist on the real NPS, the periodic peak components (halftoning) are not concerned in this thesis. In addition, we cannot find the banding defect in these examples of second laser printer, so the relationship of the graininess and streaking only analyzed in the second laser printer.

The range of graininess of actual flat-field prints from second laser printer exactly follows the definition [2] and random streaking is roughly linear only on the horizontal and/or vertical axis [37]. Though we do not know the upper spectral range of random streaking, we assume the range of linear trend at the horizontal and vertical profiles. Therefore, it is reasonable for streaking range to choose between 0.4 and 3 cycles/mm in the specific examples of the second laser printer.

Figure 3.7, 3.8, 3.8, and 3.10 show the diagonal, horizontal, and vertical profile with streaking fitted line and granularity fitted line. These test patterns have a few energy of random streaking in both directions. However, we will analyze the relationship of the graininess and vertical streaking in next chapter because the slope of horizontal streaking more close to zero, which means the white noise not horizontal streaking. The spectral slopes on log-log scale of graininess and streaking defects are presented in Table 3.2. In addition, the spectral range of graininess is from 0.4 to 10 cyc/mm and the range of streaking is from 0.4 to 3 cyc/mm.

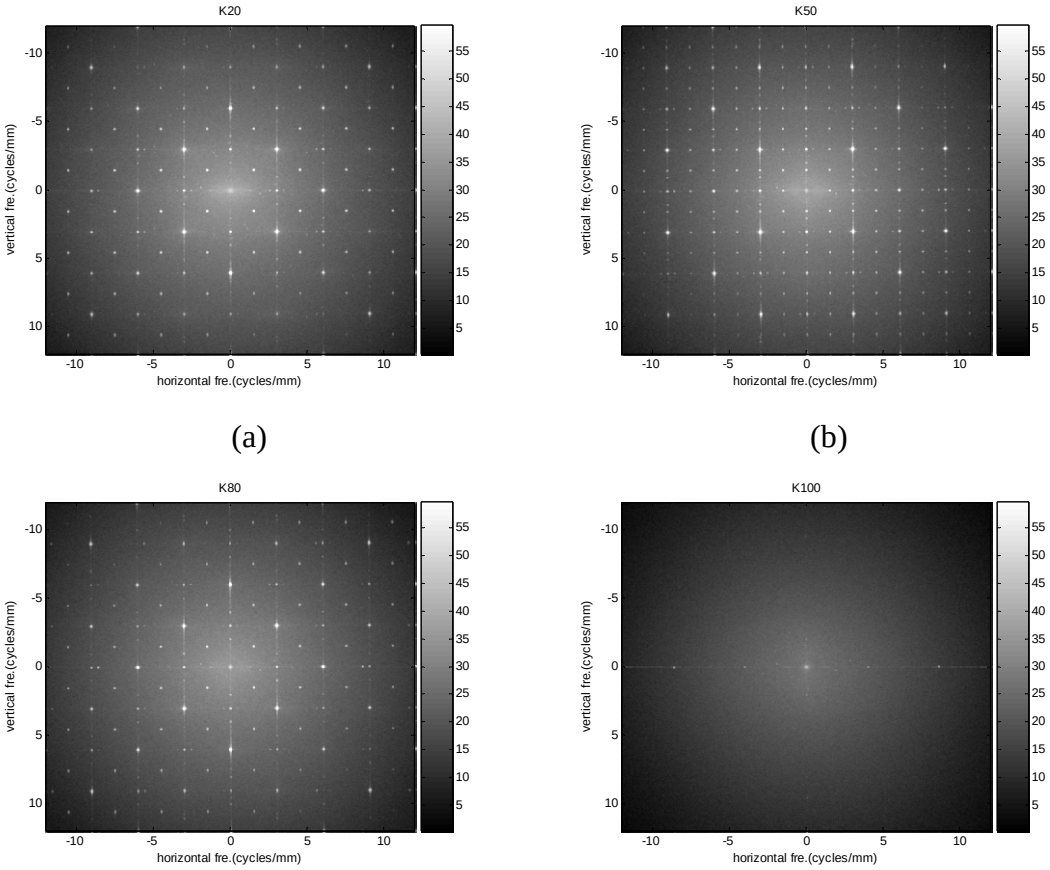

Figure 3.6 (a) 2D NPS of K20 test pattern (b) 2D NPS of K50 test pattern (c) 2D NPS of K80 test pattern (d) 2D NPS of K100 test pattern from second laser printer

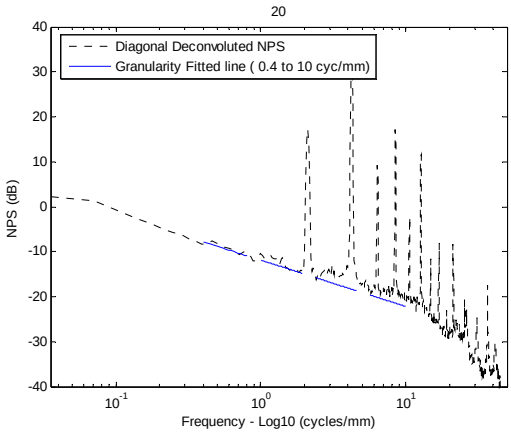

(a)

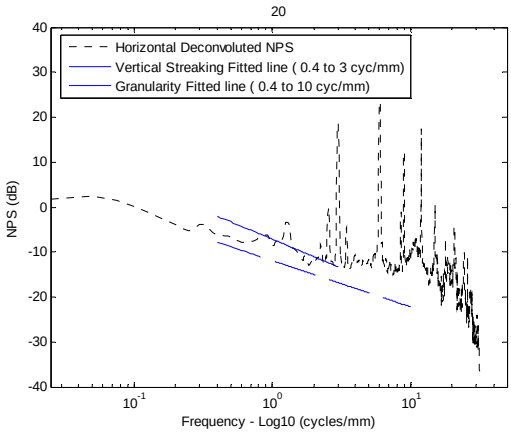

(b)

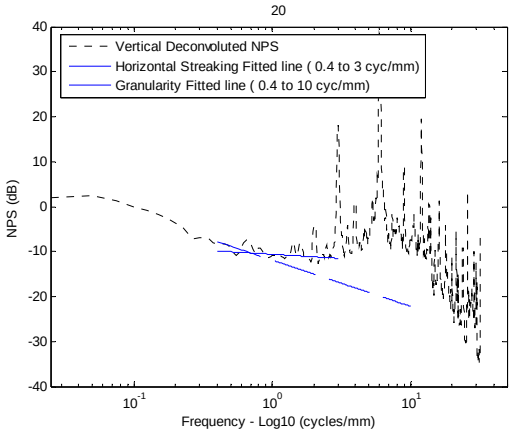

(c)

Figure 3.7 (a) The granularity fitted line on the Diagonal profile (b) Comparison of vertical streaking and granularity fitted lines on the Horizontal profile (c) Comparison of horizontal streaking and granularity fitted lines on the Vertical profile of K20 test pattern

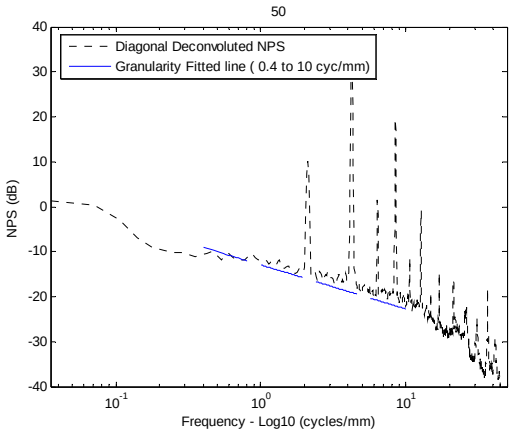

(a)

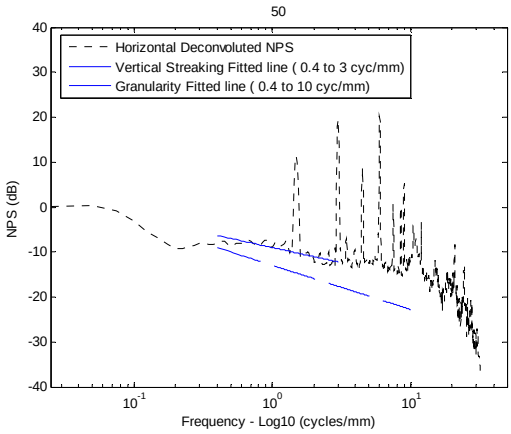

(b)

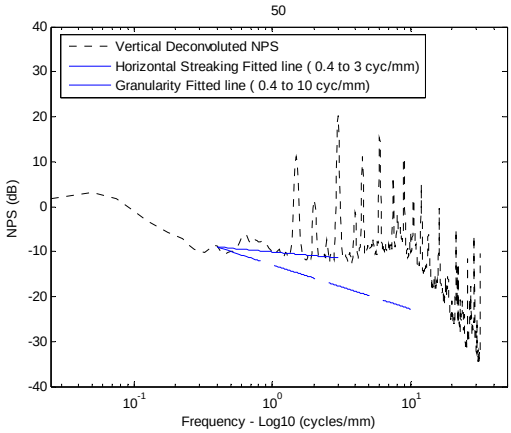

(c)

Figure 3.8 (a) The granularity fitted line on the Diagonal profile (b) Comparison of vertical streaking and granularity fitted lines on the Horizontal profile (c) Comparison of horizontal streaking and granularity fitted lines on the Vertical profile of K50 test pattern

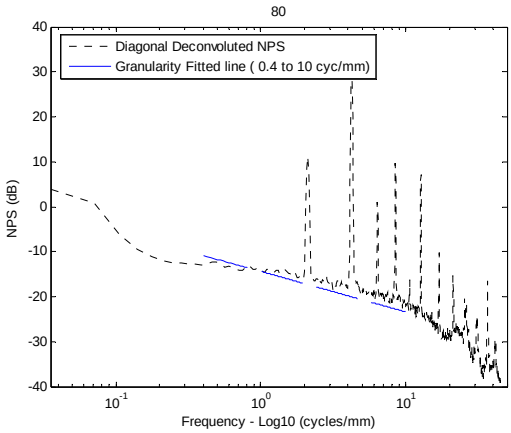

(a)

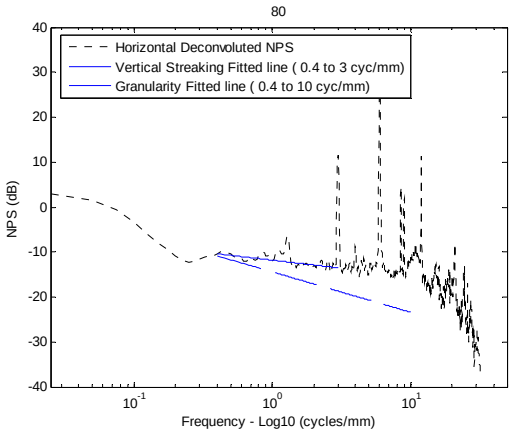

(b)

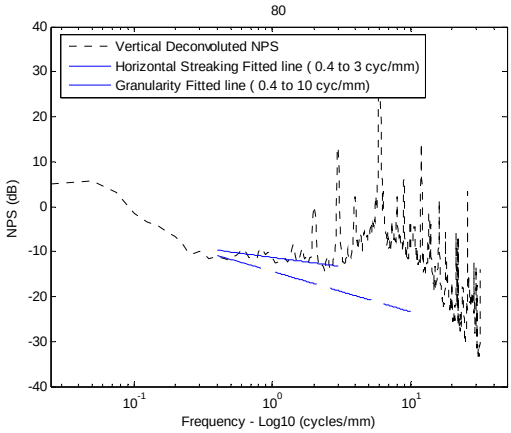

(c)

Figure 3.9 (a) The granularity fitted line on the Diagonal profile (b) Comparison of vertical streaking and granularity fitted lines on the Horizontal profile (c) Comparison of horizontal streaking and granularity fitted lines on the Vertical profile of K80 test pattern

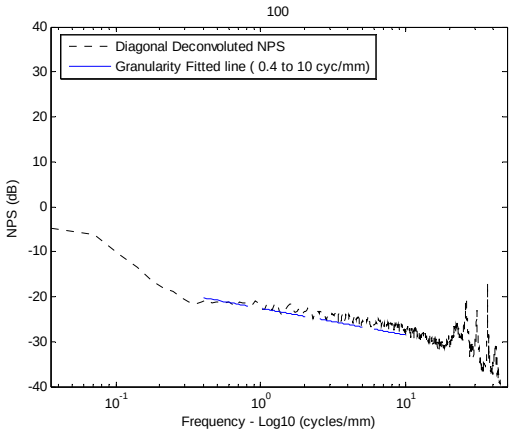

(a)

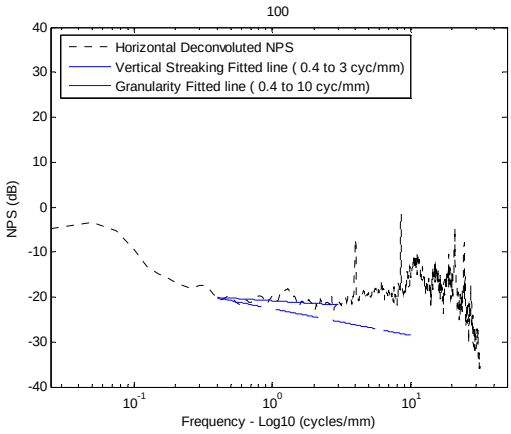

(b)

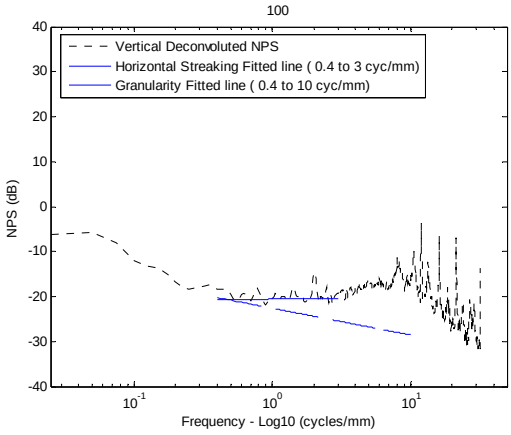

(c)

Figure 3.10 (a) The granularity fitted line on the Diagonal profile (b) Comparison of vertical streaking and granularity fitted lines on the Horizontal profile (c) Comparison of horizontal streaking and granularity fitted lines on the Vertical profile of K100 test pattern

3.2.3 Analysis for First Inkjet Printer

This section discusses the 2D NPS of four different density patterns, i.e., K20, K50, K80, and K100, from first inkjet printer. The 2D NPS of four patterns is shown as Figure 3.11, and these NPS will be compared to additive NPS and multiplicative NPS of simulated defects. In these examples, graininess, horizontal banding, and horizontal streaking exist on the hardcopy targets. The periodic peak component (halftoning) of inkjet printer is not clear than the halftoning of laser printers, and we will not concern halftoning components in this thesis because halftoning components are not printer defect.

Figure 3.12, 3.13, 3.14, and 3.15 show the horizontal, vertical, and diagonal profiles of the four different NPS with the graininess and streaking fitted lines. In vertical profile, the energy of horizontal streaking much larger than the energy of graininess in the diagonal profile, but the energy of vertical streaking is almost same as the graininess. Therefore, we assume that there is not vertical streaking in these test targets. The spectral slopes on log-log scale of graininess and streaking defects are presented in Table 3.3. In addition, the spectral range of graininess is from 0.4 to 12 cyc/mm and the range of streaking is from 0.4 to 3 cyc/mm. For graininess fitted line, the highest frequency is a 12 cyc/mm because this value makes better slope line than to use a 10 cyc/mm in actual flat-field prints from first inkjet printer.

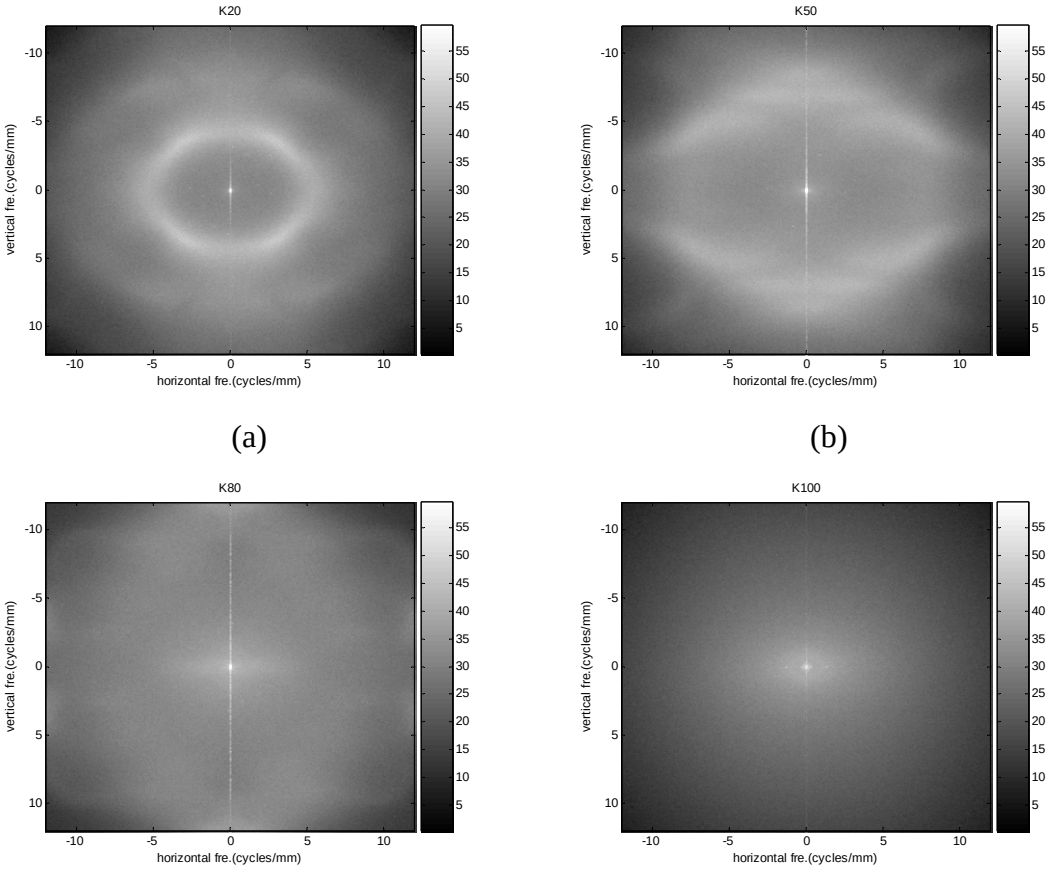

(a) (b)

(c) (d)

Figure 3.11 (a) 2D NPS of K20 test pattern (b) 2D NPS of K50 test pattern (c) 2D NPS of K80 test pattern (d) 2D NPS of K100 test pattern from first inkjet printer

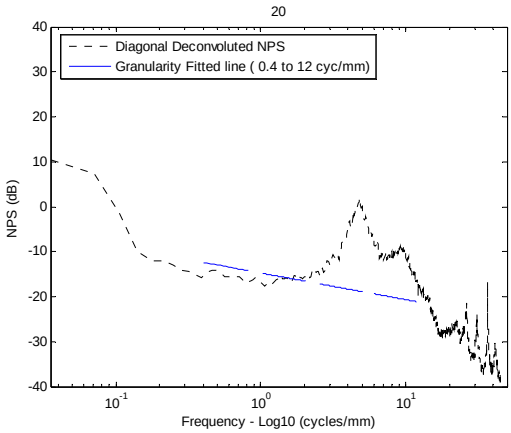

(a)

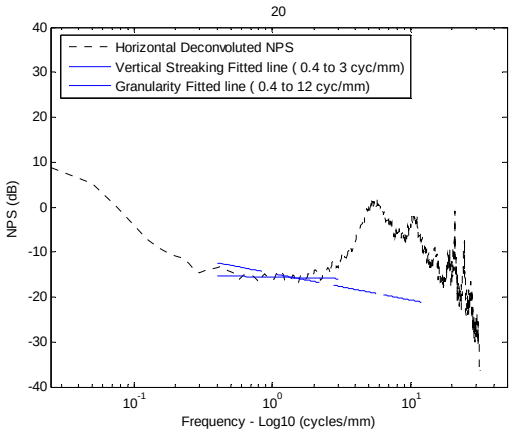

(b)

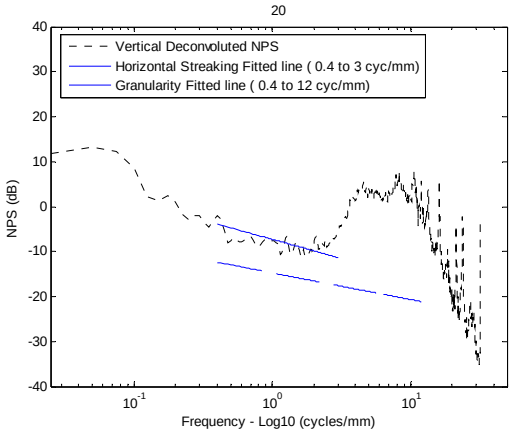

(c)

Figure 3.12 (a) The granularity fitted line on the Diagonal profile (b) Comparison of vertical streaking and granularity fitted lines on the Horizontal profile (c) Comparison of horizontal streaking and granularity fitted lines on the Vertical profile of K20 test pattern

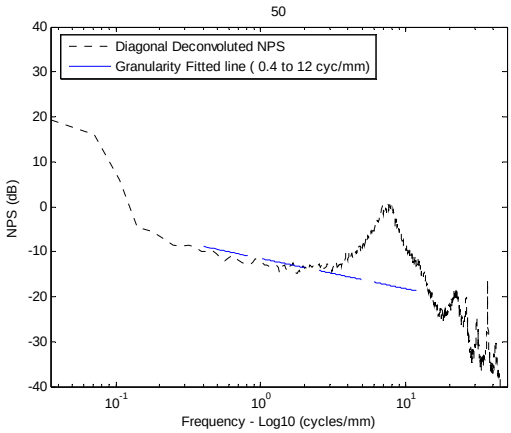

(a)

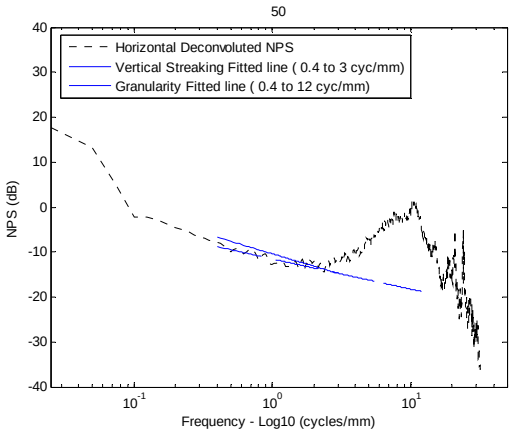

(b)

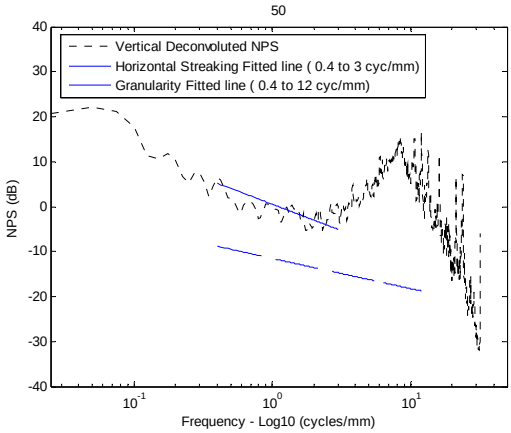

(c)

Figure 3.13 (a) The granularity fitted line on the Diagonal profile (b) Comparison of vertical streaking and granularity fitted lines on the Horizontal profile (c) Comparison of horizontal streaking and granularity fitted lines on the Vertical profile of K50 test pattern

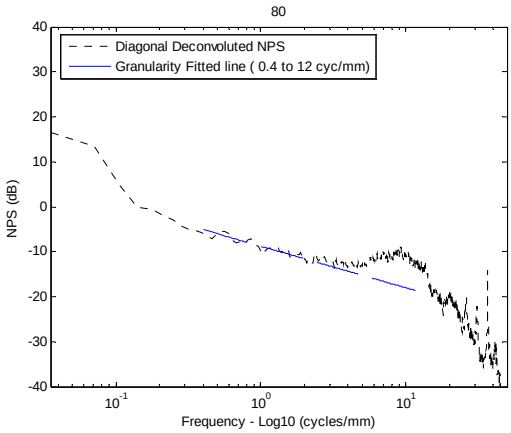

(a)

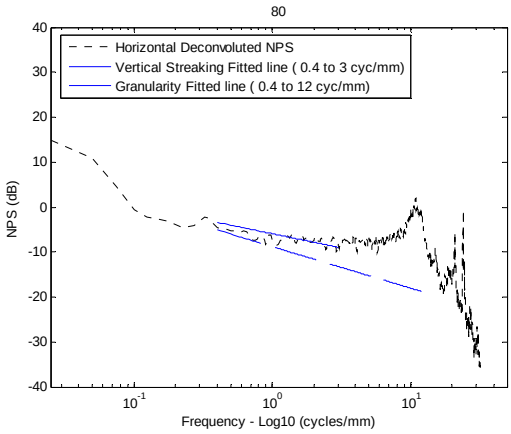

(b)

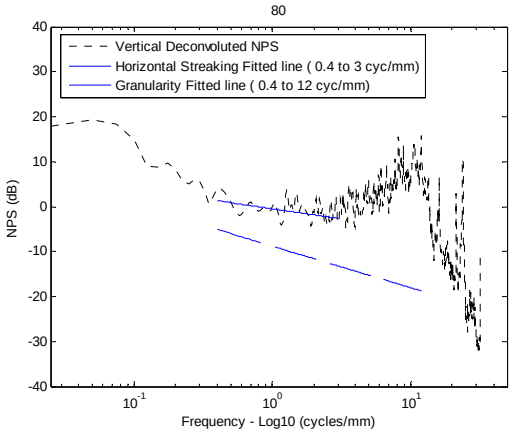

(c)

Figure 3.14 (a) The granularity fitted line on the Diagonal profile (b) Comparison of vertical streaking and granularity fitted lines on the Horizontal profile (c) Comparison of horizontal streaking and granularity fitted lines on the Vertical profile of K80 test pattern

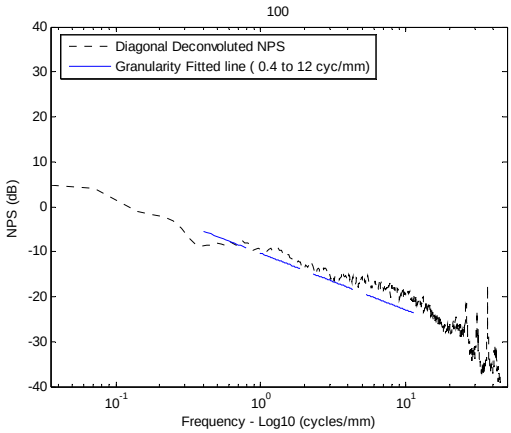

(a)

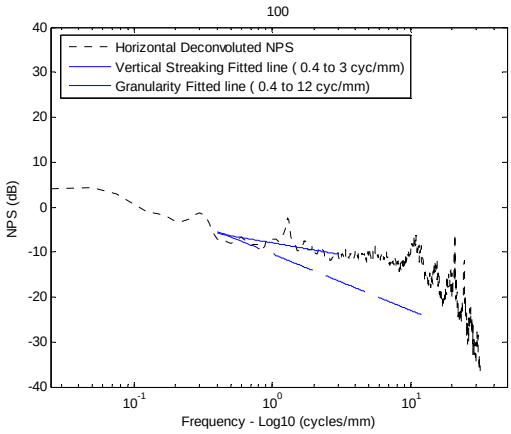

(b)

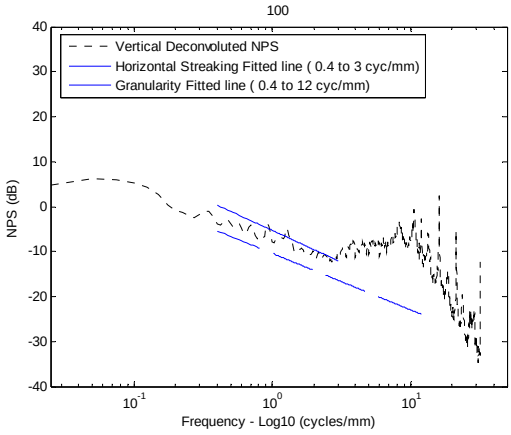

(c)

Figure 3.15 (a) The granularity fitted line on the Diagonal profile (b) Comparison of vertical streaking and granularity fitted lines on the Horizontal profile (c) Comparison of horizontal streaking and granularity fitted lines on the Vertical profile of K100 test pattern

3.2.4 Analysis for Second Inkjet Printer

The approach method is exactly same as previous sections, and this case also discusses about four different density patterns, i.e., K20, K50, K80, and K100. Figure 3.16 shows the 2D NPS of four patterns from second inkjet printer and each NPS will be compared to additive NPS and multiplicative NPS of two defects in Chapter 4. Though halftone components exist on the real NPS, we will not concern the periodic peak components (halftoning). In addition, we cannot see the banding defect in these specific examples, so the relationship of the graininess and streaking only analyzed in the second inkjet printer. We also use the same range of linear trend at the horizontal and vertical profiles from 0.4 to 3 cycles/mm in the specific examples of the second inkjet printer.

Figure 3.17, 3.18, 3.19, and 3.20 represent the diagonal, horizontal, and vertical profile with streaking fitted line and granularity fitted line. Though these test patterns have a few energy of random streaking in both directions, horizontal streaking will be analyzed in next Chapter. The spectral slopes on log-log scale of graininess and streaking defects are presented in Table 3.4. In addition, the spectral range of graininess is from 0.4 to 10 cyc/mm and the range of streaking is from 0.4 to 3 cyc/mm.

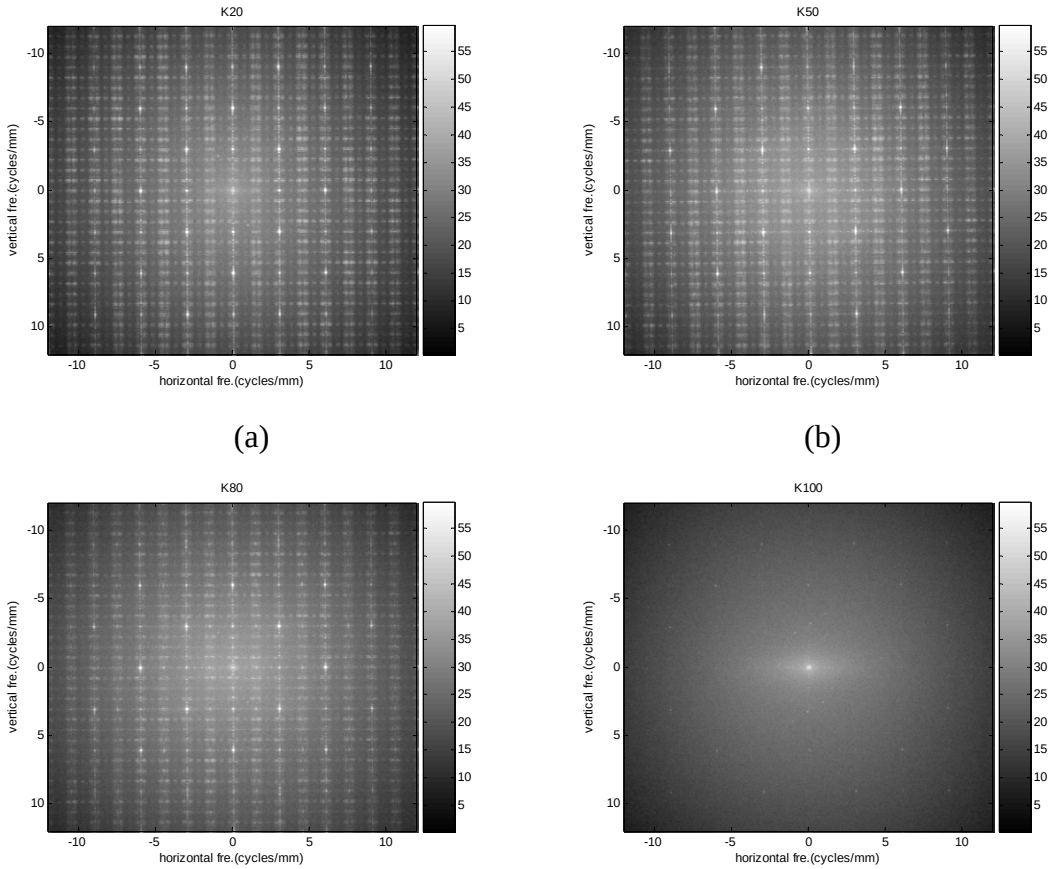

Figure 3.16 (a) 2D NPS of K20 test pattern (b) 2D NPS of K50 test pattern (c) 2D NPS of K80 test pattern (d) 2D NPS of K100 test pattern from second inkjet printer

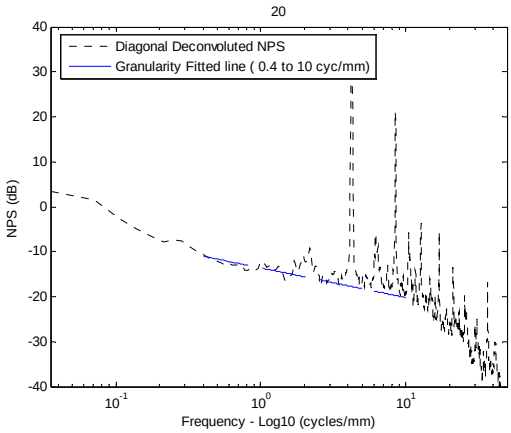

(a)

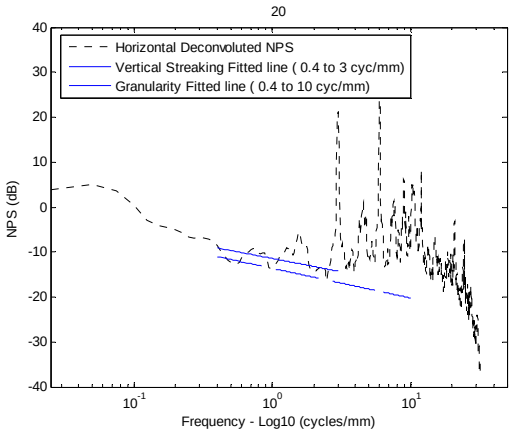

(b)

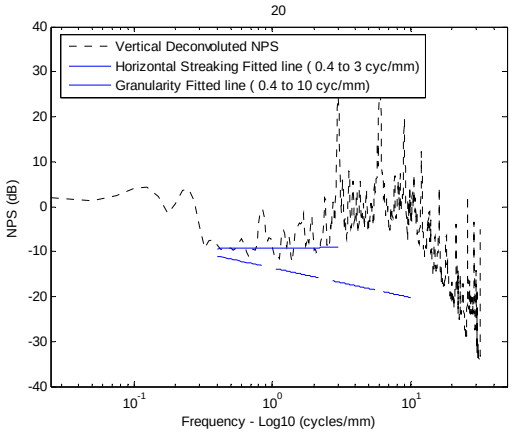

(c)

Figure 3.17 (a) The granularity fitted line on the Diagonal profile (b) Comparison of vertical streaking and granularity fitted lines on the Horizontal profile (c) Comparison of horizontal streaking and granularity fitted lines on the Vertical profile of K20 test pattern

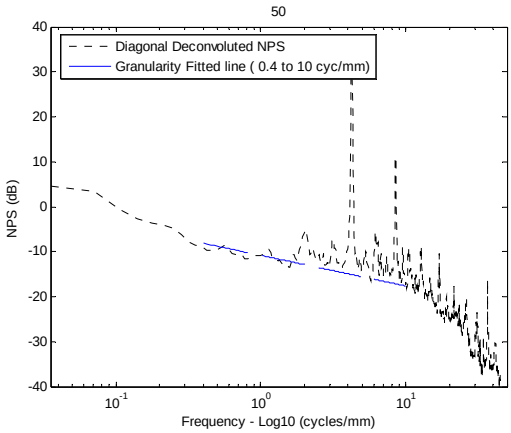

(a)

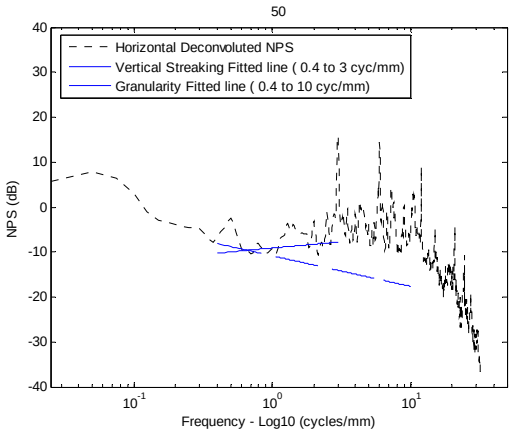

(b)

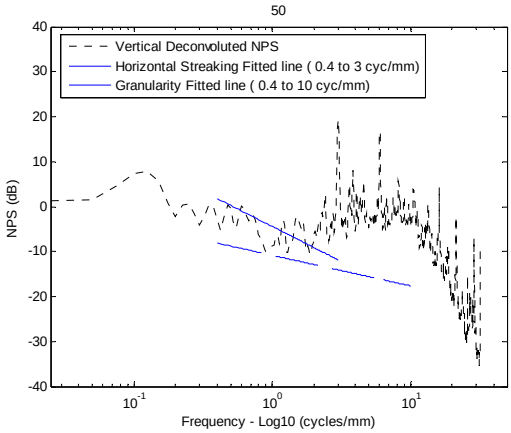

(c)

Figure 3.18 (a) The granularity fitted line on the Diagonal profile (b) Comparison of vertical streaking and granularity fitted lines on the Horizontal profile (c) Comparison of horizontal streaking and granularity fitted lines on the Vertical profile of K50 test pattern

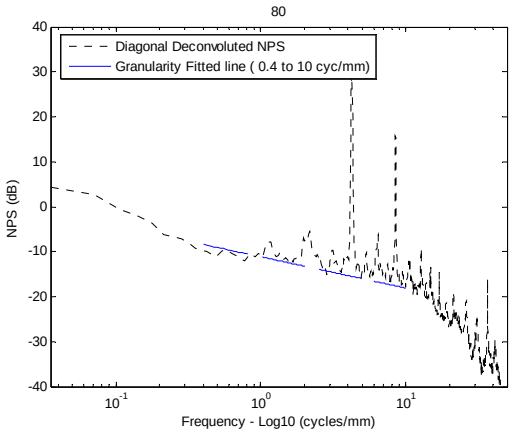

(a)

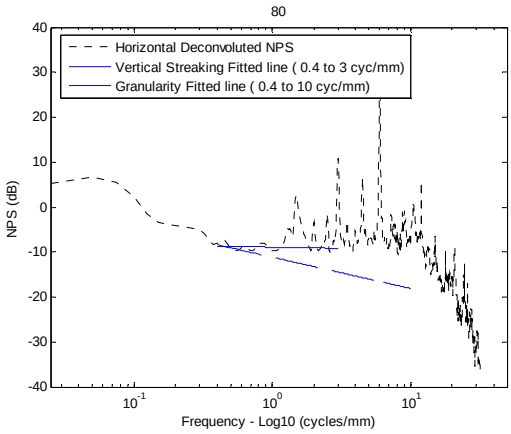

(b)

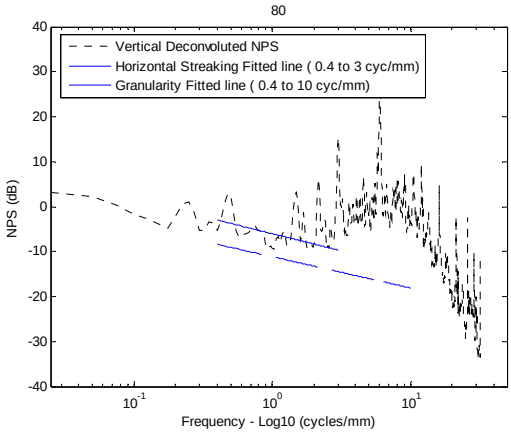

(c)

Figure 3.19 (a) The granularity fitted line on the Diagonal profile (b) Comparison of vertical streaking and granularity fitted lines on the Horizontal profile (c) Comparison of horizontal streaking and granularity fitted lines on the Vertical profile of K80 test pattern

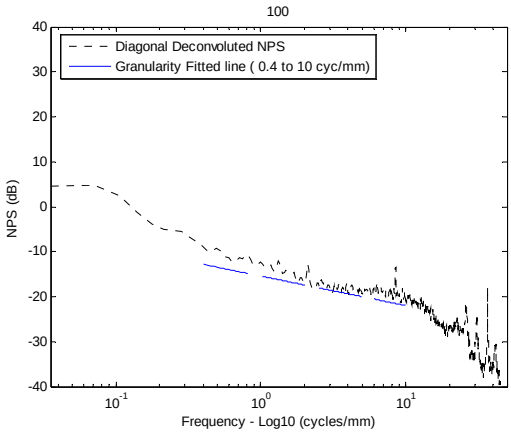

(a)

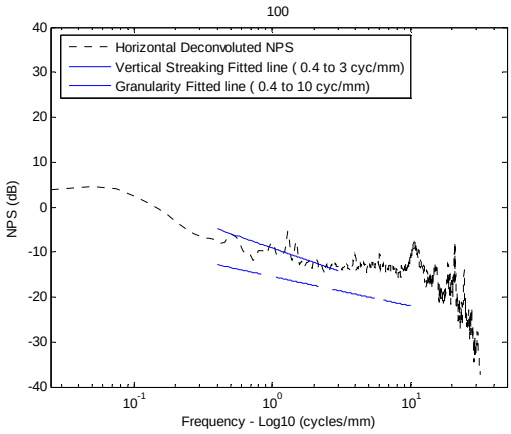

(b)

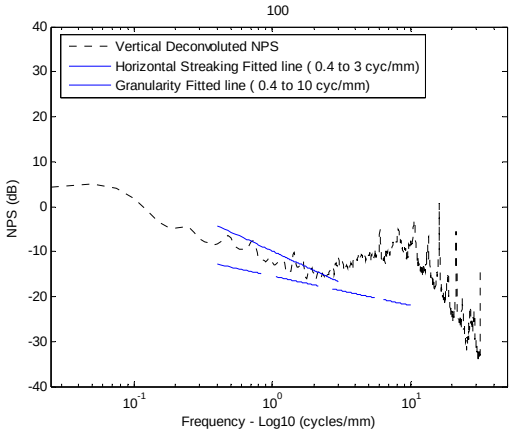

(c)

Figure 3.20 (a) The granularity fitted line on the Diagonal profile (b) Comparison of vertical streaking and granularity fitted lines on the Horizontal profile (c) Comparison of horizontal streaking and granularity fitted lines on the Vertical profile of K100 test pattern

Table 3.1: The spectral slopes on log-log scale of graininess and streaking defects from First Laser Printer. The spectral ranges of graininess and streaking are from 1.3 to 10 cyc/mm.

	Graininess	Vertical Streaking	Horizontal Streaking
K20	-1.2349	-0.7720	1.1491
K50	-1.4805	-0.9405	0.8573
K80	-1.5661	-1.3452	1.0321
K100	-1.2218	-0.6631	0.2504

Table 3.2: The spectral slopes on log-log scale of graininess and streaking defects from Second Laser Printer. The spectral range of graininess is from 0.4 to 10 cyc/mm and the range of streaking is from 0.4 to 3 cyc/mm.

	Graininess	Vertical Streaking	Horizontal Streaking
K20	-1.0255	-1.2861	-0.1913
K50	-0.9763	-0.6703	-0.2756
K80	-0.8951	-0.3571	-0.4003
K100	-0.5922	-0.1916	0.0342

Table 3.3: The spectral slopes on log-log scale of graininess and streaking defects from First Inkjet Printer. The spectral range of graininess is from 0.4 to 12 cyc/mm and the range of streaking is from 0.4 to 3 cyc/mm.

	Graininess	Vertical Streaking	Horizontal Streaking
K20	-0.5898	-0.0711	-0.8501
K50	-0.6693	-0.9119	-1.1677
K80	-0.9201	-0.6285	-0.4457
K100	-1.2532	-0.5292	-1.4056

Table 3.4: The spectral slopes on log-log scale of graininess and streaking defects from Second Inkjet Printer. The spectral range of graininess is from 0.4 to 10 cyc/mm and the range of streaking is from 0.4 to 3 cyc/mm.

	Graininess	Vertical Streaking	Horizontal Streaking
K20	-0.6551	-0.5920	0.0322
K50	-0.6779	0.2795	-1.5439
K80	-0.6920	-0.0544	-0.7566
K100	-0.6510	-1.0611	-1.4105

CHAPTER 4

Results and Discussions

This chapter presents and discussed the results obtained from the additive test and multiplicative tests for graininess, streaking, and banding interactions. Section 4.1 presents additive and multiplicative results of graininess and streaking artifacts as well as the 2D real NPS from four different digital printers. These results are compared the NPS of actual flat-field prints from digital printers to draw conclusion actual artifact interaction. Section 4.2 provides the additive and multiplicative results of graininess and banding artifacts and these results are also compared the NPS of actual flat-field prints from digital printers. The results of banding and streaking artifacts are discussed in Section 4.3.

4.1 Additive and Multiplicative Results of Graininess and Streaking

This section only focuses on the relationship of graininess and streaking artifacts from four different digital printers. We simulated each graininess and streaking artifacts from four different densities such as K20, K50, K80, and K100 test prints of each digital printer. Figure 4.1, 4.2, and 4.3 show the real NPS at the top (a), horizontal profiles of real NPS, additive, and multiplicative results at the top (b), additive image in space domain at the left of middle (c), additive NPS at the right of middle (c), multiplicative image in space domain at the left of bottom (d), and multiplicative NPS at the right of bottom (d) of simulated graininess and vertical streaking artifacts from first laser printer with appropriate amplitudes. The shape of graininess in multiplicative model has moved to the streaking region of simulated NPS. However, the graininess of real NPS does not

change their shape, and it looks more obvious that the horizontal profiles of the additive model more close to the real horizontal profiles. Therefore, the interaction of the graininess and streaking artifacts of first laser printer is more appropriate additive than multiplicative relationship.

The NPS of additive and multiplicative results of graininess and vertical streaking with appropriate amplitudes represent in Figure 4.4, 4.5, 4.6, and 4.7, respectively. As similar to the results of the first laser printer, the graininess of real NPS has not affect on the streaking, and it is obvious that vertical streaking is independent to the graininess of the second printer. Therefore, the interaction of the graininess and streaking of second laser printer is more appropriate additive than multiplicative relationship.

Figure 4.8, 4.9, 4.10, and 4.11 present the NPS of additive and multiplicative results of graininess and horizontal streaking with appropriate amplitudes for the first inkjet printer. Though horizontal banding defect at low frequency seems like to horizontal streaking, we assume the component over the 0.4 cyc/mm is the horizontal streaking. The shape of graininess in multiplicative model of the K20 test pattern has moved to the streaking region of simulated NPS. In other patterns of the multiplicative model, the streaking has been reduced by the graininess artifact. However, the graininess of real NPS does not change their shape, and it looks more obvious that horizontal streaking is not depends on the graininess. Therefore, the interaction of the graininess and streaking artifacts of first inkjet printer is more appropriate additive than multiplicative relationship.

Figure 4.12, 4.13, 4.14, and 4.15 present the NPS of additive and multiplicative results of graininess and horizontal streaking with appropriate amplitudes for the second inkjet printer. As similar to the results of the first inkjet printer, the graininess of real NPS has

not affect on the streaking, and it is obvious that horizontal streaking artifact is independent to the graininess of the second inkjet printer. Therefore, the interaction of the graininess and streaking of second inkjet printer is more appropriate additive than multiplicative relationship.

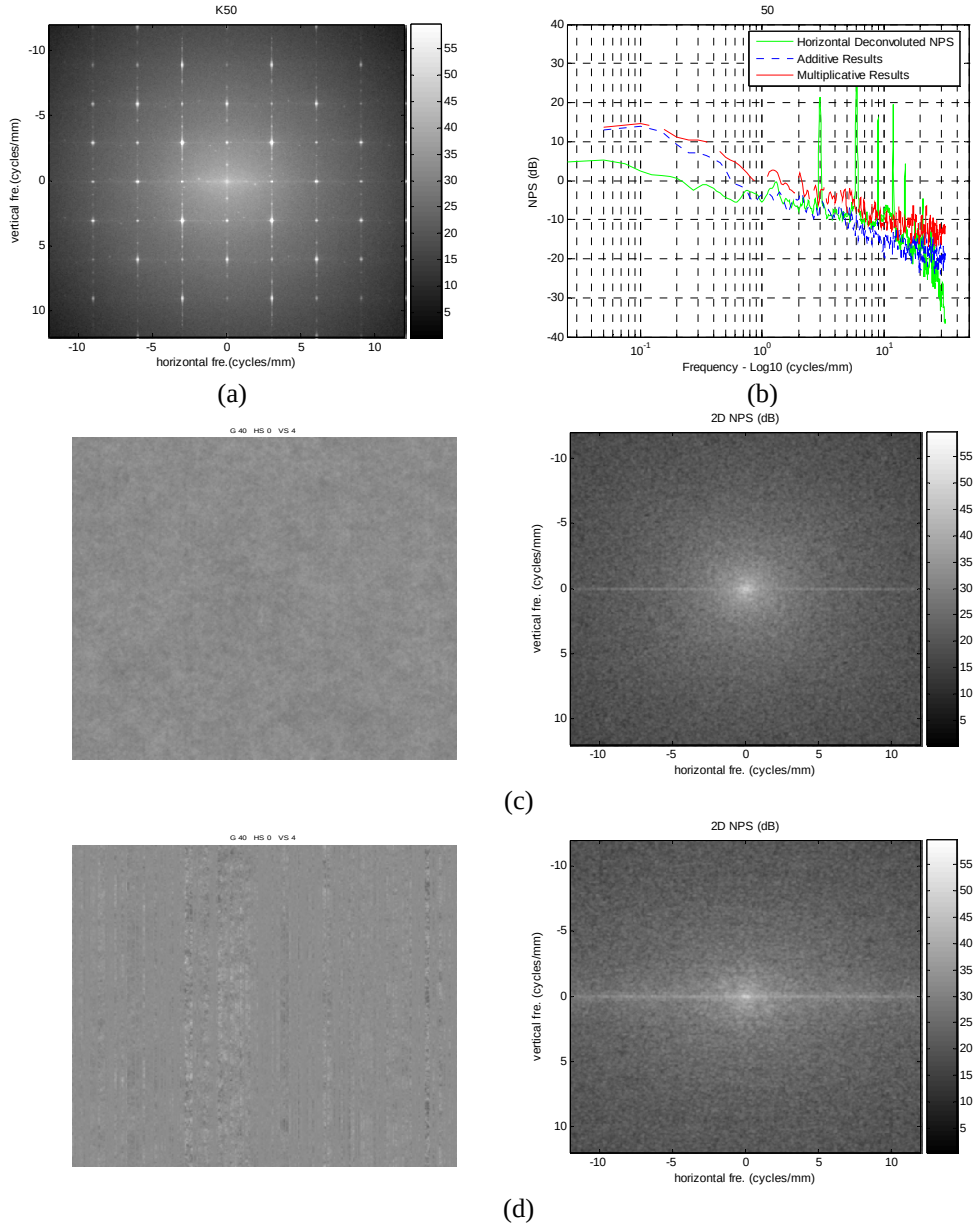

Figure 4.1 (a) 2D NPS of K50 test pattern (b) Horizontal Profiles of real NPS, additive, and multiplicative results (c) Additive image in space domain (left) and 2D NPS (right) (d) Multiplicative image in space domain (left) and 2D NPS (right) of simulated graininess and vertical streaking from first laser printer with appropriate amplitudes

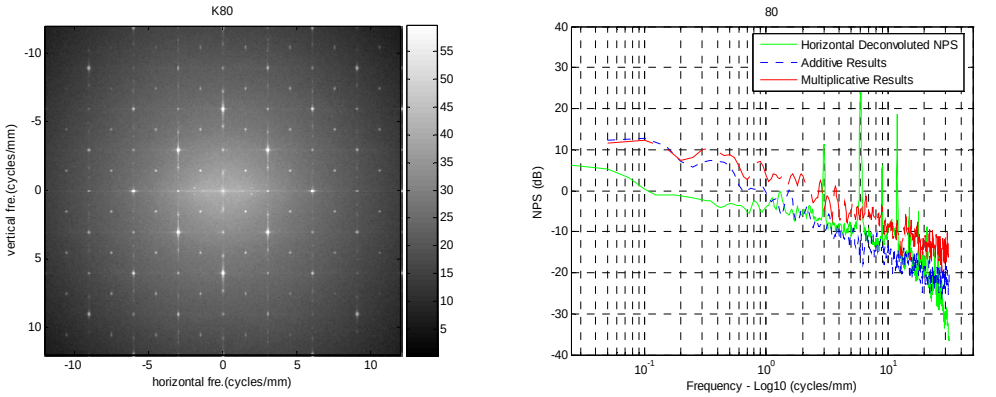

(a)

(b)

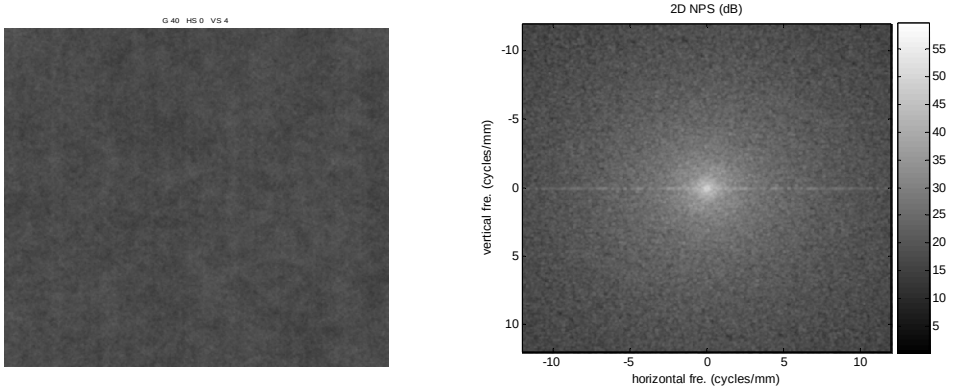

(c)

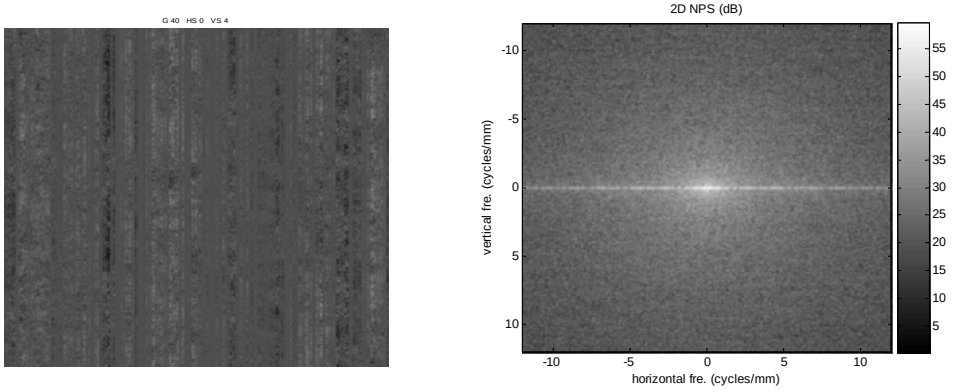

(d)

Figure 4.2 (a) 2D NPS of K80 test pattern (b) Horizontal Profiles of real NPS, additive, and multiplicative results (c) Additive image in space domain (left) and 2D NPS (right) (d) Multiplicative image in space domain (left) and 2D NPS (right) of simulated graininess and vertical streaking from first laser printer with appropriate amplitudes

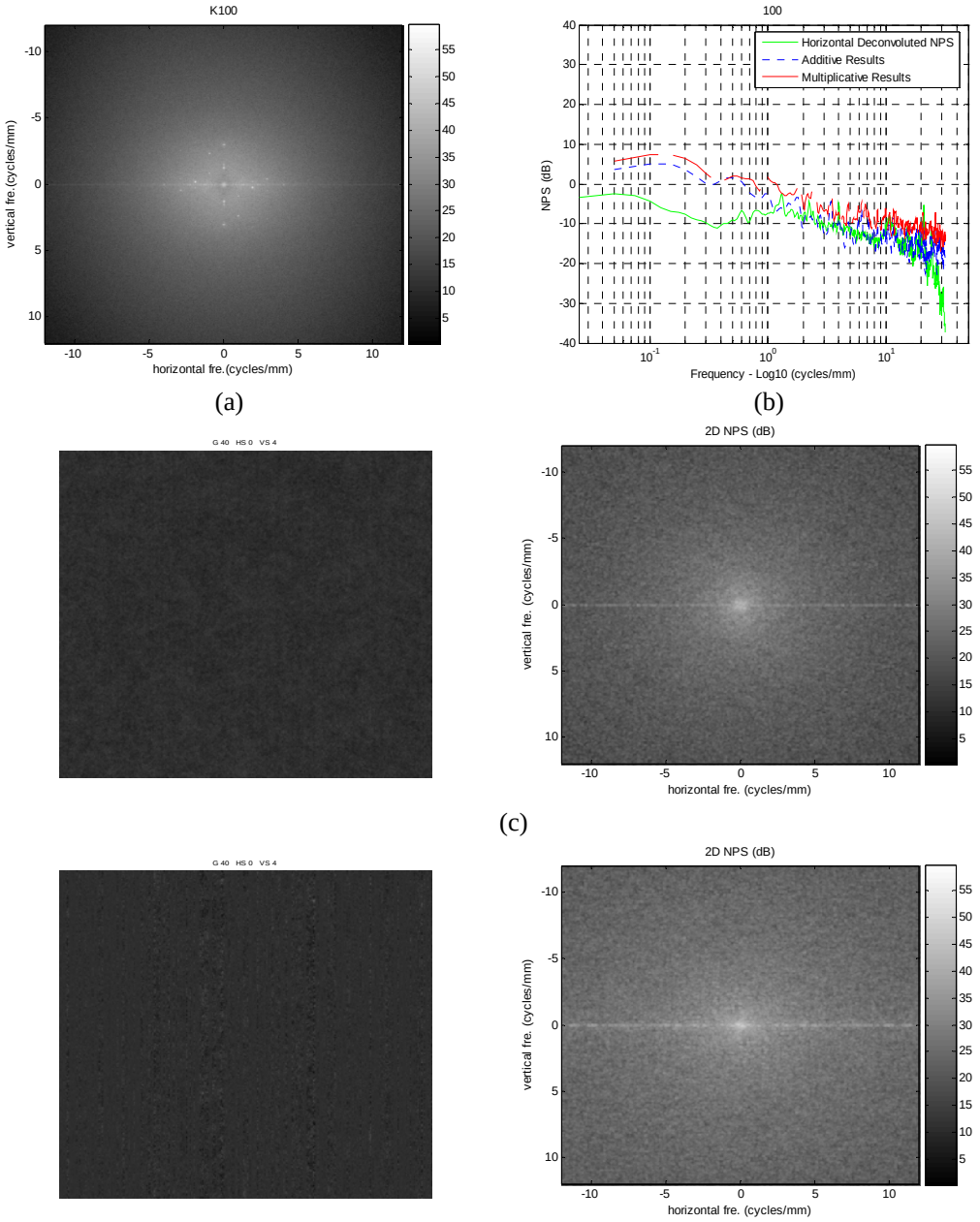

Figure 4.3 (a) 2D NPS of K100 test pattern (b) Horizontal Profiles of real NPS, additive, and multiplicative results (c) Additive image in space domain (left) and 2D NPS (right) (d) Multiplicative image in space domain (left) and 2D NPS (right) of simulated graininess and vertical streaking from first laser printer with appropriate amplitudes

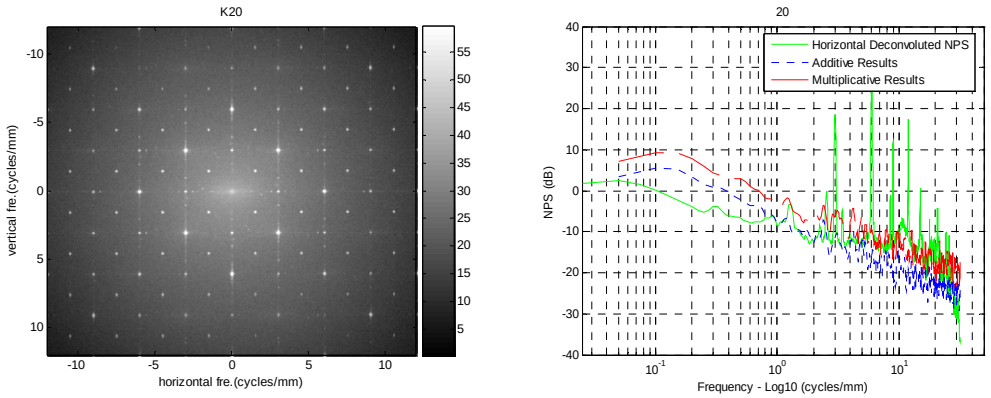

(a) (b)

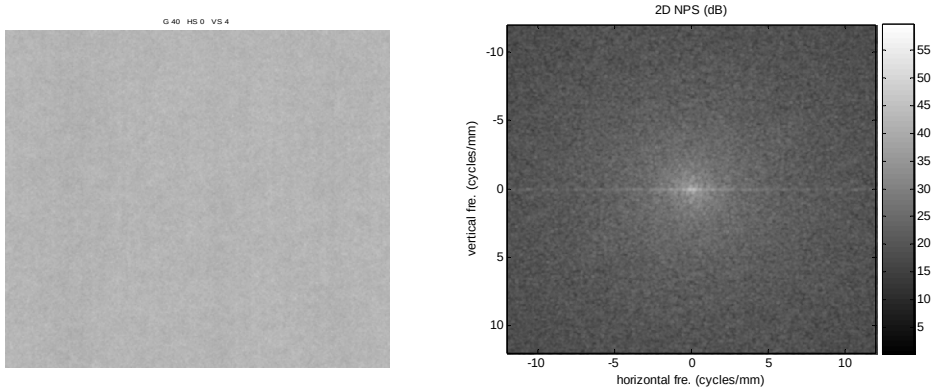

(c)

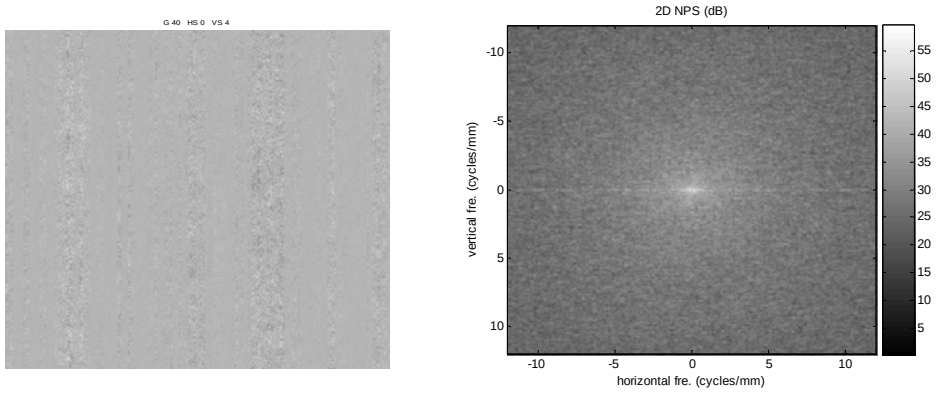

(d)

Figure 4.4 (a) 2D NPS of K20 test pattern (b) Horizontal Profiles of real NPS, additive, and multiplicative results (c) Additive image in space domain (left) and 2D NPS (right) (d) Multiplicative image in space domain (left) and 2D NPS (right) of simulated graininess and vertical streaking from second laser printer with appropriate amplitudes

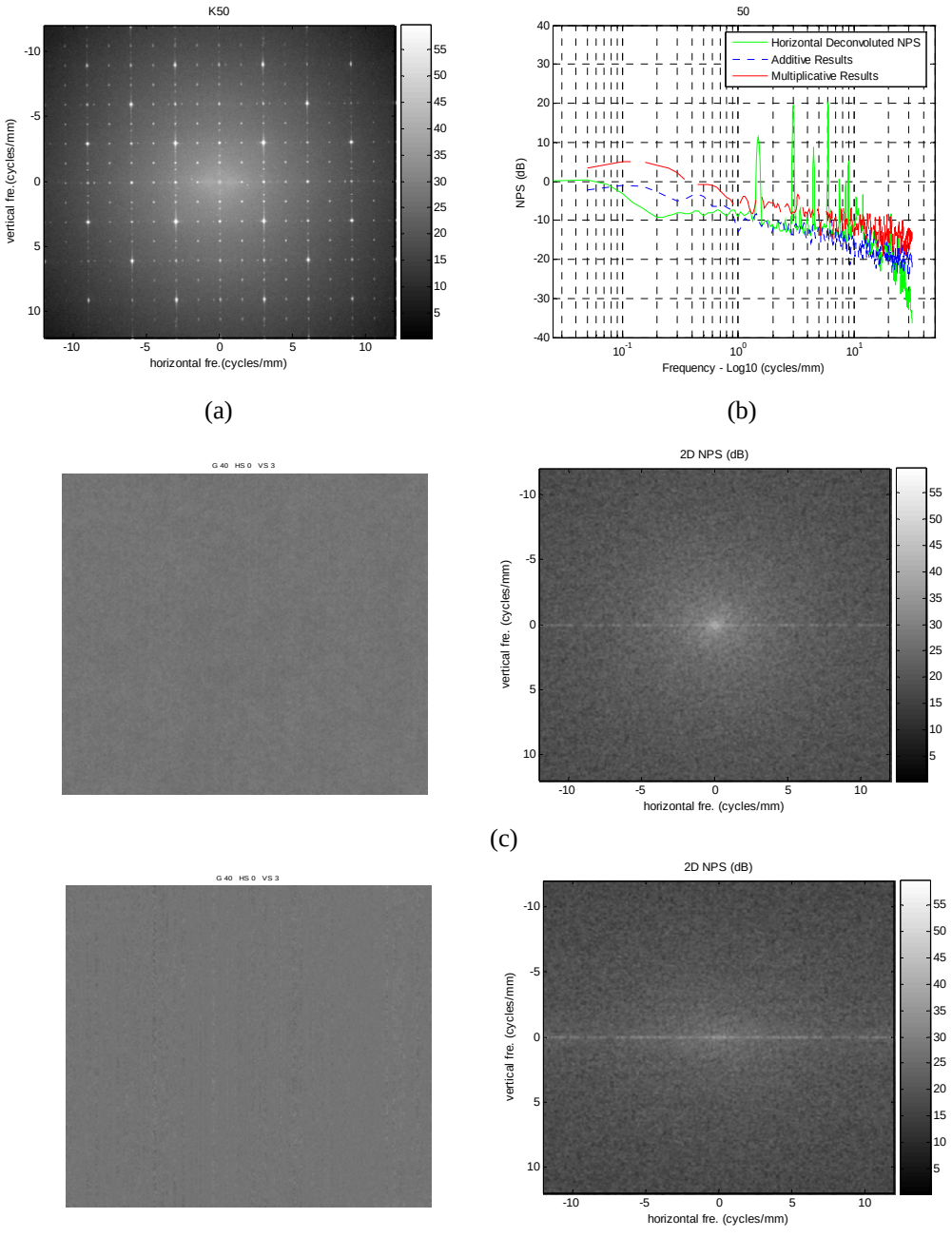

Figure 4.5 (a) 2D NPS of K50 test pattern (b) Horizontal Profiles of real NPS, additive, and multiplicative results (b) Additive image in space domain (left) and 2D NPS (right) (c) Multiplicative image in space domain (left) and 2D NPS (right) of simulated graininess and vertical streaking from second laser printer with appropriate amplitudes

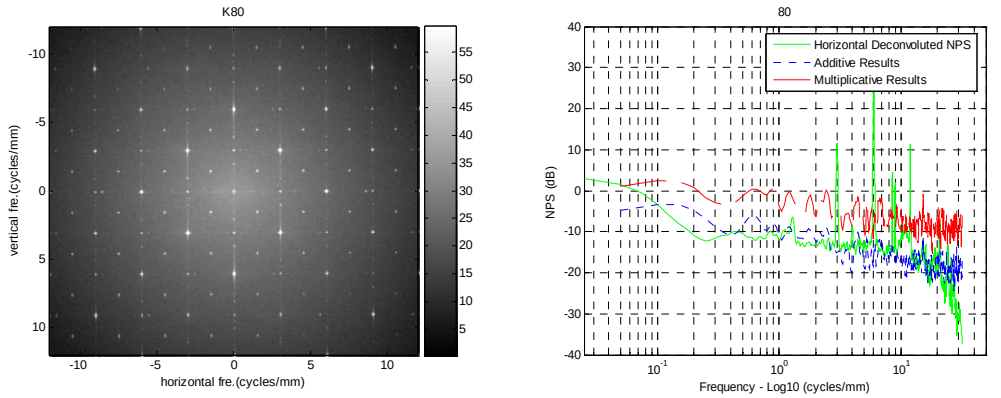

(a) (b)

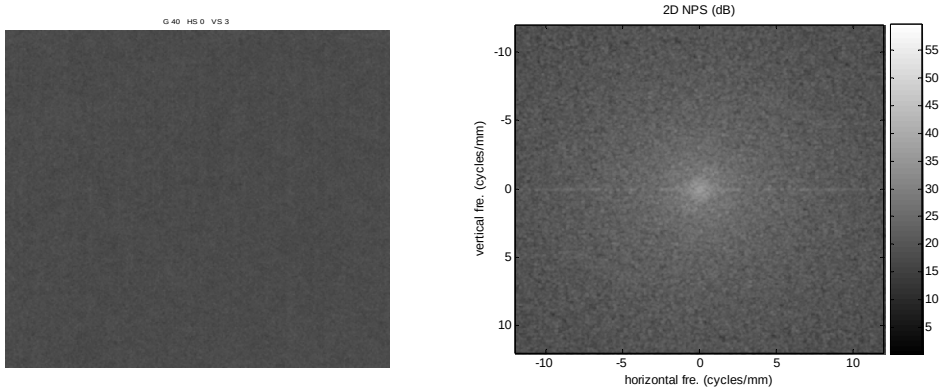

(c)

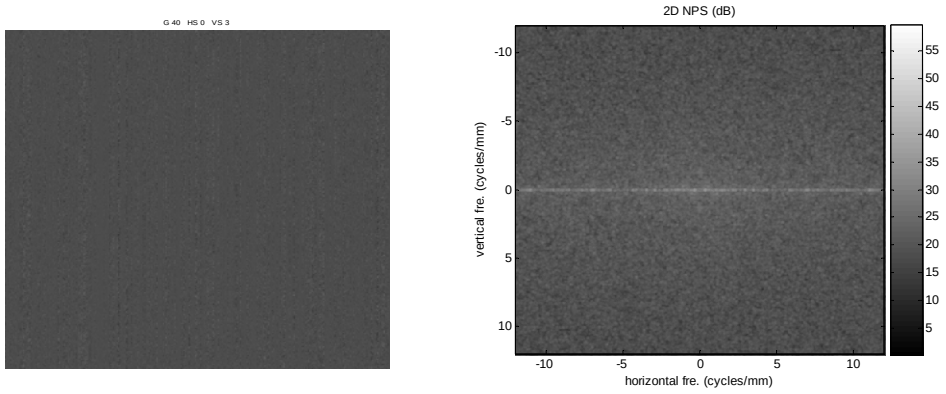

(d)

Figure 4.6 (a) 2D NPS of K80 test pattern (b) Horizontal Profiles of real NPS, additive, and multiplicative results (c) Additive image in space domain (left) and 2D NPS (right) (d) Multiplicative image in space domain (left) and 2D NPS (right) of simulated graininess and vertical streaking from second laser printer with appropriate amplitudes

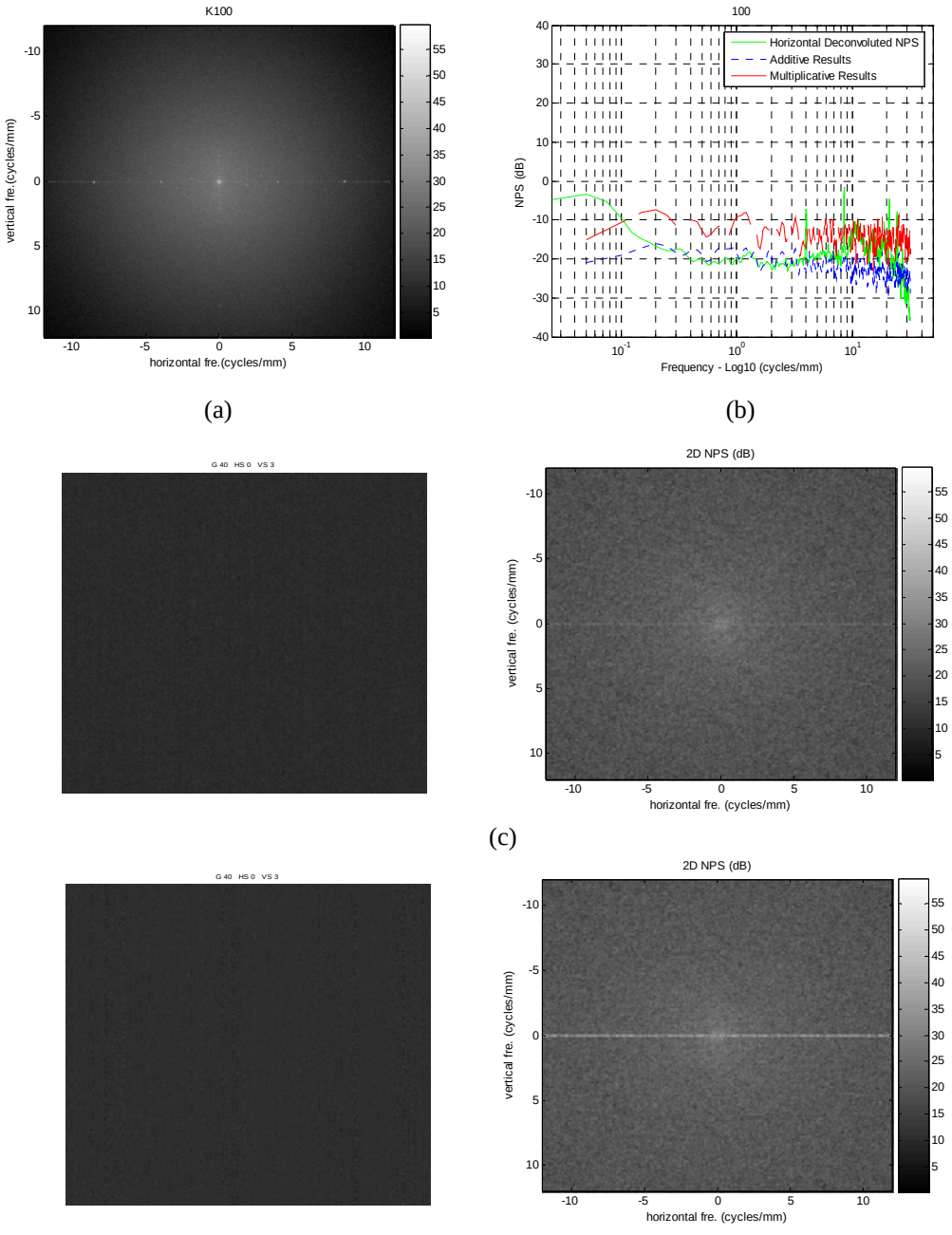

Figure 4.7 (a) 2D NPS of K100 test pattern (b) Horizontal Profiles of real NPS, additive, and multiplicative results (c) Additive image in space domain (left) and 2D NPS (right) (d) Multiplicative image in space domain (left) and 2D NPS (right) of simulated graininess and vertical streaking from second laser printer with appropriate amplitudes

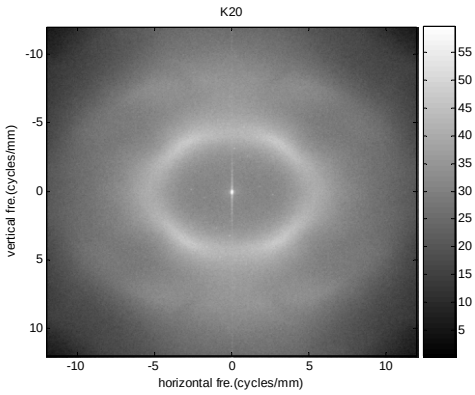

(a)

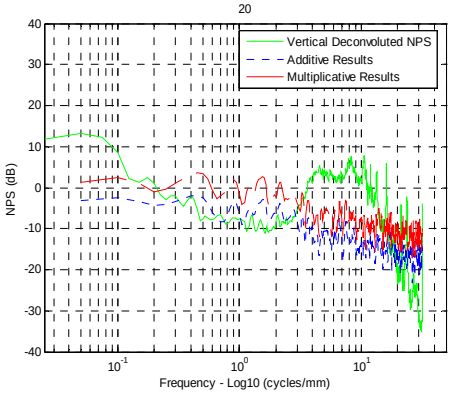

(b)

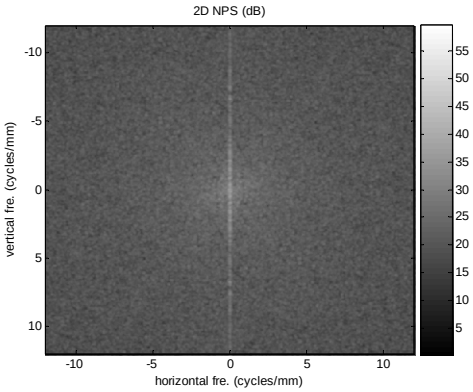

(c)

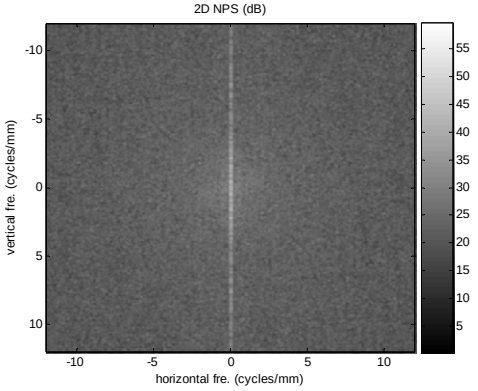

(d)

Figure 4.8 (a) 2D NPS of K20 test pattern (b) Vertical Profiles of real NPS, additive, and multiplicative results (c) Additive image in space domain (left) and 2D NPS (right) (d) Multiplicative image in space domain (left) and 2D NPS (right) of simulated graininess and horizontal streaking from first inkjet printer with arbitrary amplitudes

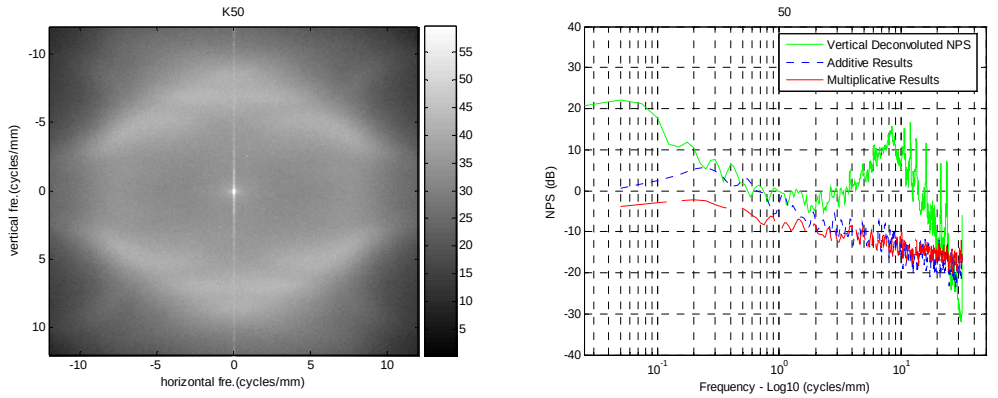

(a)

(b)

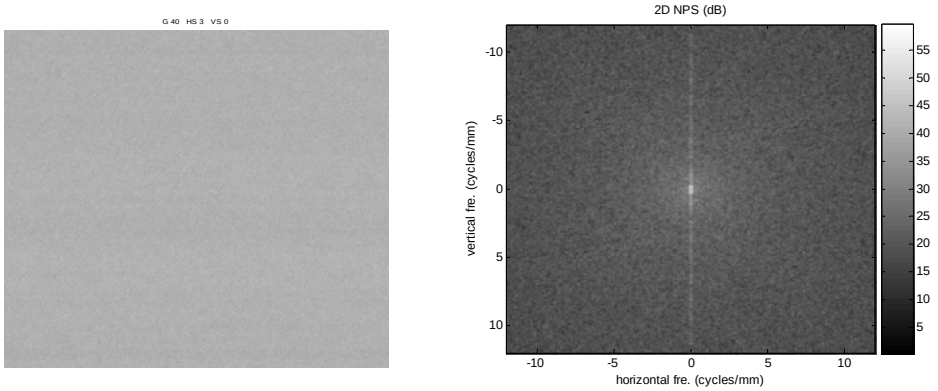

(c)

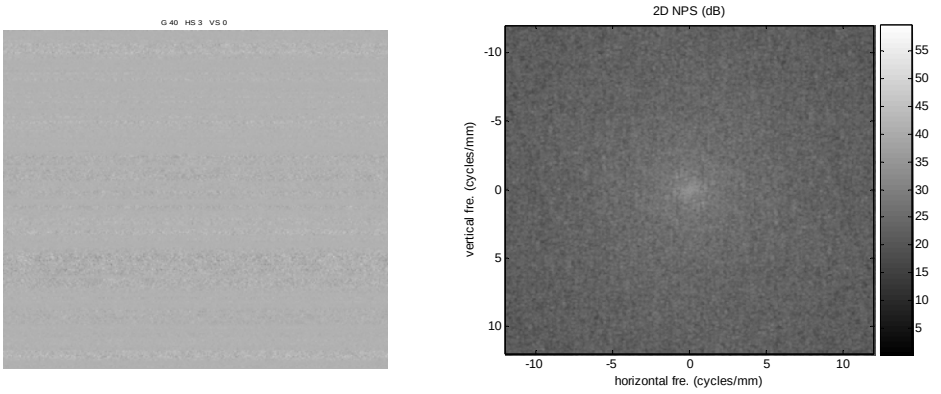

(d)

Figure 4.9 (a) 2D NPS of K50 test pattern (b) Vertical Profiles of real NPS, additive, and multiplicative results (c) Additive image in space domain (left) and 2D NPS (right) (d) Multiplicative image in space domain (left) and 2D NPS (right) of simulated graininess and horizontal streaking from first inkjet printer with arbitrary amplitudes

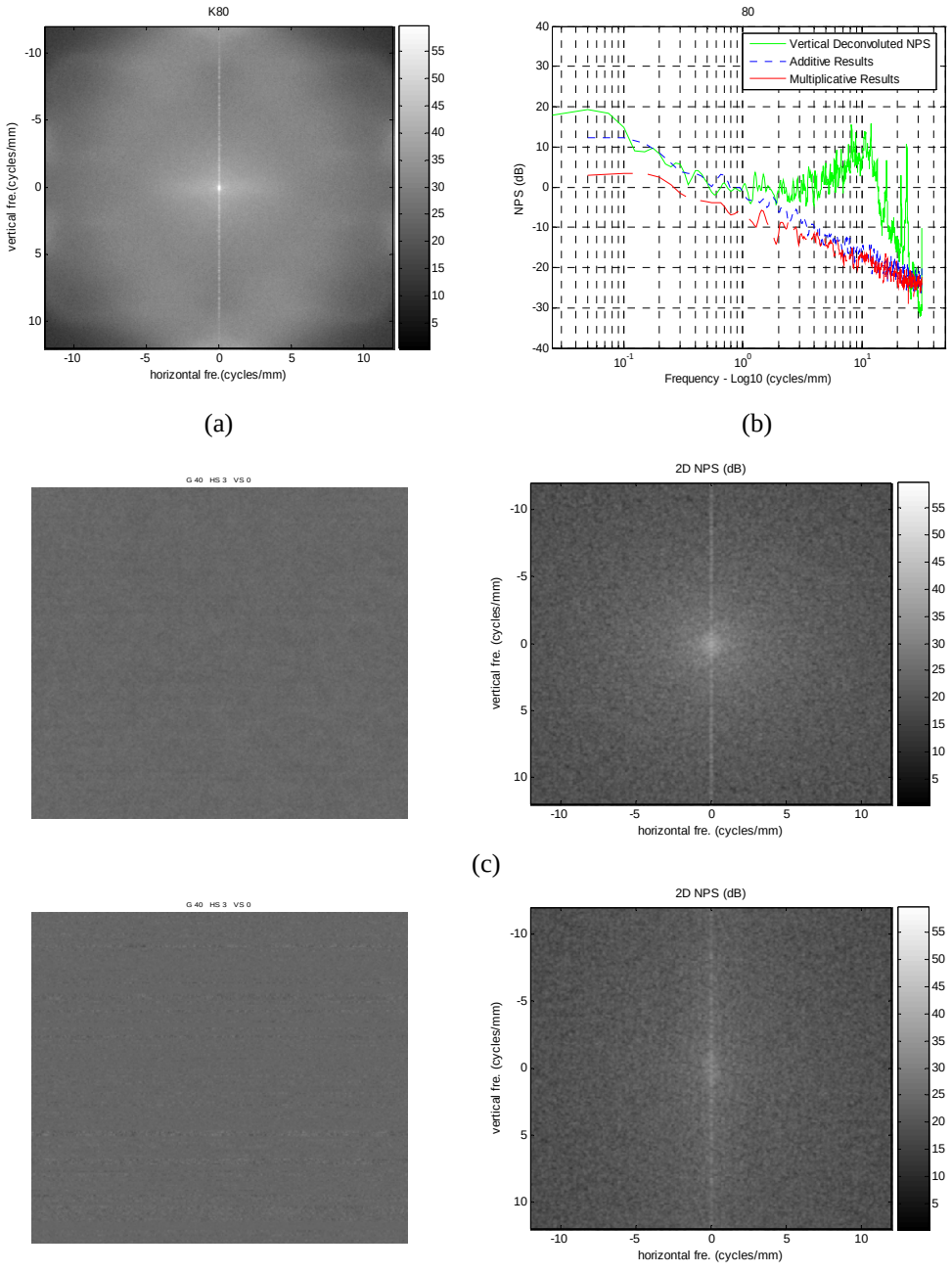

Figure 4.10 (a) 2D NPS of K80 test pattern (b) Vertical Profiles of real NPS, additive, and multiplicative results (c) Additive image in space domain (left) and 2D NPS (right) (d) Multiplicative image in space domain (left) and 2D NPS (right) of simulated graininess and horizontal streaking from first inkjet printer with arbitrary amplitudes

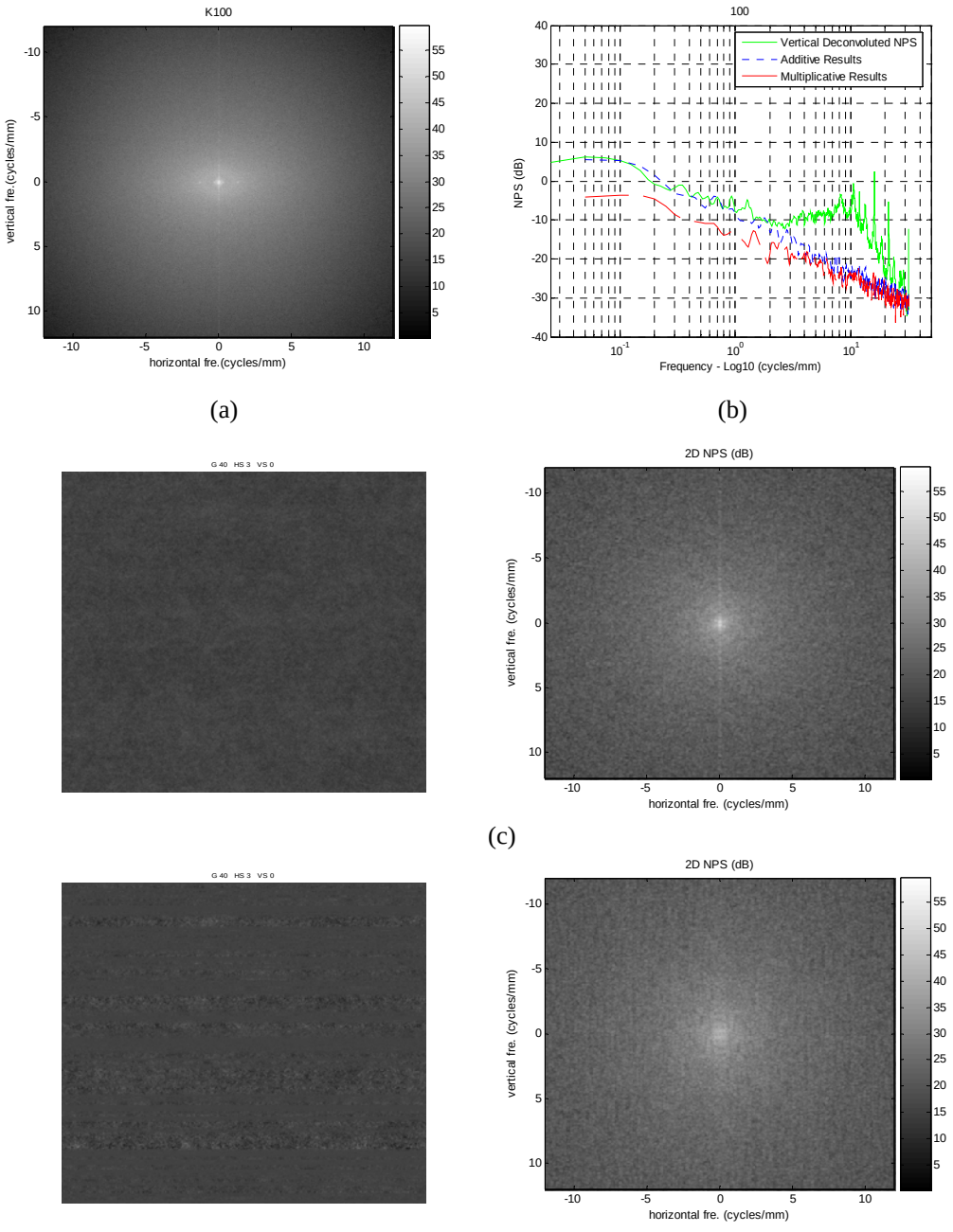

Figure 4.11 (a) 2D NPS of K100 test pattern (b) Vertical Profiles of real NPS, additive, and multiplicative results (c) Additive image in space domain (left) and 2D NPS (right) (d) Multiplicative image in space domain (left) and 2D NPS (right) of simulated graininess and horizontal streaking from first inkjet printer with arbitrary amplitudes

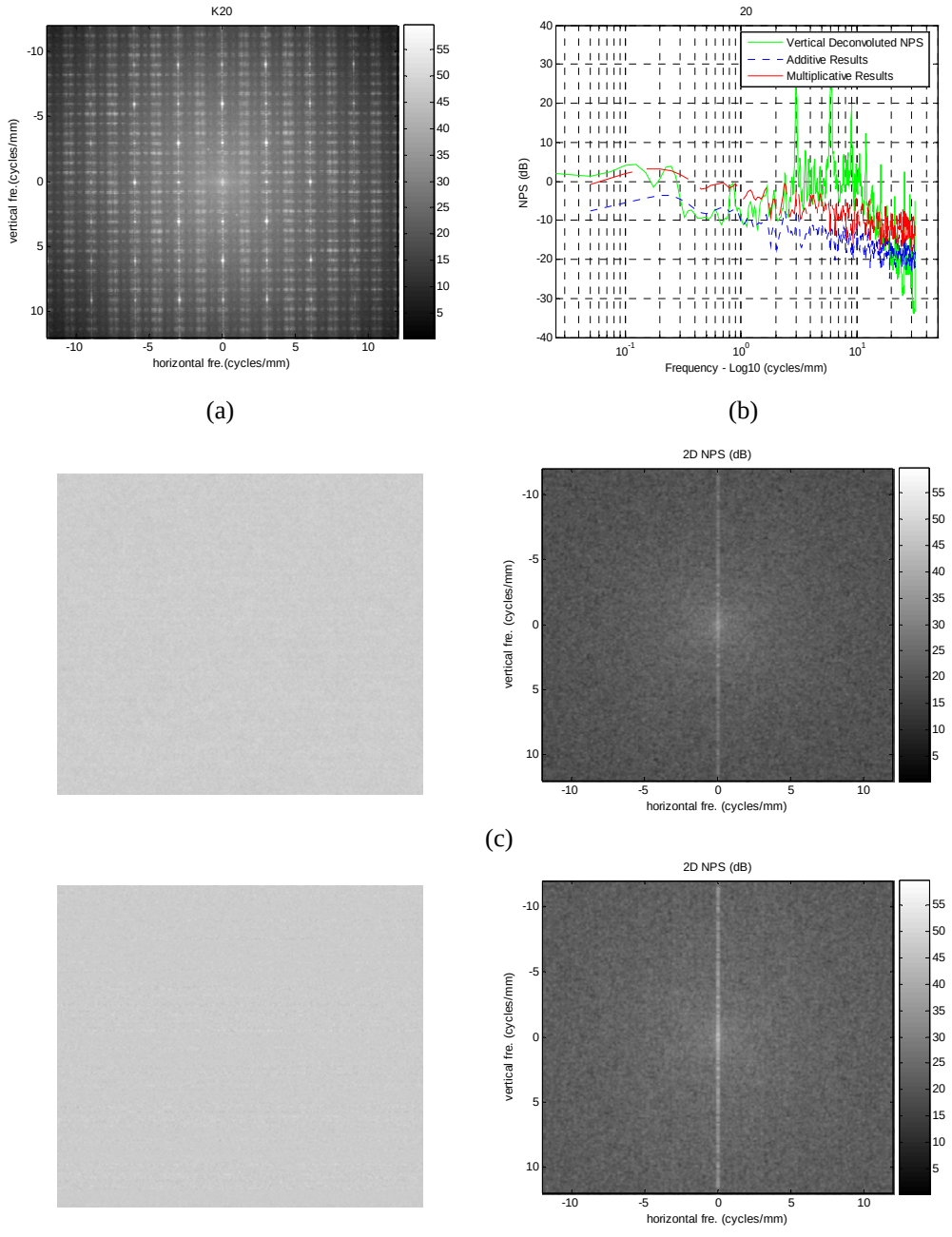

Figure 4.12 (a) 2D NPS of K20 test pattern (b) Vertical Profiles of real NPS, additive, and multiplicative results (c) Additive image in space domain (left) and 2D NPS (right) (d) Multiplicative image in space domain (left) and 2D NPS (right) of simulated graininess and horizontal streaking from second inkjet printer with arbitrary amplitudes

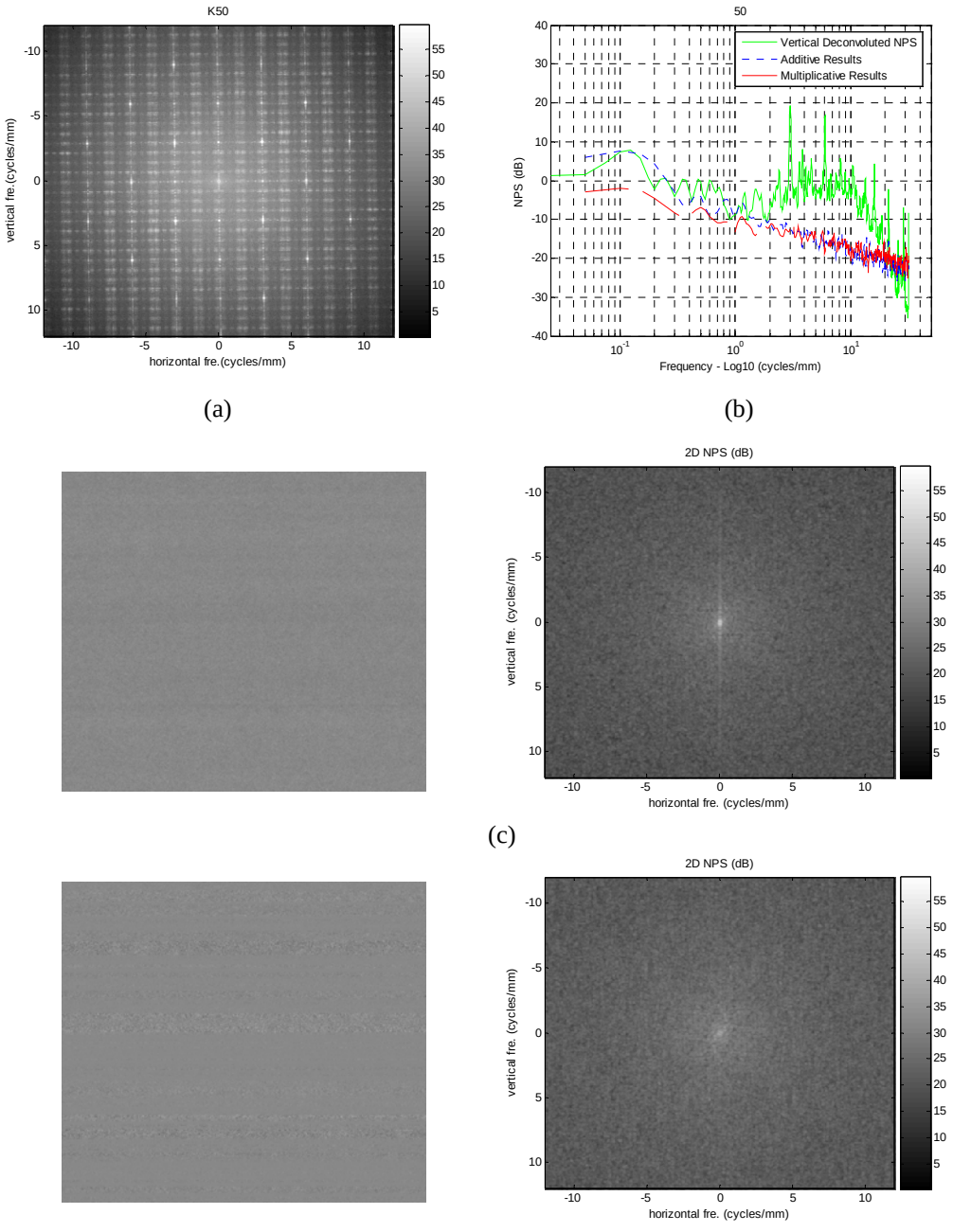

Figure 4.13 (a) 2D NPS of K50 test pattern (b) Vertical Profiles of real NPS, additive, and multiplicative results (c) Additive image in space domain (left) and 2D NPS (right) (d) Multiplicative image in space domain (left) and 2D NPS (right) of simulated graininess and horizontal streaking from second inkjet printer with arbitrary amplitudes

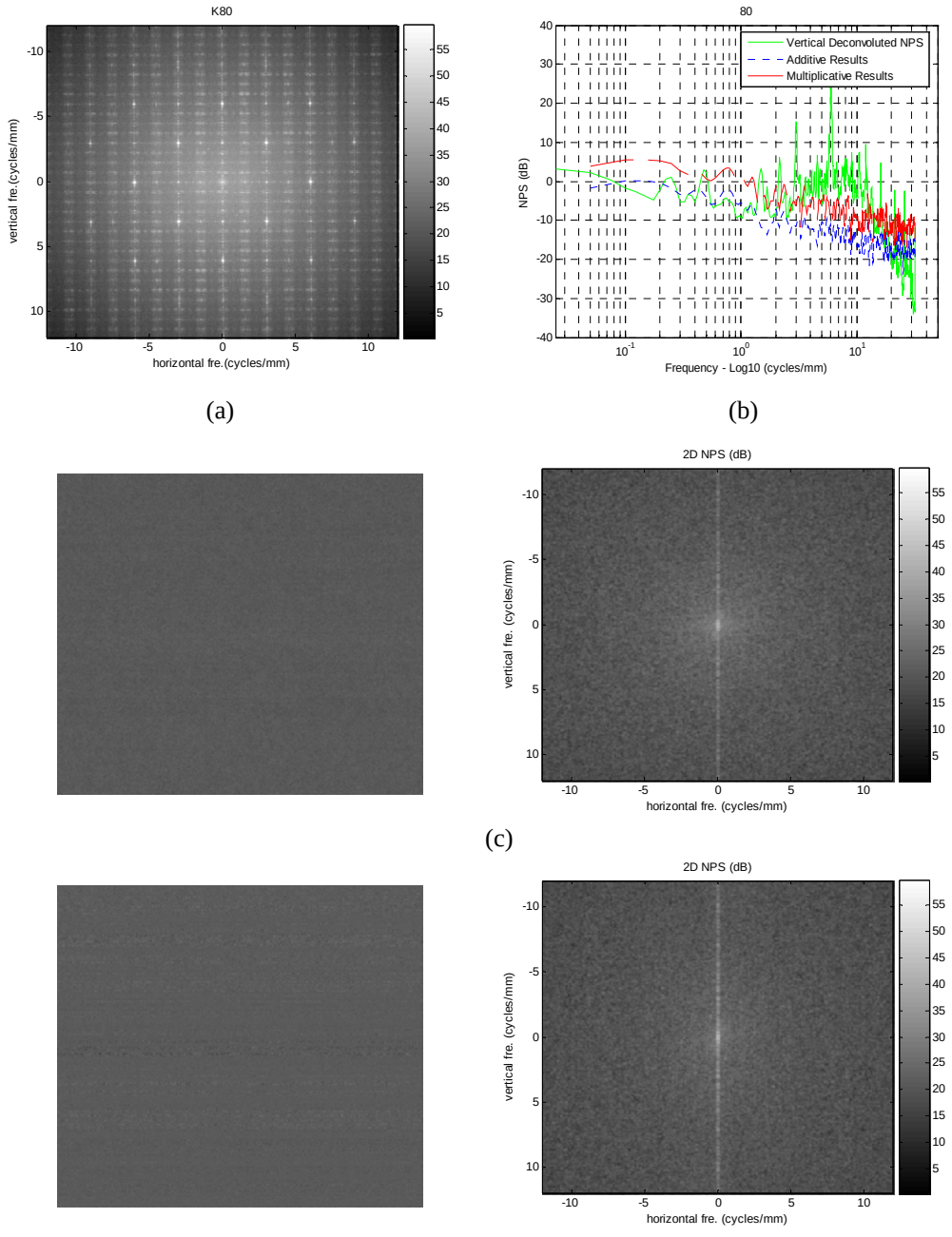

Figure 4.14 (a) 2D NPS of K80 test pattern (b) Vertical Profiles of real NPS, additive, and multiplicative results (c) Additive image in space domain (left) and 2D NPS (right) (d) Multiplicative image in space domain (left) and 2D NPS (right) of simulated graininess and horizontal streaking from second inkjet printer with arbitrary amplitudes

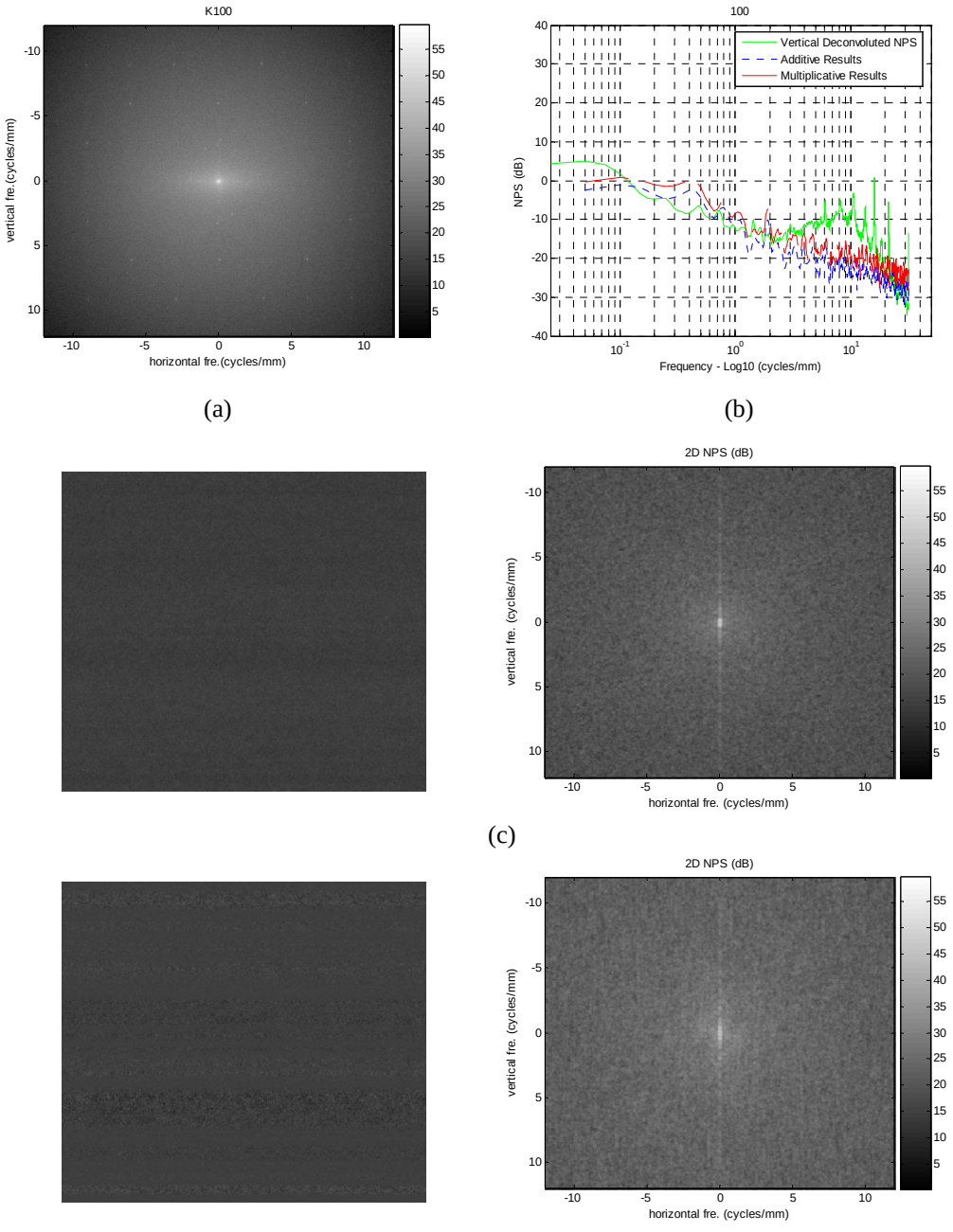

Figure 4.15 (a) 2D NPS of K100 test pattern (b) Vertical Profiles of real NPS, additive, and multiplicative results (c) Additive image in space domain (left) and 2D NPS (right) (d) Multiplicative image in space domain (left) and 2D NPS (right) of simulated graininess and horizontal streaking from second inkjet printer with arbitrary amplitudes

4.2 Additive and Multiplicative Results of Graininess and Banding

This section presents the relationship of graininess and banding defects for first laser and first inkjet printers because there are not any banding artifacts from the second laser and second inkjet printers. The additive results are shown in the Figure 4.16(c)-4.19(c), which left figures are the space results and right figures are the spectral results of banding and graininess artifacts of K20, K50, K80, and K100 test samples, respectively. In addition, Figure 4.16(d)-4.19(d) are the multiplicative results of same configuration for the first laser printer. Using the same method previous section, we compared the real NPS, i.e., Figure 4.16(a)-4.19(a), with the additive and multiplicative NPS. From Equation (3-2), the multiplicative model includes the additive model and the multiplicative component of the graininess and banding artifacts. If the multiplicative value of graininess and banding did not affect to the simulated NPS of multiplicative model, this multiplicative model will be closed to the additive model. For the K20, K50, and K80 results, the additive model is enough to close to the real NPS because there is a little multiplicative component that is just a random noise as shown in the Figure 4.16(d)-4.18(d). For K100 result, the banding artifact was reduced by the multiplicative energy, but this is also not look like to real NPS.

The results of graininess and banding defects from first inkjet printer are shown in the Figure 4.20-4.23. Figure 4.20(a)-4.23(a) are the real NPS, and the additive results are shown in the Figure 4.20(c)-4.23(c), which left figures are the space results and right figures are the spectral results of banding and graininess artifacts of K20, K50, K80, and K100 test samples, respectively. In addition, Figure 4.20(d)-4.23(d) are the multiplicative results of same configuration for the first inkjet printer. At the multiplicative model, the

banding defect (periodic component) disappears at the both (special and spectral) domain. However, the real banding defect has not affect on the graininess, and it is most likely to the additive model.

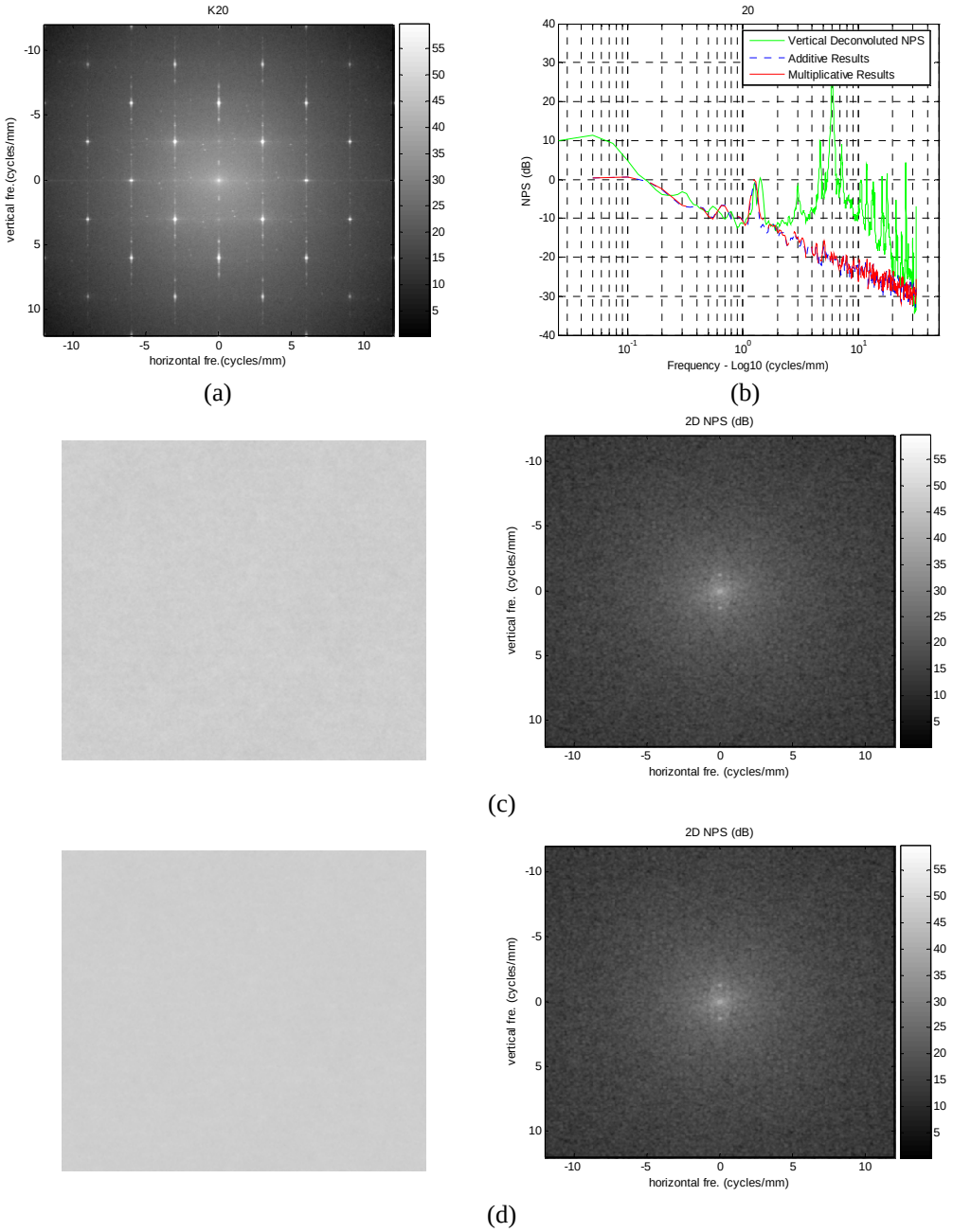

Figure 4.16 (a) 2D NPS of K20 test pattern (b) Vertical Profiles of real NPS, additive, and multiplicative results (c) Additive image in space domain (left) and 2D NPS (right) (d) Multiplicative image in space domain (left) and 2D NPS (right) of simulated graininess and vertical banding from first laser printer with appropriate amplitudes

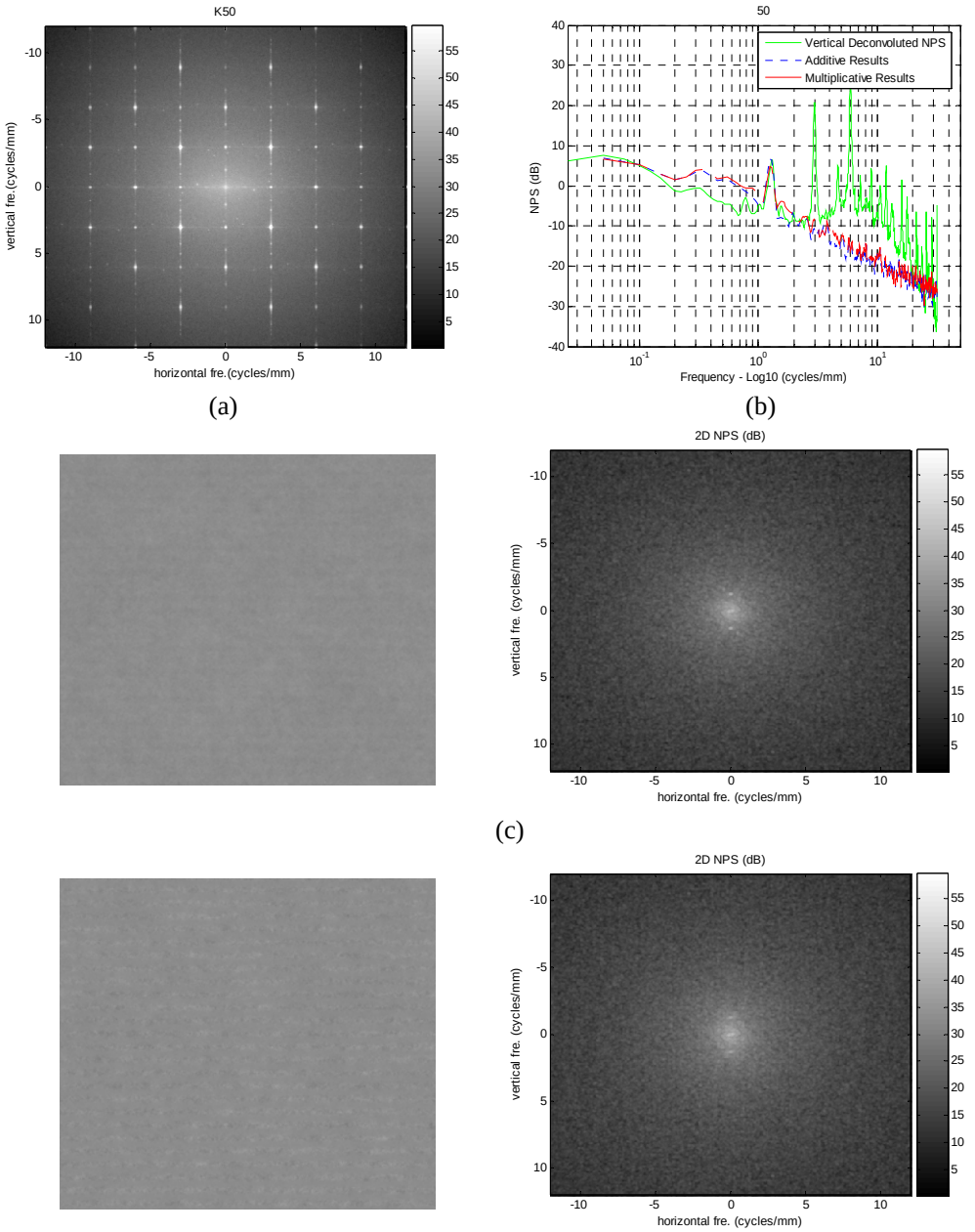

Figure 4.17 (a) 2D NPS of K50 test pattern (b) Vertical Profiles of real NPS, additive, and multiplicative results (c) Additive image in space domain (left) and 2D NPS (right) (d) Multiplicative image in space domain (left) and 2D NPS (right) of simulated graininess and vertical banding from first laser printer with appropriate amplitudes

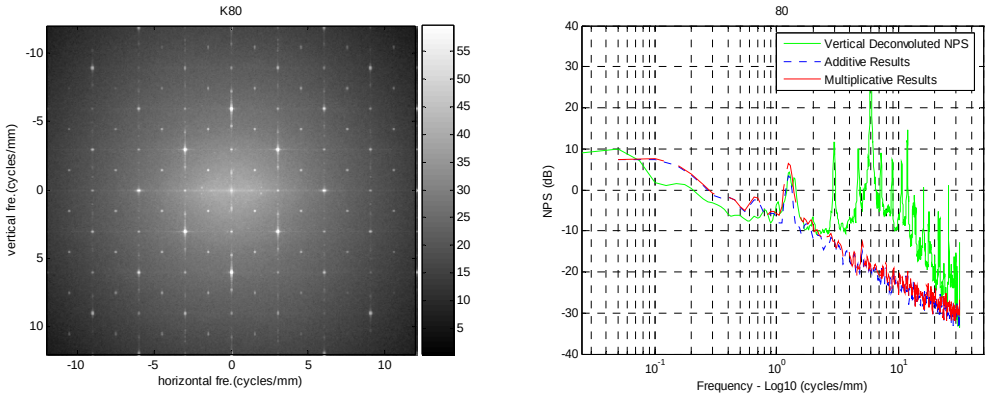

(a)

(b)

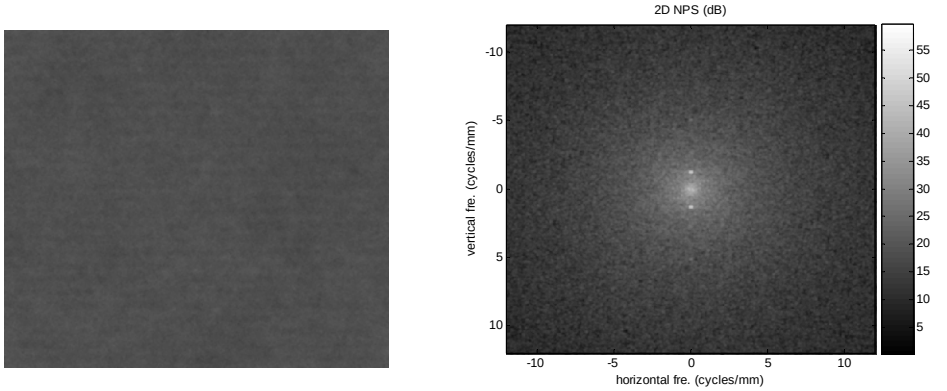

(c)

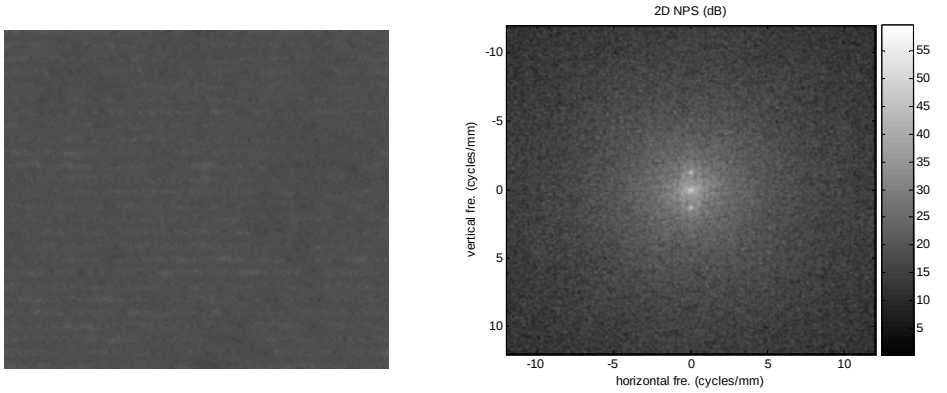

(d)

Figure 4.18 (a) 2D NPS of K80 test pattern (b) Vertical Profiles of real NPS, additive, and multiplicative results (c) Additive image in space domain (left) and 2D NPS (right) (d) Multiplicative image in space domain (left) and 2D NPS (right) of simulated graininess and vertical banding from first laser printer with appropriate amplitudes

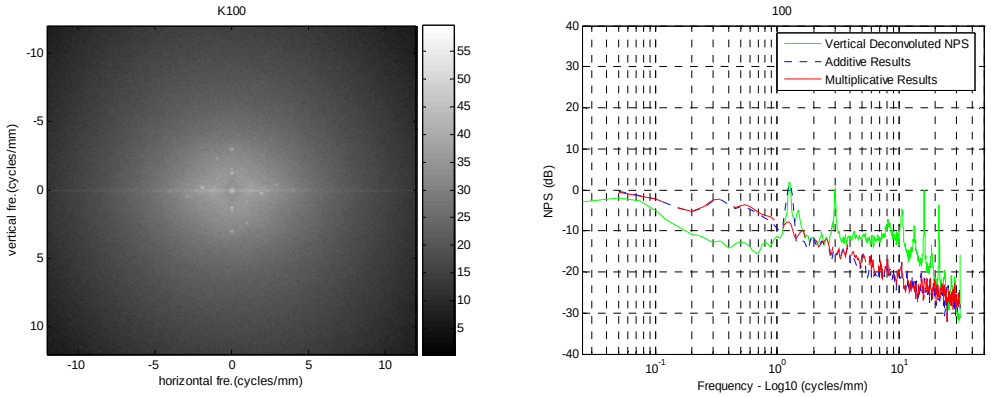

(a)

(b)

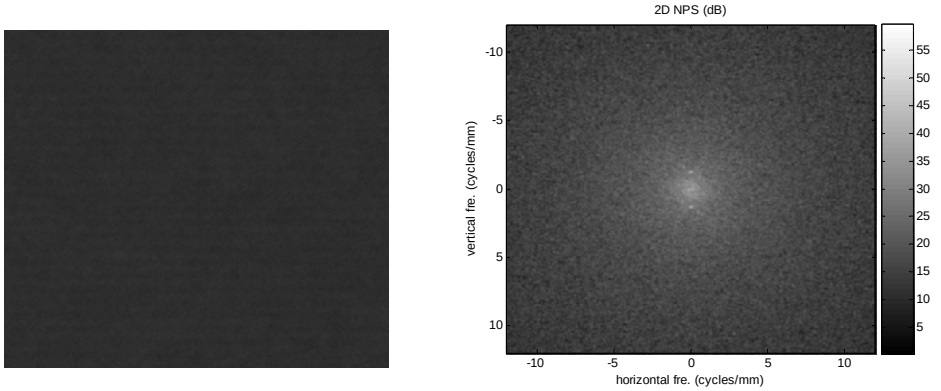

(c)

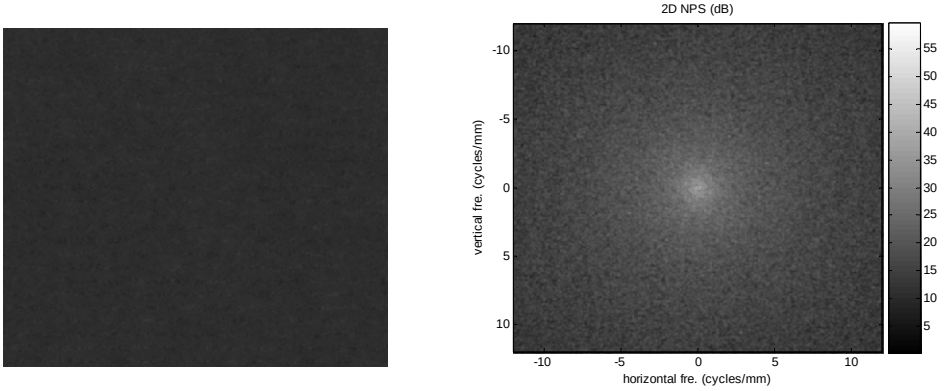

(d)

Figure 4.19 (a) 2D NPS of K100 test pattern (b) Vertical Profiles of real NPS, additive, and multiplicative results (c Additive image in space domain (left) and 2D NPS (right) (d) Multiplicative image in space domain (left) and 2D NPS (right) of simulated graininess and vertical banding from first laser printer with appropriate amplitudes

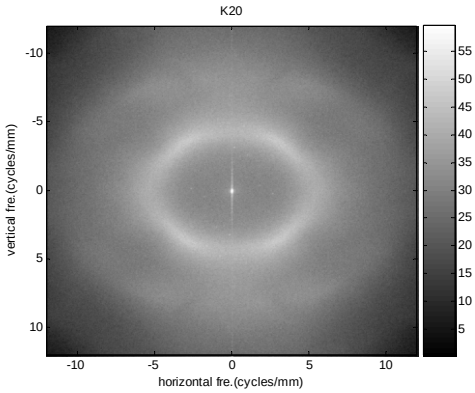

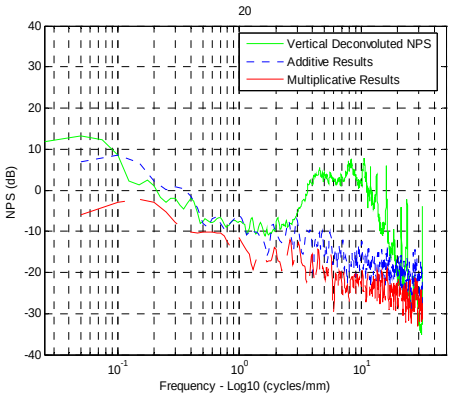

(a) (b)

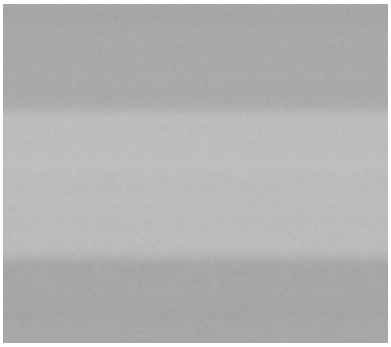

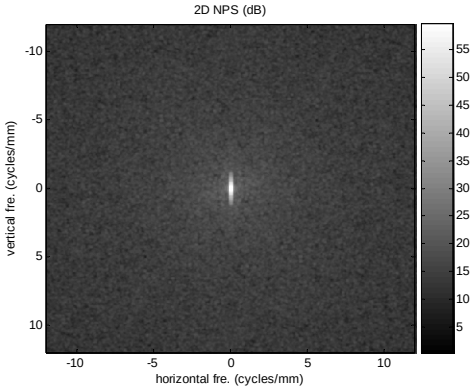

(c)

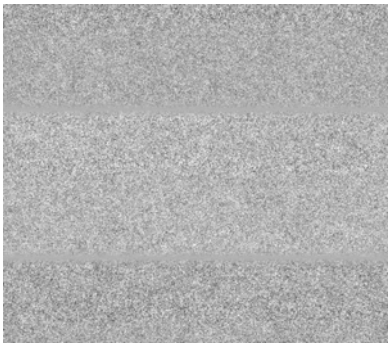

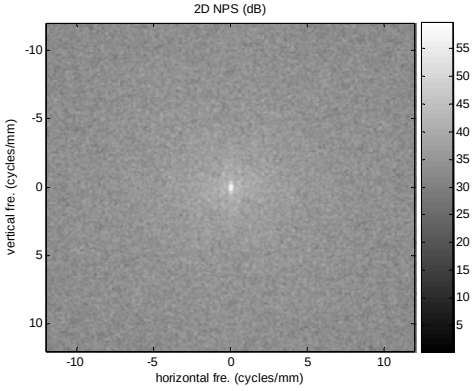

(d)

Figure 4.20 (a) 2D NPS of K20 test pattern (b) Vertical Profiles of real NPS, additive, and multiplicative results (c) Additive image in space domain (left) and 2D NPS (right) (d) Multiplicative image in space domain (left) and 2D NPS (right) of simulated graininess and horizontal banding from first inkjet printer with appropriate amplitudes

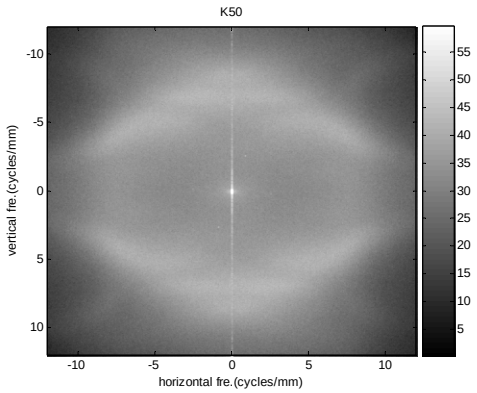

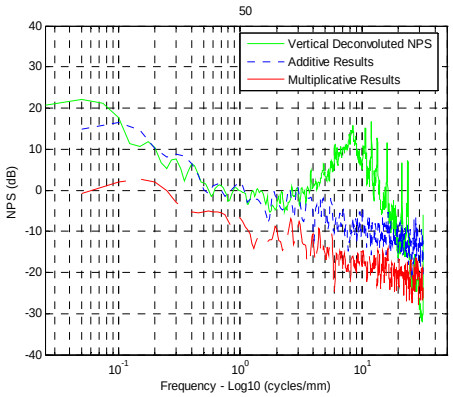

(a) (b)

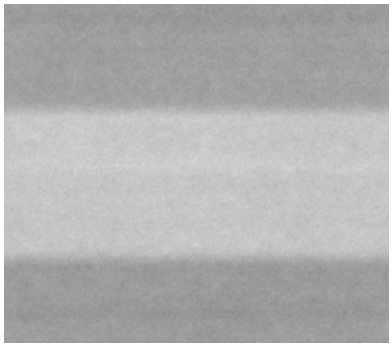

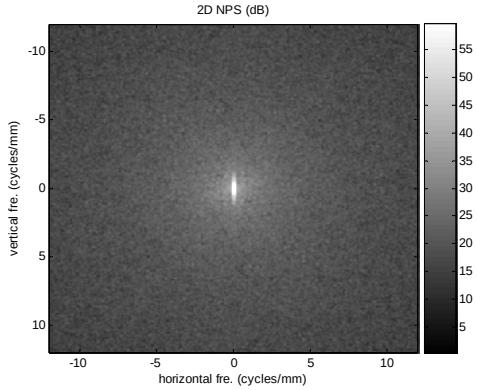

(c)

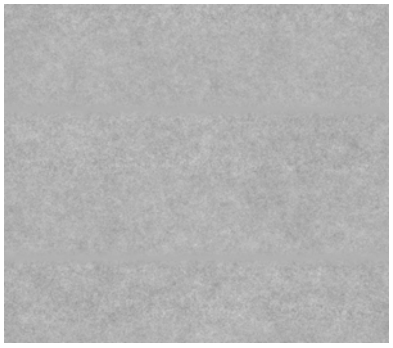

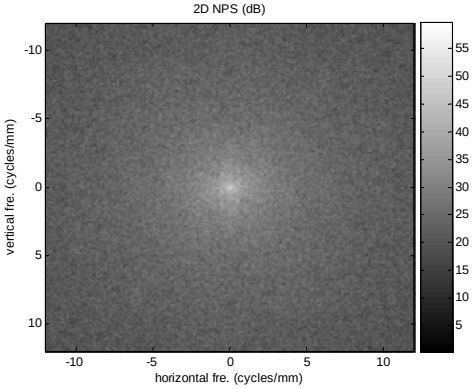

(d)

Figure 4.21 (a) 2D NPS of K50 test pattern (b) Vertical Profiles of real NPS, additive, and multiplicative results (c) Additive image in space domain (left) and 2D NPS (right) (d) Multiplicative image in space domain (left) and 2D NPS (right) of simulated graininess and horizontal banding from first inkjet printer with appropriate amplitudes

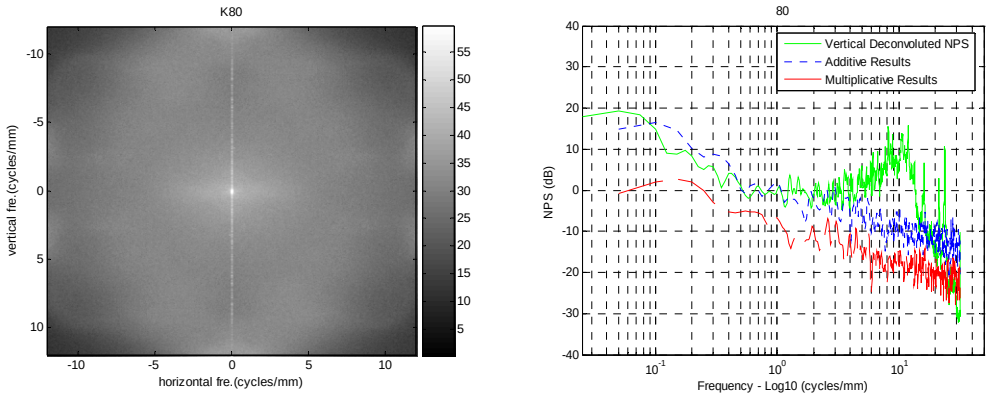

(a) (b)

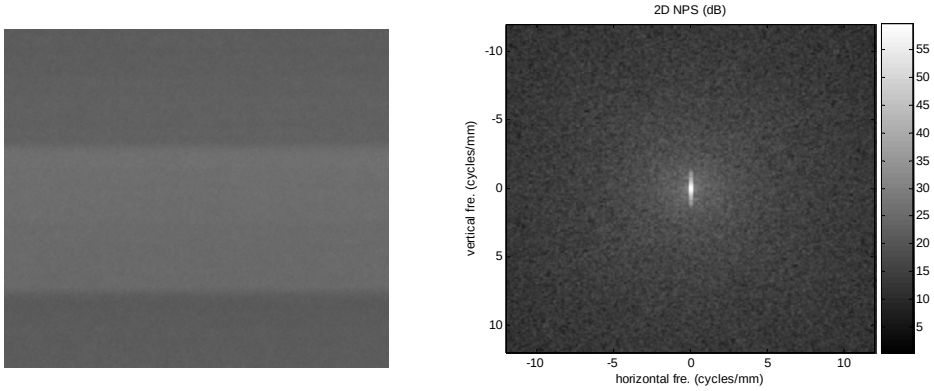

(c)

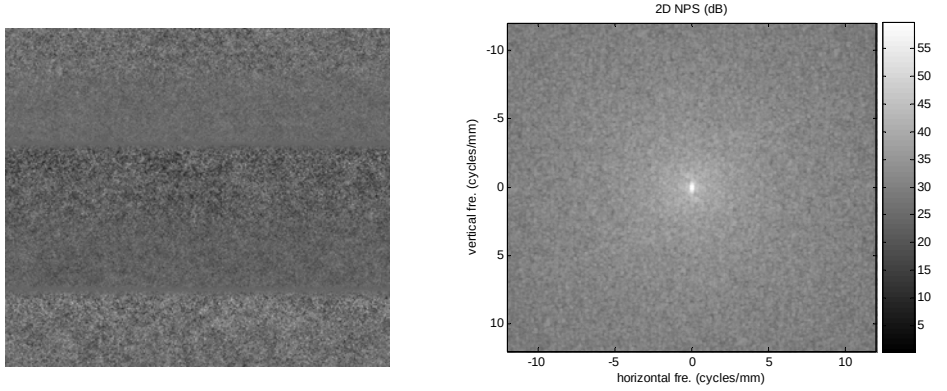

(d)

Figure 4.22 (a) 2D NPS of K80 test pattern (b) Vertical Profiles of real NPS, additive, and multiplicative results (c) Additive image in space domain (left) and 2D NPS (right) (d) Multiplicative image in space domain (left) and 2D NPS (right) of simulated graininess and horizontal banding from first inkjet printer with appropriate amplitudes

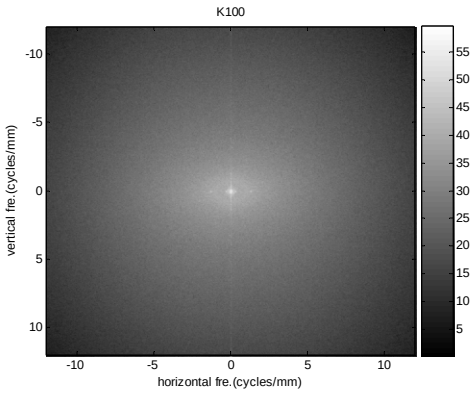

(a)

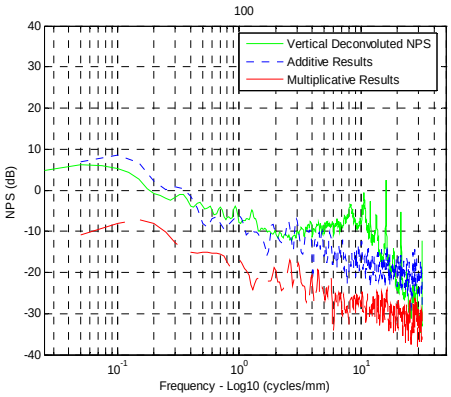

(b)

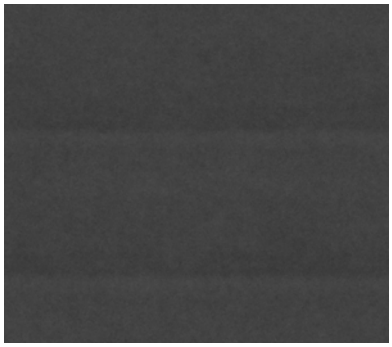

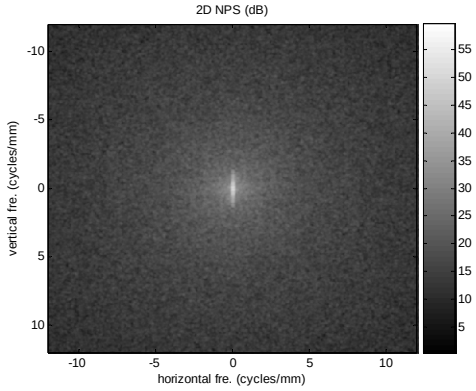

(c)

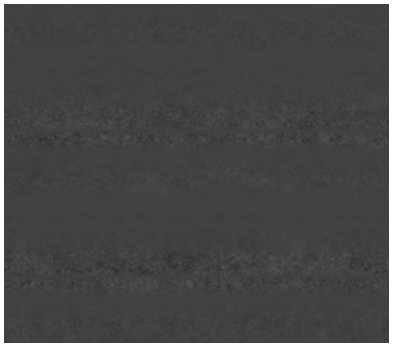

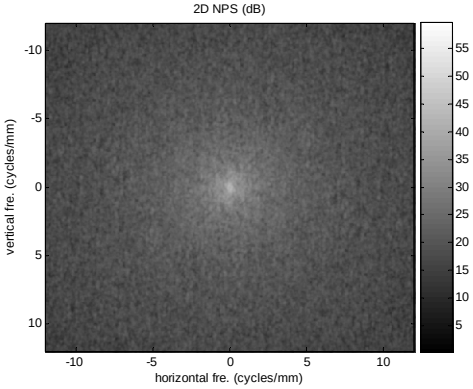

(d)

Figure 4.23 (a) 2D NPS of K100 test pattern (b) Vertical Profiles of real NPS, additive, and multiplicative results (c) Additive image in space domain (left) and 2D NPS (right) (d) Multiplicative image in space domain (left) and 2D NPS (right) of simulated graininess and horizontal banding from first inkjet printer with appropriate amplitudes

4.3 Additive and Multiplicative Results of Banding and Streaking

This section shows the interaction results of banding and streaking defects for first laser and first inkjet printers because there are not any banding artifacts from the second laser and second inkjet printers. As similar to the banding and graininess results, the additive results are shown in the Figure 4.24(c)-4.26(c), which left figures are the space results and right figures are the spectral results of banding and graininess artifacts of K20, K50, K80, and K100 test samples, respectively. In addition, Figure 4.24(d)-4.26(d) are the multiplicative results of same configuration for the first laser printer. Using the same method previous section, we compared the real NPS with the additive and multiplicative NPS. At the multiplicative model, we can see some streaking artifact to move to the banding defect, but the streaking of real NPS is not changed by the banding defect. As similar as graininess, streaking is also seems to the independent to the banding, which looks more close to the additive model of all test samples. In addition, the banding artifact has not been changed in both additive and multiplicative model as shown in Figure 4.24(b)-4.26(b).

Figure 4.27-4.30 present the interaction results of banding and streaking defects from first inkjet printer. The additive results are shown in the Figure 4.27(c)-4.30(c), which left figures are the space results and right figures are the spectral results of banding and graininess artifacts of K20, K50, K80, and K100 test samples, respectively. The multiplicative results are shown in Figure 4.27(d)-4.30(d). The multiplicative results of horizontal banding and streaking look same as only horizontal streaking. In other words, the multiplicative result of periodic and random component is the random value.

Therefore, banding defect is independent to the random streaking, and it is reasonable for additive model to close the real NPS.

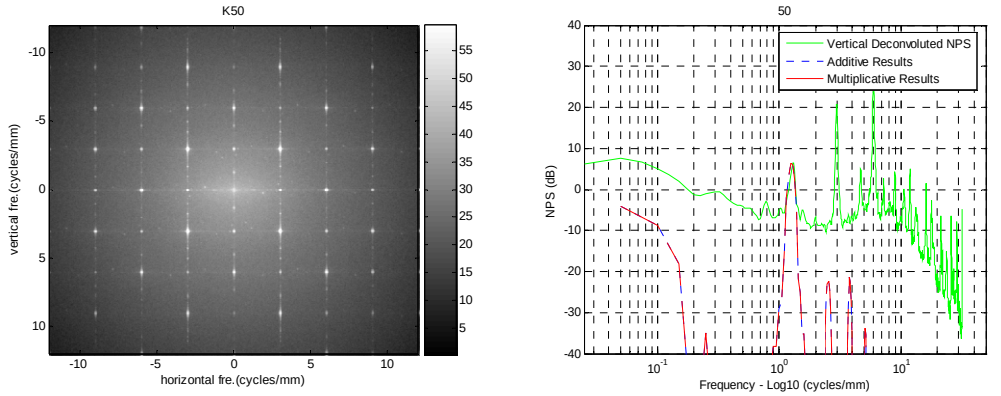

(a)

(b)

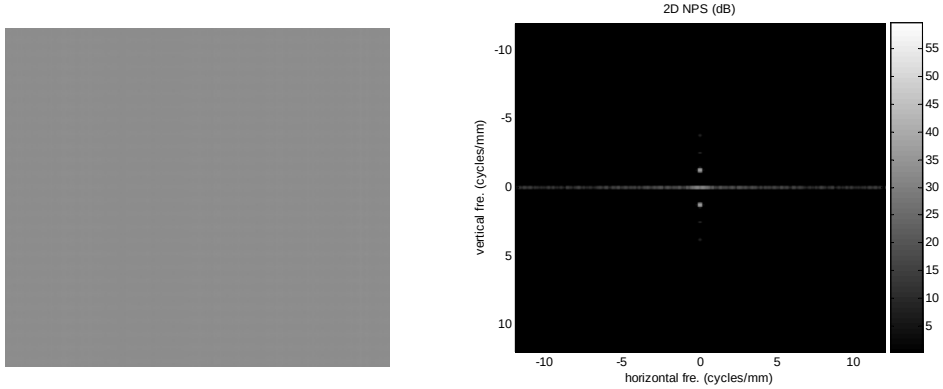

(c)

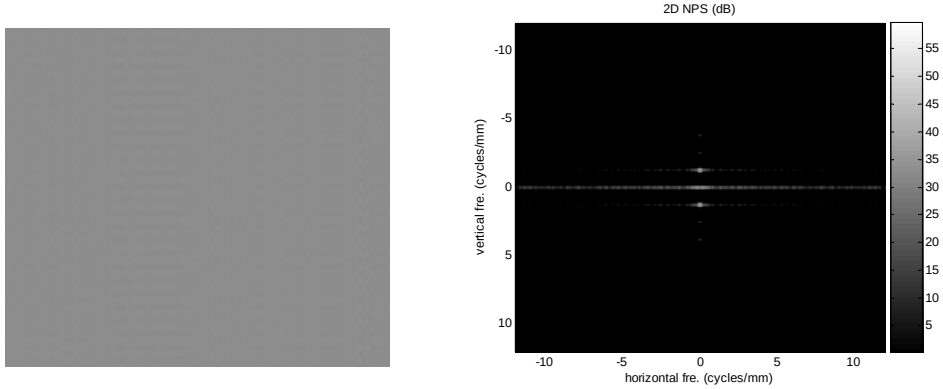

(d)

Figure 4.24 (a) 2D NPS of K50 test pattern (b) Vertical Profiles of real NPS, additive, and multiplicative results (c) Additive image in space domain (left) and 2D NPS (right) (d) Multiplicative image in space domain (left) and 2D NPS (right) of simulated vertical banding and vertical streaking from first laser printer with appropriate amplitudes

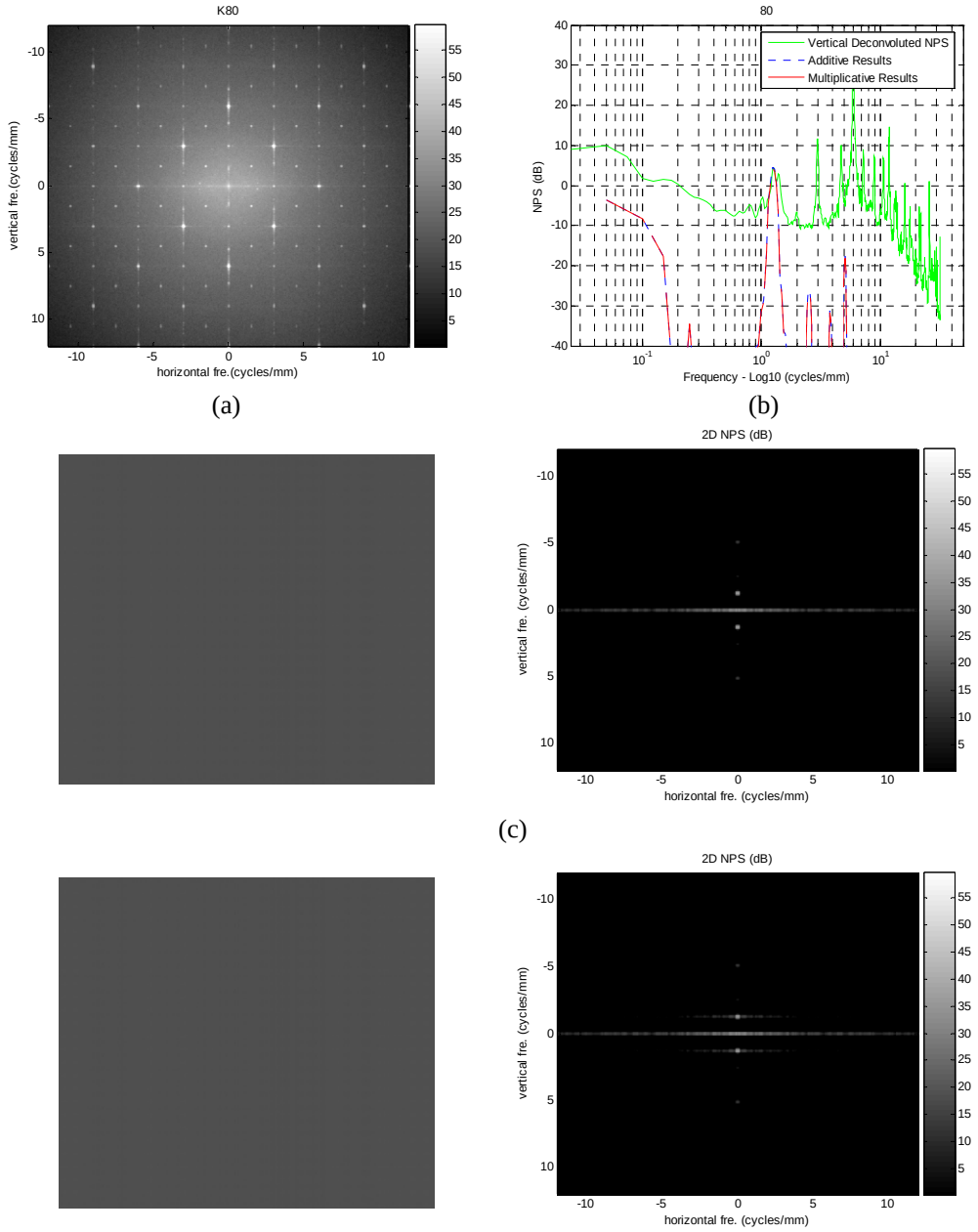

Figure 4.25 (a) 2D NPS of K80 test pattern (b) Vertical Profiles of real NPS, additive, and multiplicative results (c) Additive image in space domain (left) and 2D NPS (right) (d) Multiplicative image in space domain (left) and 2D NPS (right) of simulated vertical banding and vertical streaking from first laser printer with appropriate amplitudes

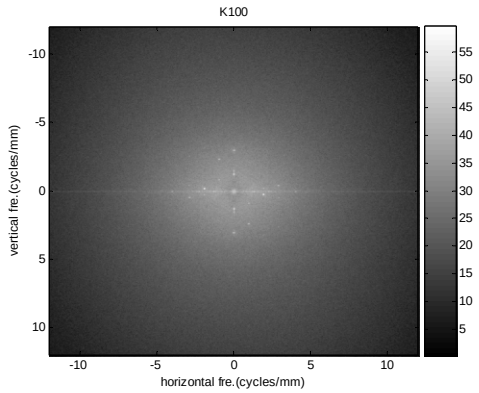

(a)

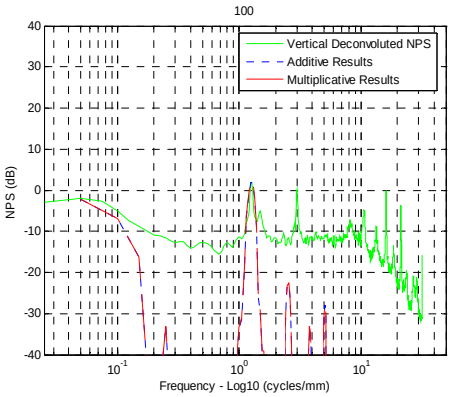

(b)

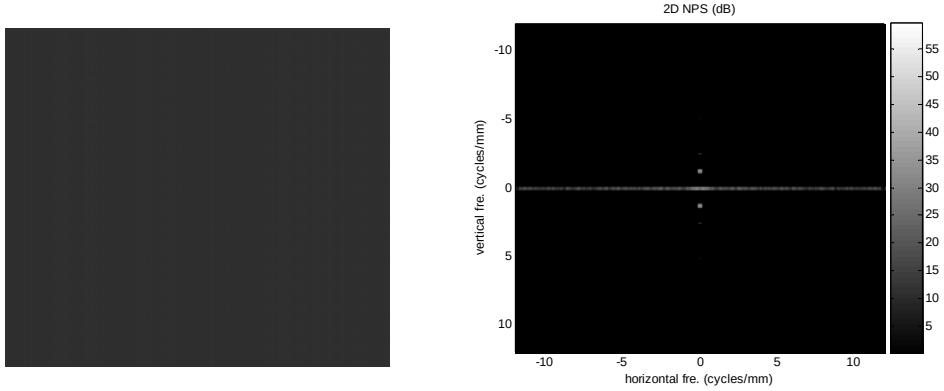

(c)

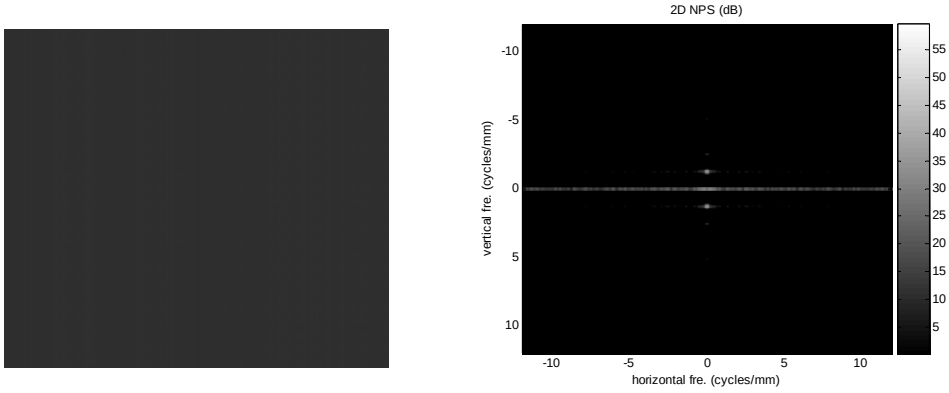

(d)

Figure 4.26 (a) 2D NPS of K100 test pattern (b) Vertical Profiles of real NPS, additive, and multiplicative results (c) Additive image in space domain (left) and 2D NPS (right) (d) Multiplicative image in space domain (left) and 2D NPS (right) of simulated vertical banding and vertical streaking from first laser printer with appropriate amplitudes

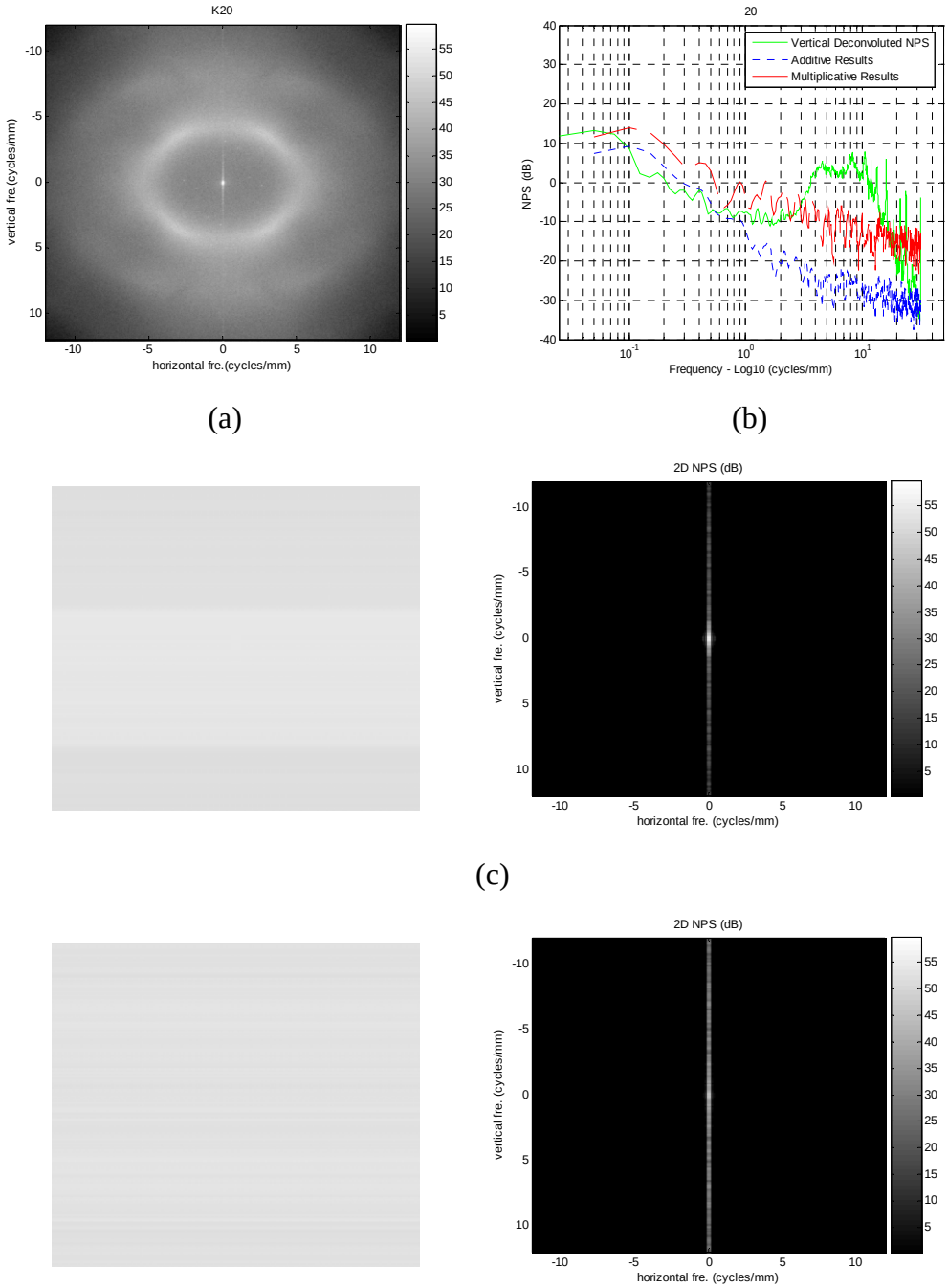

Figure 4.27 (a) 2D NPS of K20 test pattern (b) Vertical Profiles of real NPS, additive, and multiplicative results (c) Additive image in space domain (left) and 2D NPS (right) (d) Multiplicative image in space domain (left) and 2D NPS (right) of simulated horizontal banding and horizontal streaking from first laser printer with appropriate amplitudes

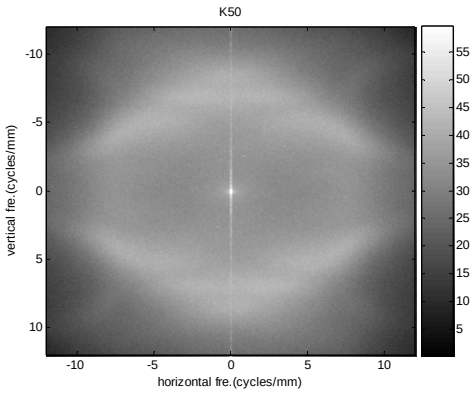

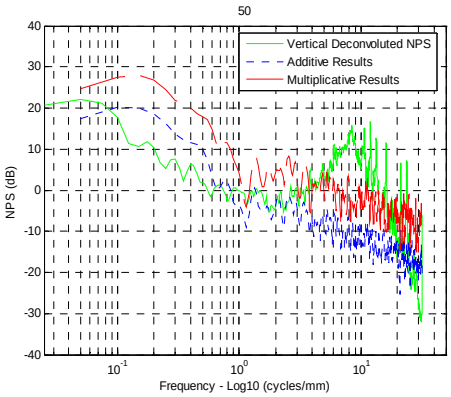

(a) (b)

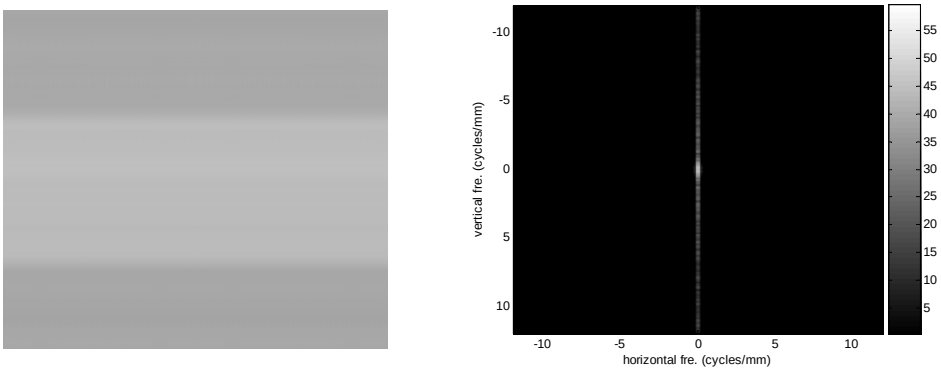

(c)

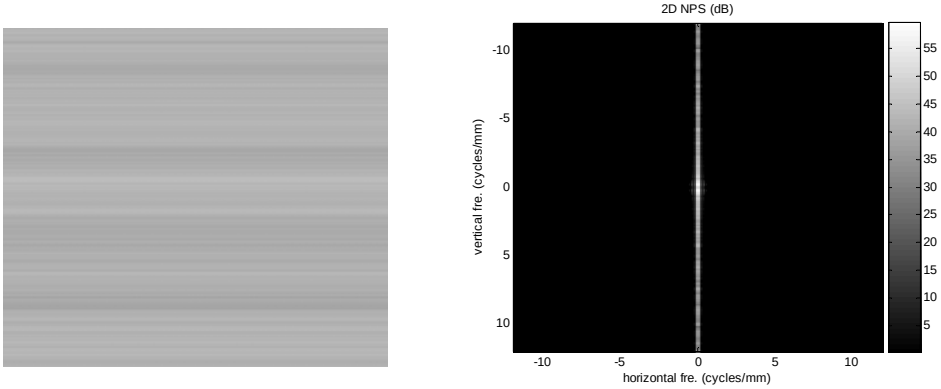

(d)

Figure 4.28 (a) 2D NPS of K50 test pattern (b) Vertical Profiles of real NPS, additive, and multiplicative results (c) Additive image in space domain (left) and 2D NPS (right) (d) Multiplicative image in space domain (left) and 2D NPS (right) of simulated horizontal banding and horizontal streaking from first laser printer with appropriate amplitudes

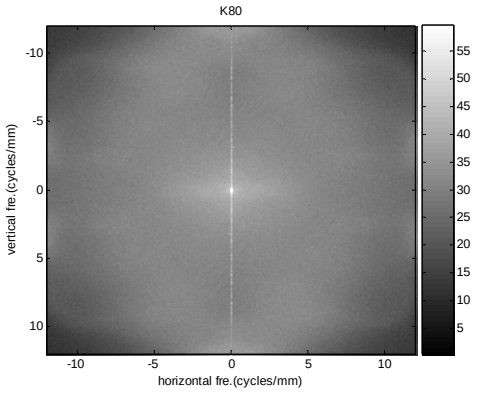

(a)

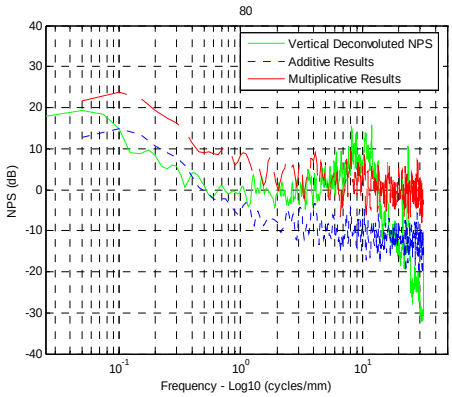

(b)

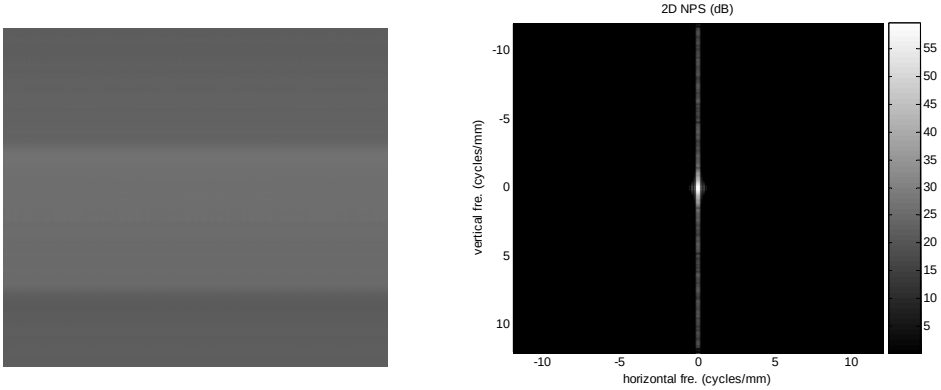

(c)

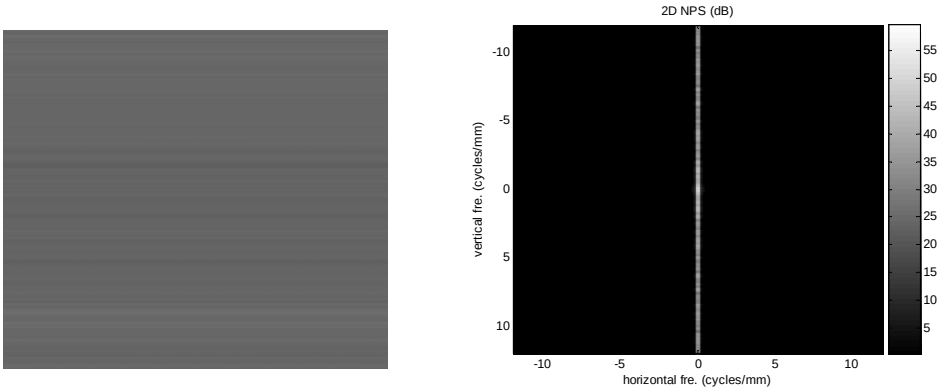

(d)

Figure 4.29 (a) 2D NPS of K80 test pattern (b) Vertical Profiles of real NPS, additive, and multiplicative results (c) Additive image in space domain (left) and 2D NPS (right) (d) Multiplicative image in space domain (left) and 2D NPS (right) of simulated horizontal banding and horizontal streaking from first laser printer with appropriate amplitudes

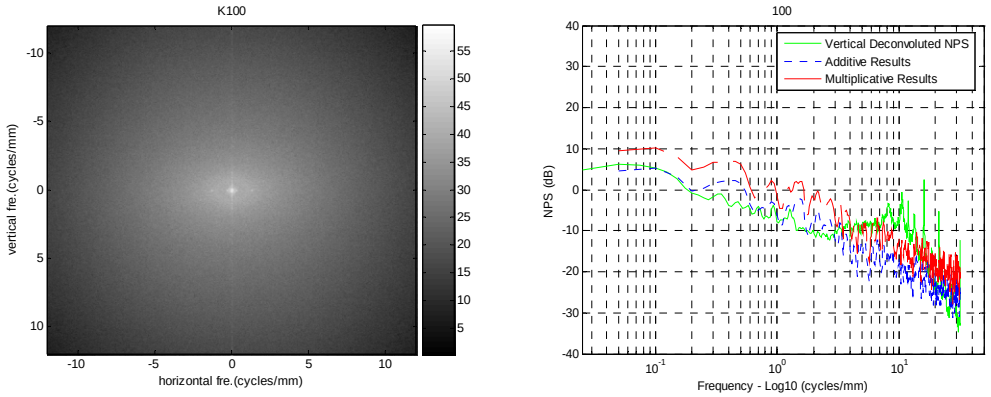

(a) (b)

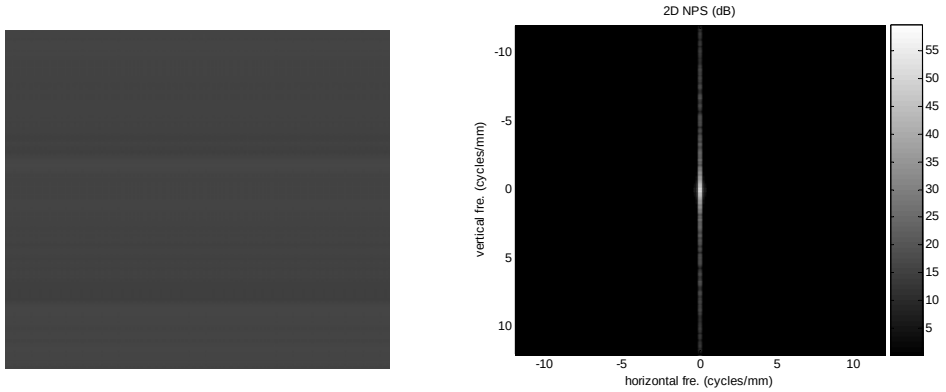

(c)

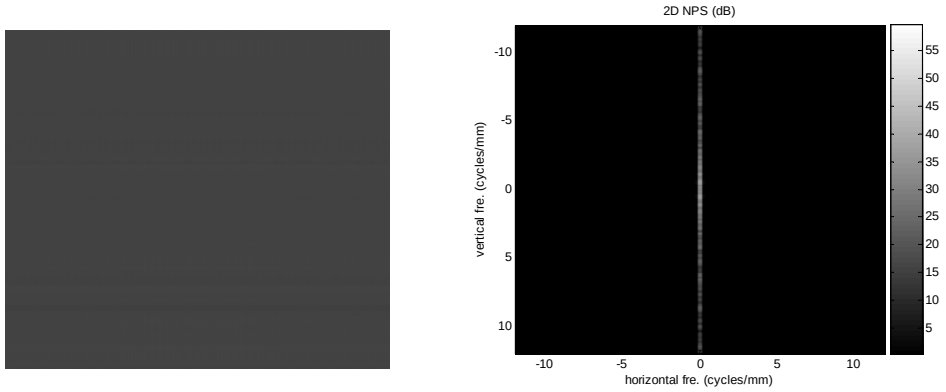

(d)

Figure 4.30 (a) 2D NPS of K100 test pattern (b) Vertical Profiles of real NPS, additive, and multiplicative results (c) Additive image in space domain (left) and 2D NPS (right) (d) Multiplicative image in space domain (left) and 2D NPS (right) of simulated horizontal banding and horizontal streaking from first laser printer with appropriate amplitudes

CHAPTER 5

Conclusions and Future Work

The chapter focuses on the contributions made and the inferences that can be derived based on the results of additive and multiplicative test of simulated printer defects. The summary and conclusion of the two suggested test models are discussed on section 5.1. Section 5.2 describes the possible future research directions and suggestions for print quality evaluations.

5.1 Summary and Conclusions

The objective of this thesis was to determine the interactive relationships of print defect patterns such as graininess, streaking, and banding under flat-field hardcopy outputs. The characterization tool used in this work was the power spectral density (PSD) of flat-field printer outputs. The additive and multiplicative models were considered for describing the interaction between printer defects. Simulated print defect patterns and metrics based on the NPS were use to demonstrate the patterns generated by multiplicative and additive processes. These results were compared the noise power spectrum (NPS) of actual flat-field prints from digital printers (two laser printers and two inkjet printers) to draw conclusion concerning actual artifact interaction.

The result of graininess and streaking artifacts was an additive interaction. The reason is that the shape of graininess in multiplicative model has changed by the streaking artifact. However, the graininess of real NPS does not change their shape, and in other words, the graininess of real NPS has not affect on the streaking artifact. Therefore, the interaction

of the graininess and streaking artifacts is more appropriate additive than multiplicative relationship.

The result of graininess and banding artifacts was an additive interaction. At the multiplicative model, we found out there is no multiplicative components in the results of first laser printer and the banding defect (periodic component) disappears at the both (special and spectral) domain in the results of first inkjet printer. Furthermore, graininess is seems to the independent to the banding, which is look to more close to the additive model of all test images.

The result of banding and streaking artifacts was an additive interaction. At the multiplicative model, we found out some streaking energy to move to the location of the banding defect, but the streaking of real NPS is not changed by the banding defect. As similar as graininess, streaking is also seems to the independent to the banding, which looks more close to the additive model of all test samples.

5.2 Future Work

The contribution of this thesis focused on finding the interaction between printer defects that affect uniformity such as graininess, streaking, and banding, and being able to model these interactions in the NPS. There are two different types of uniformity such as Macro-uniformity and Micro-uniformity. The contributors of Macro-uniformity are streaks, bands, mottle, gradients, moiré, etc and the contributors of Micro-uniformity are streaks, bands, voids, mottle, granularity, textures, noise, etc. An understanding of the interaction of many different contributors of uniformity could lead to better models for combining metrics for perceptual scoring of image quality. In addition, some other multiplicative

models also need to consider comparing an additive model with automatic and systemic method.

APPENDIX

A: The Properties of Printers

A-1 The Properties of First Inkjet Printer

Property	Setting
Print Quality (mode)	Normal (300 * 300 dpi)
Paper Setting	Plain Paper
Paper Size	Letter [8.5 * 11 in.]
Orientation	Portrait
Print in Grayscale	Black Inks only for test patterns
Saturation	50% (Muted – Vibrant)
Brightness	50% (Darker – Lighter)
Ink Volume	50 % (Light – Heavy)

A-2 The Properties of Second Inkjet Printer

Property	Setting
Print Quality (mode)	Normal (300 * 300 dpi)
Paper Setting	Plain Paper
Paper Size	Letter [8.5 * 11 in.]
Orientation	Portrait
Print in Grayscale	Black Inks only for test patterns
Shading (Halftone)	Auto
Brightness	50% (Darker – Lighter)
Contrast	50 % (Light – Heavy)

A-3 The Properties of First Laser Printer

Property	Setting
Print Quality (mode)	Normal (600 * 600 dpi)
Paper Setting	Plain Paper
Paper Size	Letter [8.5 * 11 in.]
Orientation	Portrait
Print in Grayscale	Black Inks only for test patterns
Saturation	50% (Muted – Vibrant)
Brightness	50% (Darker – Lighter)
Ink Volume	50 % (Light – Heavy)

A-4 The Properties of Second Laser Printer

Property	Setting
Print Quality (mode)	Normal (600 * 600 dpi)
Paper Setting	Plain Paper
Paper Size	Letter [8.5 * 11 in.]
Orientation	Portrait
Print in Grayscale	Black Inks only for test patterns
Shading (Halftone)	Auto
Brightness	50% (Darker – Lighter)
Contrast	50 % (Light – Heavy)

B: The Properties of Scanners

B-1 The Properties of Flatbed Scanner (Epson 1650)

Property	Setting
Image type	Color Photo → Pixel Depth : 24-bit color
Destination	EPSON Stylus Printer (Photo)
Resolution	300, 600, 1300, and 1600dpi
Source (ROI)	80 mm * 80 mm (Figure 2.2)
Scale	100%
Exposure	0
Gamma	1.8
Highlight	246
Shadow	40
Tone correction	Linear
Gray Balance Intensity	100
Saturation	0

REFERENCES

1. Brian Keelan, Handbook of Image Quality, Marcel Dekker, Inc., 2002.
2. International Standard ISO/IEC 13660:2001.
3. The Print Quality Toolkit: An Integrated Print Quality Assessment Tool.
4. International Committee for Information Technology Standards (INCITS) W1.1 – Image Quality for Printer System. Available from: <http://www.incits.org/tc_home/w11htm/incits_w11.htm >
5. B.Girod, “What’s wrong with Mean-squared Error”, Digital Images and Human Vision, A. B. Watson (Ed.), Chapter 15, MIT Press, 1993, pg. 207-220.
6. B. A. Wandell, Foundations of Vision, Sinauer Associates, Inc., 1995.
7. A. B. Poirson, and B. A. Wandell, “Appearance of colored patterns: pattern-color separability”, Journal of Optical society America A, vol. 10, no. 12, Dec. 1993, pg. 2458-2470.
8. A. B. Poirson, and B. A. Wandell, “Pattern-color separable pathways predict sensitivity to simple colored patterns”, Vision research, vol.36, no. 4, 1996, pg. 515-526.
9. C. M. Bird, G. B. Hemming, F. A. Wichmann, “Contrast discrimination with sinusoidal gratings of different spatial frequency”, Journal of Optical Society of America, vol.19, no.7, July 2002, pg. 1267-1273.
10. A. B. Watson, “The cortex transform: Rapid computation of simulated neural images”, Computer Vision, Graphics and Image Processing, vol. 39, no. 3, September 1987, pg. 311-327.

11. E. N. Dalal, D. R. Rassmussen, F. Nakaya, P. A. Crean and M. Sato, “Evaluating the Overall Image Quality of Hardcopy Output”, Proc. PICS, 1998, pg. 169-173.

12. Z. Wang, A. C. Bovik, H. R. Sheikh, and E. P. Simoncelli, “Image Quality Assessment: From Error Visibility to Structural Similarity”, IEEE Transactions on Image Processing, Vol. 13, No. 4, 2004, pg. 600-612.

13. D. Towner, N. Burningham, E. Schneider, “An Objective Resolution Metric for Digital Printers”, Proc. PICS, 2002, pg. 115-120.

14. D. R. Rasmussen, P. A. Crean, F. Nakaya, M. Sato, and E. N. Dalal, “Image Quality Metrics: Applications and Requirements”, Proc. PIC Conference, Portland (1998).

15. A. Kenney and S. Chapman, “Digital Resolution Requirements for Replacing Text-Based Material: Methods for Benchmarking Image Quality”, Commission on Preservation and Access, Washington, D.C., 1995.

16. Weber E H, *De* Pulsu, Resorptione, Auditu et Tactu (Leipzig: Koehler), 1834.

17. J. L. Mannos, D. J. Sakrison, “The Effects of a Visual Fidelity Criterion on the Encoding of Images”', IEEE Transactions on Information Theory, Vol. 20, No 4, 1974, pg. 525-535.

18. G.E.Legge and J.M.Foley, “Contrast masking in human vision”, JOSA, Vol-70, No. 12, December, 1980, pg. 1458-1471.

19. J. H. Siewerdsen, I. A. Cunningham, D. A. Jaffray, “A framework for noise-power spectrum analysis of multidimensional images”, Med. Phys. 29 (11), November 2002, pg. 2655-2671.

20. M. L. Giger, K. Doi, and C. E. Metz, “Investigation of basic imaging properties in digital radiography. 2. Noise Wiener spectrum,” Med. Phys. 11, 1984, pg. 797-805.

21. Paul J. Kane, Theodore F. Bouk, Peter D. Burns, and Andrew D. Thompson, “Quantification of Banding, Streaking and Grain in Flat Field Images”, IS&T, Portland, OR, 2000, pg. 79-83.

22. J. C. Dainty and R. Shaw, Image Science, Academic Press, London, 1974, ch. 8.

23. P. D. Burns, Proc. Advances in Non-Impact Printing Tech., 1984, pg. 139.

24. P. C. Bunch and R. Van Metter, Proc, SPIE, 914, 877, (1988).

25. J. Vranckx, P. Breesch and M. DeBelder, Photgr. Sci. Eng., 28, 134 (1985).

26. Kenneth M. Hanson , "A simplified method of estimating noise power spectra", in Medical Imaging: Physics of Medical Imaging, J. T. Dobbins III and J. M. Boone, eds., Proc. SPIE **3336**, 1998, pg. 243-250.

27. Oppenheim, A. V. and A. W. Schafer: Digital Signal Processing, Prentice-Hall, New Jersey, 1975, Chapter 11.

28. M. S. Bartlett, “An Introduction to Stochastic Processes with Special Reference to Methods and Applications,” Cambridge University Press, New York, 1953.

29. R. B. Blackman and J. W. Tukey, “The Measurement of Power Specta,” Dover Publications, Inc., New York, 1958.

30. Fredric J. Harris, “On the Use of Windows for Harmonic Analysis with the Discrete Fourier Transform,” Proc. IEEE, Vol. 66, 1978, pg. 51-83.

31. B. J. West and M. Shlesinger, “The Noise in Natural Phenomena,” American Scientist, Volume 78, 1990, pg. 40-45.

32. T. bouk and N. Burningham, “Measurement of Graininess for Halftone Electrophotography,” Office Imaging Research & Technology Development, Eastman Kodak Company 1994, pg. 166-170.

33. R. P. Dooley and R. Shaw, “Noise Perception in Electrophotography,” J. Appl. Photogr. Eng., 5: 190-196 (1979).

34. E. W. H. Selwyn, “A Theory of Graininess,” Photogr. J, 75: 571 (1935).

35. B. J. West and M. F. Shlesinger, “On the ubiquity of 1/f noise,” Intl. J. Mod. Phys. B3: 1989, pg. 795-819

36. Birger Streckel, Bernhard Steuernagel, Eckhard Falkenhagen, and Eggert Jung, “Objective Print Quality Measurements Using a Scanner and a Digital Camera”, DPP2003, pg. 145-147

37. Howard Mizes, Nancy Goodman, and Paul Butterfield, “The Perceptibility of Random Streaking”, IS&T, Portland, OR, 2000, pg. 89-93.

38. D. R. Rasmussen, E. D. Dalal, K. M. Hoffman, “Measurement of Macro-uniformity: Streaks, Bands, Mottle and Chromatic Variatins,” IS&T’s 2001 PICS Conference Proceedings, pg. 90-95.

39. B. Mishra and D. R. Rasmussen, “MicroUniformity: An Image Quality Metric For Measuring Nosie,” IS&T’s PICS 2000 Conference Proceedings, pg. 75-78.

40. A. C. Bovik, “Streaking in Median Filtered Images,” IEEE Transactions on Acoustics, Speech, and Signal Processing, Vol. Assp-35, No. 4, 1987, pg. 493-503

41. John C. Briggs, Mike Murphy, and Yichuan Pan, “Banding Characterization for Inkjet Printing”, IS&T, Portland, OR, 2000, pg. 84-88.

42. M. C. Chen, G. T. Chiu, J. P. Allebach, “Characterization of Chromatic banding artifact for secondary colors in a polychrome electrophotographic process,” International Conference on Digital Printing Technologies, 2004, pg. 464-469.

43. C. Cui, D. Cao, S. Love, “Measuring Visual Threshold of Inkjet Banding,” Society for Imaging Science and Technology, Image Processing, Image Quality, Image Capture, Systems Conference, 2001, pg. 84-89.

44. W. Wu, E. N. Dalal, R. D. Rasmussen, “Perceptibility of Non-sinusoidal Bands,” International Conference on Digital Printing Technologies, 2002, pg. 462-466.

45. Y. Bang, Z. Pizlo, J. P. Allebach, “Discrimination Based Banding Assessment,” International Conference on Digital Printing Technologies, 2003, pg. 745-750.

46. John C. Briggs, “MTF, CTF, and Contrast Measurements”, Application Note, Quality Engineering Associates (QEA), Inc.

VITA

Il-Won Shin was born on 31 January 1974 in Pusan, Korea. He received his Bachelor's Degree in Division of Information and Computer Engineering from Hansung University, Korea in February 2001. In pursuit of his higher education he attended The College of Engineering at University of Kentucky, Lexington. His research interests are in Signal and Image processing and he was a Research Assistant in the Visual System Lab. Currently he is working in Division of Air Quality for Kentucky States. He enjoys watching all kinds of movies, playing soccer and tennis, and computers.